UNIVERSIDADE FEDERAL DE MINAS GERAIS

ESCOLA DE ENGENHARIA

SCHOOL OF ENGINEERING

GRADUATE PROGRAM IN CHEMICAL ENGINEERING

DOCTORAL THESIS

Corrosion Study of Standard Duplex Stainless Steel UNS S31803 and Lean Duplex Stainless UNS S32304 in Liquor from Paper and Pulp Mill

Author**:** Luiza Esteves

Advisor (UFMG - Brazil): Prof[a] Dr[a] Vanessa de Freitas Cunha Lins

Advisor (OSU - USA): Prof. Dr Gerald Frankel

Belo Horizonte

December 2016

UNIVERSIDADE FEDERAL DE MINAS GERAIS

ESCOLA DE ENGENHARIA

PROGRAMA DE PÓS-GRADUAÇÃO EM ENGENHARIA QUÍMICA

Luiza Esteves

Corrosion Study of Standard Duplex Stainless Steel UNS S31803 and Lean Duplex Stainless UNS S32304 in Liquor from Paper and Pulp Mill

Tese de doutorado apresentada ao Programa de Pós-Graduação em Engenharia Química da Universidade Federal de Minas Gerais

Linha de pesquisa: Corrosão e Engenharia de Superfície

Orientadora (UFMG): Profª Drª Vanessa De Freitas Cunha Lins

Co-orientador (OSU): Prof. Dr. Gerald S. Frankel

Belo Horizonte

Dec/2016

ACKNOWLEDGEMENTS

To begin with, I'm very grateful to GOD because, without his graces and blessings, this study would not have been possible.

I would also like to express my sincere gratitude to my advisor Prof. Dra. Vanessa de Freitas Cunha Lins for the continuous support of my Ph.D. study and related research, for her patience, motivation, and immense knowledge. Her guidance helped me during my research and writing of this thesis. I could not have imagined having a better advisor and mentor for my Ph.D. study.

I would also like to thank Aperam, specially Adolfo Kalergis for his advice and Cenibra for their support

Besides my advisor, I would like to thank the rest of my thesis committee: Prof. Dra Mônica M. A. M. Schvartzman, Prof. Dr. Wagner R. C. Campos, Dr. Maria das Mercês R. de Castro and Dra. Rosa M. R. Junqueira. Not just for their insightful comments and encouragement, but also for the difficult questions which motivated me to widen my research to various perspectives.

My sincere thanks also goes to Dra. Mônica Schvartzman and Dr. Wagner Reis who gave me an opportunity to join their team, access to their laboratory and research facilities at CDTN. And also, thanks to Edicleto for his help during the performance of electrochemical tests at high temperature. Without their full support, it would not have been possible to conduct this research.

I have been aided in various laboratories over the years. I would like to thank all from Corrosion and Surface Engineering Laboratory (Cíntia, Layane, Dalila, Renata, Elisângela, Brunela, Débora, Ricardo, Amanda, Camilo, Fernanda,Túlio, Thalys, Thiago e Pedro) who have helped, in exchanging knowledge and expectations. Thanks to Prof. Dr. Dagoberto and Prof Dr. Bracarence and their entire group for sample preparation support. Thanks to Prof. Dra. Luiza de Marilac and Prof Dr. Kátia for their support.

I am grateful to Prof Dr. Frankel for his help and support and also for the opportunity to be a part of his amazing group during my sandwich doctorate at Fontana Corrosion Center (FCC) as a visiting scholar. I was blessed with a friendly and cheerful group. I cannot forget all that you did for me (Angie, Rebecca, Feng, Ben, Brandon, Xiaolei, Huang, Anup, Jinwook, Shanshan, Dadi, Jichao, Jinheon, Santiago, Sara, Xi, Katsuya and Zhicao, Aline in special).

Last but not the least, I would like to thank my family: my parents, Neuza e Luiz, my brothers: Guilherme, Cleiton e Diego *in memorian,* my nephews: Luiz Gustavo, Henrique, Otávio Vinícius and Gabriel, my sisters in law for supporting me spiritually throughout the writing of this thesis and my life in general not forgetting my boyfriend Fábio Lucas for being patient and for his attention.

Our greatest weakness lies in giving up.

The most certain way to succeed is always to try just one more time.”

Thomas A. Edison

SUMMARY

FIGURES

TABLES

RESUMO

A microestrutura do aço inoxidável duplex foi analisada utilizando microscopia de força magnética (MFM) e microscopia de sondagem Kelvin de varredura (SKPFM). O SKPFM foi aplicado para avaliar a variação do potencial de Volta entre austenita (γ) e ferrita (α). O MFM foi usado para distinguir as fases austenita e ferrite, devido às características magnéticas (ferrita é ferromagnética e austenita é paramagnética). Além disso, as técnicas MFM/SKPFM mostraram ser uma ferramenta poderosa para estudar as fases em aços inoxidáveis duplex sem ataque químico.

Neste estudo, a difração de raios-X (DRX) e o refinamento de Rietveld foram realizados para identificar e quantificar a fase de ferrita e austenita nos aços dúplex laminados à frio e à quente (UNS S31803) e aços inoxidáveis lean duplex (UNS S32304). A espectroscopia de impedância eletroquímica (EIE) foi utilizada para avaliar o comportamento químico dos aços inoxidáveis dúplex e o lean duplex em licores branco, verde e negro da indústria de papel e celulose. Os resultados da análise de Rietveld mostraram um maior teor de austenita do que o limite padrão para os aços duplex na condição de laminados à quente. A condição de laminação à quente mostrou uma melhoria da resistência à corrosão no licor branco, principalmente para o lean duplex.

O comportamento de polarização potenciodinâmica cíclica do aço inoxidável duplex (DSS) e lean duplex (LDSS) foram estudados em licores branco e verde fornecidos por uma fábrica americana de papel e celulose e comparada com licores sintéticos. As curvas de polarização dos aços dúplex em licor branco sintético foram deslocadas para potenciais mais baixos e maiores densidades de corrente em relação ao licor branco industrial, que se mostrou menos agressivo ao aço duplex. Os aços dúplex também apresentaram os maiores valores de potencial transpassivação em licor branco industrial. Os aços dúplex e o lean duplex em licor verde em ambos os processos de laminação, apresentaram os menores valores de potencial transpassivação.

As amostras de aço inoxidável duplex (DSS) foram expostas a alta temperatura (200 ° C) em licor branco industrial de uma fábrica brasileira usando uma autoclave para simular as mesmas condições de processamento de um digestor. O método de extrapolação de Tafel e a perda de

massa foram utilizados para avaliar o comportamento de corrosão dos aços. Os resultados mostraram que as taxas de corrosão dos DSSs aumentam com o aumento de temperatura. Além disso, foi observada uma dissolução seletiva da fase ferrita.

ABSTRACT

Duplex stainless steel (DSS) was employed to distinguish between two phases: austenite and ferrite. The microstructure was analyzed using magnetic force microscope (MFM) and scanning Kelvin probe microscopy (SKPFM). MFM was used to distinguish the phases austenite and ferrite, due to magnetic features (ferrite is ferromagnetic and austenite is paramagnetic). SKPFM was applied to evaluate the variation of Volta potential between austenite (γ) and ferrite (α). Also, MFM/SKPFM technique showed to be a powerful tool in studying the phases in duplex stainless steels without surface etching necessarily.

In this study, X-Ray Diffraction (XRD) and Rietveld Refinement were performed to identify and quantify the ferrite and austenite phase of cold and hot rolled duplex stainless steels (UNS S31803) and lean duplex stainless steels (UNS S32304). Electrochemical impedance spectroscopy (EIS) was applied to evaluate the chemical behavior of duplex and lean duplex stainless steels in white, green, and black liquors of paper and pulp industry. Rietveld analysis results showed a higher austenite content than the standard limit for duplex steels in the hot rolled condition. The hot rolling condition plays a major role in improving corrosion resistance in white liquor mainly for the lean duplex steel.

The cyclic potentiodynamic polarization behavior of duplex stainless steel (DSS) and lean duplex stainless steel (LDSS) was studied in white and green liquors from a pulp and paper processing plant. The corrosion behavior in industrial and also synthetic liquors was compared. The polarization curves of the duplex steels in synthetic white liquor were shifted to lower potentials and higher current densities in relation to the steel in industrial white liquor, which proved to be less aggressive to the duplex steel. The duplex steels also showed the highest values of transpassive potential in industrial white liquor. Cold and hot rolled duplex and lean duplex steels in green liquor showed the lowest values of transpassive potential.

Specimens of duplex stainless steel (DSS) were exposed at high temperature (200 ºC) in industrial white liquor from a Brazilian kraft mill using an autoclave to simulate the same conditions as a digester processing. Tafel extrapolation method and weight loss were used to evaluate corrosion behavior of steels. The results showed that the corrosion rates of DSSs increase with temperature increases. As well as selective dissolution of the ferrite phase.

1 INTRODUCTION

This present study is aimed to investigate the influence of microstructure on the electrochemical properties of standard and lean duplex stainless steels (DSS) in white, green, and black liquors of pulp and paper mill. This study has also investigated the influence of microstructure of cold and hot rolled duplex steels on electrochemical properties of the duplex and lean duplex steels in white, green, and black liquors from Pine and southern hardwood mix of an American pulp and paper industry, and also from a Brazilian company.

The work in this thesis was carried out at Fontana Corrosion Center (FCC) at Ohio State University (OSU), USA and also at Corrosion and Surface Engineering Laboratory – Chemical Engineering at Belo Horizonte (UFMG), Brazil. The first section consists of a review of literature about DSS and pulp and paper mill and electrochemical techniques in **Chapter 3.** The following parts consist of chapter 4, 5, 6, 7, 8, 9, 10, 11 and 12.

Chapter 4: Rietveld and impedance analysis of cold and hot rolled duplex and lean duplex steels for application in paper and pulp industry;

Chapter 5: Scanning Kelvin probe force and magnetic force microscopy and impedance characterization of standard and lean duplex stainless steel;

Chapter 6: Electrochemical behavior of Duplex stainless steels in liquor from paper mill;

Chapter 7: Corrosion Behavior of duplex and lean duplex stainless steels in industrial and synthetic liquors;

Chapter 8: Corrosion behavior of duplex and lean duplex stainless steels in black liquors;

Chapter 9: High-Temperature and High-Pressure Corrosion Behavior of Duplex Stainless Steel in White Liquor from Brazilian Paper and Pulp Mill;

Chapter 10: Microelectrochemical Testing: Microcell Technique;

Chapter 11: Characterization of Passive Film on Duplex Stainless Steel in White Liquor;

Chapter 12: Future works.

2 GOALS

Evaluate the corrosion behavior of standard stainless duplex (UNS 31803) and lean duplex stainless steels (UNS S32304) in environments of pulp and paper mill.

2.1 Specific Goals

- Evaluate the effect of microstructure on corrosion resistance of UNS S31803 and UNS S32304 steel with different processing: cold and hot rolling in black, white and green liquors of pulp and paper industry;
- Evaluate the passivation and repassivation using cyclic potentiodynamic polarization and electrochemical behavior using electrochemical impedance spectroscopy in different solution supplied by North American and Brazilian industry;
- Evaluate the influence of industrial and synthetic liquors;
- Evaluate the effect of high temperature and high pressure on duplex steels in white liquor using autoclave to simulate the same conditions of a digester processing;
- Perform laboratory characterization of microstructure duplex stainless steel and corrosion products using techniques such as optical microscopy, scanning electron microscopy (SEM), X-Ray Diffraction and energy dispersive spectroscopy (EDS).

3 LITERATURE REVIEW

3.1 Duplex Stainless Steels (DSS)

Duplex stainless steels (DSS) have increasing applications as a structural material in critical components of nuclear power plants, chemical industries, oil and gas sectors, pulp and paper digesters (Shulz *et al.,* 2014), liquor tanks and paper machines, transportation (Sahu *et al.,*2009), biofuel power, solar power (Baddoo, 2008), corrosive chemical containment pressure vessels (Farina, 2000) and other general engineering applications because of their high strength, superior resistance to stress, corrosion, cracking and weldability.

Duplex grades have been used for structural applications, which offer a combination of higher mechanical strength compared with the austenitic (and also the great majority of carbon steels) with similar or superior corrosion resistance (Baddoo, 2008; Schweitzer, 2006).

The uses of lean duplex are mostly considered for the less aggressive environments due to economic reasons such as the use of lean duplex in liquor tanks and suction roll (Charles, 2008).

DSS contain roughly 22 to 25%wt.Cr, 5 to 7%wt. Ni, up to 4%wt. Mo, as well as additions of copper (Cu) and nitrogen (N) (ASM, 2000) and exhibit good properties such as high mechanical strength, corrosion resistance and good weldability (Kawaguchi *et al*., 1997). DSS have lower amounts of nickel than the austenitic grades, with the result that some of the austenite transforms to ferrite (Jones, 2001). DSS have a dual phase microstructure with equal amounts of austenite and ferrite (Krauss, 2005; Marcus, 2006).

A comparative study among AISI 304L, 316L stainless steels and duplex stainless were performed by Senatore (2007) that showed that the duplex stainless are alternatives to austenite stainless steel in 3% NaCl solution (Senatore *et al.*, 2007). However, the lower raw material costs for duplex steels compared to austenitic steels are make up for by higher hot-working costs conducted to avoid deleterious phase such as sigma due to high chromium/molybdenum contents (Talbot, 1998).

The use of DSS has increased drastically as shown in Figure 3.1 (Gagnepain, 2008; Tuomi *et al*., 2000, Schulz *et al.,* 2014). Nickel ore and other raw elements, such as chromium and molybdenum are subject to market variations, making DSS a more competitive cost (Schulz *et al.,* 2014).

DSS are known best for the following performance characteristics such as: lower life-cycle cost, high resistance to stress corrosion cracking (SCC), excellent resistance to pitting and crevice corrosion, high resistance to erosion and general corrosion in many environments, high mechanical strength, low thermal expansion, and good weldability (Schweitzer,2006).

The corrosion resistance of duplex steels is comparable to the austenitic steels: lean duplex (S32304) as type 316 and duplex (S31803) as type 317 (Sastri *et al.,* 2012; Schweitzer, 2006).

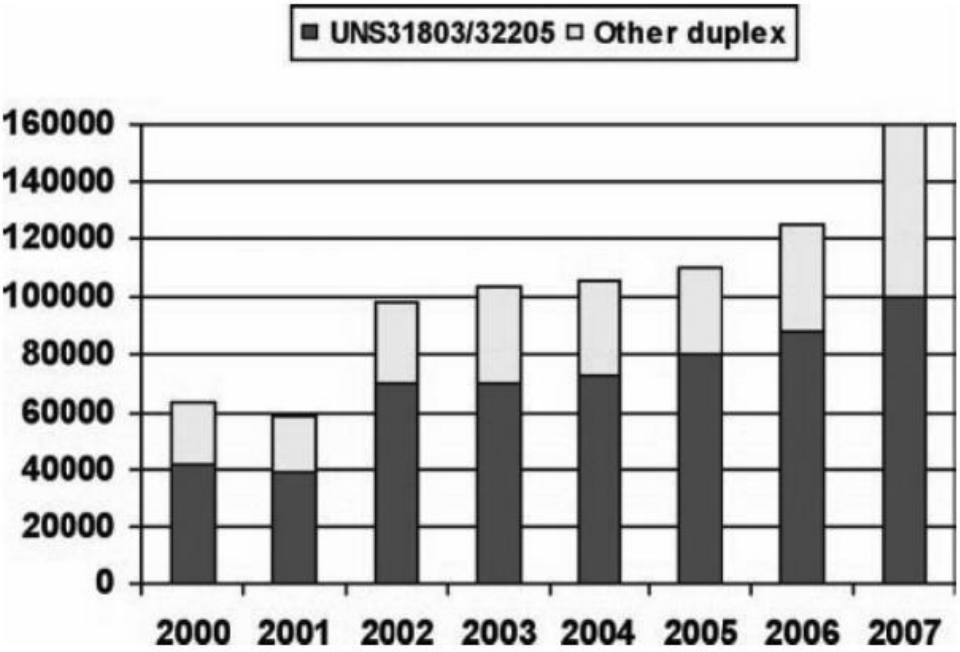

Figure 3.1: Crude productions of DSS according to Global markets (metric tons). Source: Gagnepain, 2008, Schulz *et al.,* 2014).

Schaeffler diagram (Figure 3.2) shows the three plotted classical families of Duplex grades: the UNS S32304 Mo free grades, standard Duplex type UNS S32205 and super duplex grades of UNS S32507 type, with (Charles, 2008; Talbot, 1998). The Cr (ferrite former) and Ni (austenite former) equivalents that form the two axes of the Schaeffler diagram (Pierre, 1999).

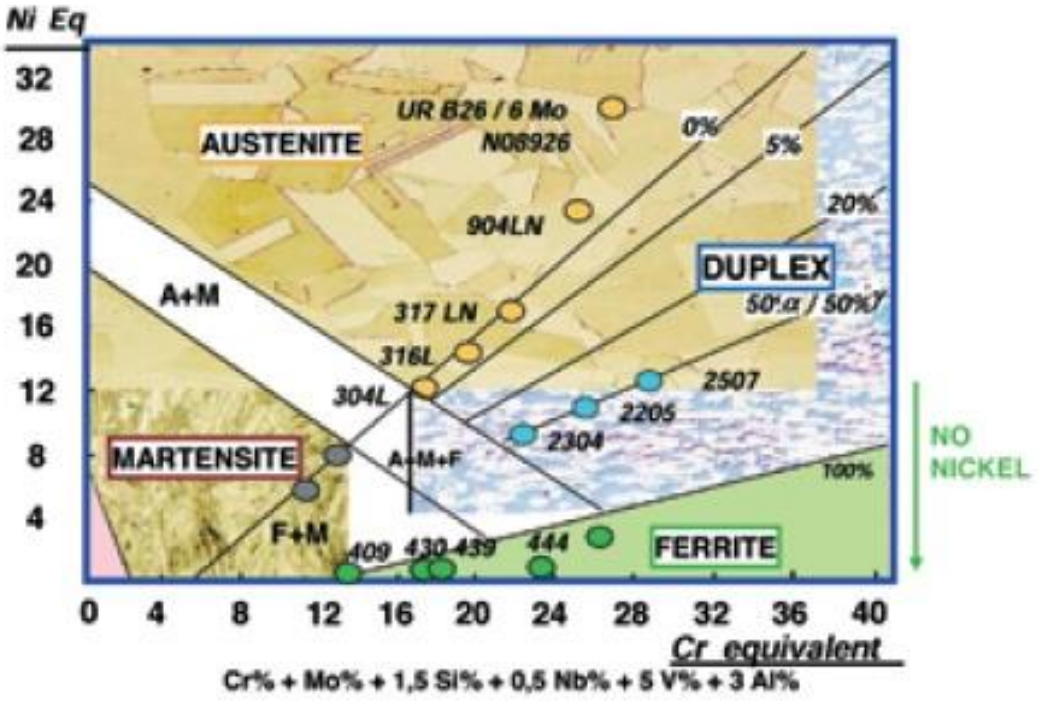

Figure 3.2: The Schaeffler diagram for estimating the constitutions of stainless steels. Ni equivalent = wt-% Ni + 30 wt-% C + 25 wt-% N + 0.5 wt-% Mn. Cr equivalent = wt-% Cr + wt-% Mo + 1.5 wt- % Si + 0.5 wt-% Nb + 1.5 wt-% Ti. α = F= Ferrite; α′ = M = martensite; and γ = A = austenite (Charles, 2008, Talbot, 1998).

3.1.1 Hot Working

Hot working occurs when deformation is achieved at a temperature above where recrystallization can occur (Callister, 2001). UNS S32205 DSS can be readily forged, upset and hot headed. Uniform heating of the steel in the range from 1150°C to 1250°C is required. Initial hot working should be performed without large reductions or change of shape. The finishing temperature should not be below 950°C. If the temperature after forging is still above 1000°C, rapid cooling (water quenching) can be carried out directly at working temperature. Otherwise, all hot-working operations should be followed by annealing, pickling and passivating to restore the mechanical properties and corrosion resistance (NAS, 2010).

3.1.2 Cold Working

When a metal is plastically deformed at temperatures that are low relative to its melting point it is referred to as is called cold worked. Cold working is known greatly to increase the number of dislocations in a metal (Reed-Hill, 2009). The UNS S32205 DSS has good formability, due to the increase in strength (Callister, 2001) and the fact that more power is required for most cold-forming operations than for austenitic stainless steels (NAS, 2010).

3.2 Dss: Composition and Microstructure

DSS, means those with a mixed microstructure of about equal proportions of γ-austenite (face centered cubic - FCC) and α-ferrite (body centered cubic - BCC), have existed for more than 70 years. Both constituent phases contain at least about 11wt% chromium (Lai *et al*., 2012).

Chromium, molybdenum, tungsten and nitrogen contents are responsible for the pitting resistance and crevice corrosion resistance (IMOA, 2009; Sastri *et. al.,* 2012; Gunn, 1997).The high localized corrosion resistance of these alloys could be observed by Pitting Resistance Equivalent Number (PREN), which was developed to associate the amount of these elements with the potential corrosion of the alloy shown in Equation 1. The higher the PREN, the better the pitting resistance is (Deng *et al., 2008)*.

PREN = %Cr +3.3 x (%Mo) + 16 x (%N) **Equation 1**

The duplex grade is given by the Unified Numbering System (UNS) from United States of America and is given by their chromium and nickel contents. For instance, UNS S32304 (SAF 2304) contains 23% Cr and 4% Ni and UNS S32205 (2205) contains 22% Cr and 5% Ni (ASM, 2000). The PREN of S32205 steel is 35 and of S32304 is 24 (Shulz *et al.,* 2014).

During the 1980s, the development of the S32304 occurred, that is a lean alloy grade with lesser Mo than the UNS S32205 steel, with a lower cost, but a lower pitting resistance (Gunn, 1997; Westin, 2010). The corrosion resistance of the lean duplex is compared with the 304 L (Schulz *et al.,* 2014).

The microstructure depends on the chemical composition of the alloy and the heat treatment conditions (Itman *et al.,* 2014). Three main types of microstructure exist in stainless steels: ferritic,

austenitic and martensitic (Lo *et al.,* 2009). There are two types of alloy elements: ferrite stabilizers (chromium, silicon, molybdenum, titanium and niobium) and austenite stabilizers (nickel, carbon, copper, nitrogen, manganese) (Yonekubo, 2010).

The optimal phase balance for modern products can be in a range between 45% and 60% austenite. The microstructure is obtained by a simultaneous control of the chemical composition and annealing temperature (manufacturing process). A microstructure of rolled duplex steels is shown in Figure 3.3 (Gunn, 1997; Jones, 2001).

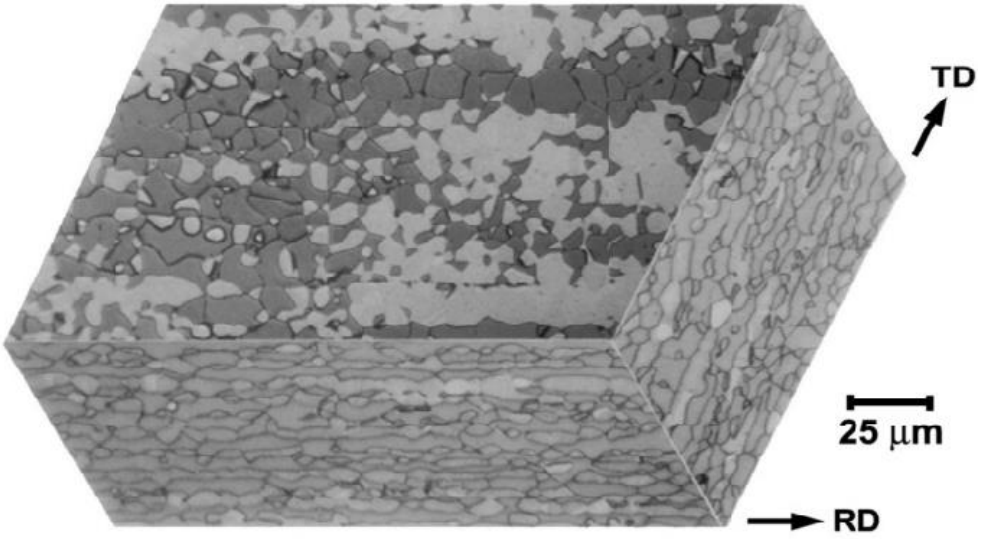

Figure 3.3: 3D composed micrograph of rolled DSS. Optical microscopy. Ferrite is the darker phase. Etched with Behara II (Armas, 2009).

Microstructural evaluation of DSSs must be performed with the proper etching techniques in order to use an optical light microscope (OLM) or scanning electron microscope (SEM). Numerous etchants and electro-chemical etching techniques have been identified for the revelation of the microstructures in DSS. The following etching techniques 10% KOH electrolytical etchant, 5 V; Kallings reagent; 10% Oxalic Acid, 40% NaOH, and Glyceregia electrolytical etching and Behara reagent (Russell, 2005).

Jimenez studied the microstructural features of DSS in the as-received after the annealing at a temperature range between 850 to 1100 °C. The chemical etching used was a solution of 15 mL HNO_3 and 30 mL HCl to evaluate the microstructure. DSS in the as-received sheet showed a microstructure

of austenitic grains elongated along the rolling direction in a ferrite matrix and after annealing (Jimenez *et al*., 2000).

In DSSs, Cr, Mo, Ni and N are not uniformly distributed between ferrite and austenite phase and this heterogeneity may lead to galvanic interactions, which may result in difference in corrosion behavior between these phases (Femenia, 2004).

Sigma phase is a hard, brittle intermetallic phase compound of Fe, Cr and, to a smaller extent of Mo (Sopousek and Kruml, 1996; Michalska, 2006) and can influence mechanical and corrosion properties (Pohl, 2004). Additional secondary phases can be represented by the different precipitates that have been found in DSSs such as phase, Chi (χ) phase, R-phase, π-phase, secondary austenite (γ_2), Cr_2N, carbides M23C and M7C3 and Cu-rich epsilon (ε) phase that are mainly found in hot processing steels (Russell, 2005).

Quantitative image analysis was employed to evaluate intermetallic phase precipitation in UNS S32205 DSS after aging at 750 °C condition. 20% NaOH solution was particularly useful in selective etching austenite–ferrite phase boundaries, grain boundaries in ferrite, intermetallic σ, and χ phases. The precipitation of σ and χ phases was primarily affected by the volume fractions of matrix phases and corresponding portioning of alloying elements (Michalska, 2006).

Sigma and Chi phases form in high chromium, high molybdenum stainless steels and ferrite is the preferential precipitate (IMOA, 2009). The UR 52N DSS was aged at 475ºC for various periods to evaluate the effect of alpha prime on mechanical and chemical resistance (Fontes, 2009). Alpha prime phase leads to decreased corrosion resistance and mechanical properties losses of DSS.

X-ray diffraction (XRD) analysis evaluates microstructural parameters easily, reliable, quicker and in a non-destructive way (Feng *et al*., 2013). Garin (2012) quantified the cast super duplex steel fraction using the Rietveld method together with conventional X-ray powder diffraction techniques after having realized on a series of heat-treated weldments that permitted an accurate quantification of the microstructural components such as austenite, ferrite, and sigma-phase in all studied samples. Figure 3.4 shows the XRD patterns of the parent allow and the sample annealed weldments at 1133 K for 3 h. Formation of sigma all detected in all heat-treated samples (Garin, 2012, Dubiel, 2011).

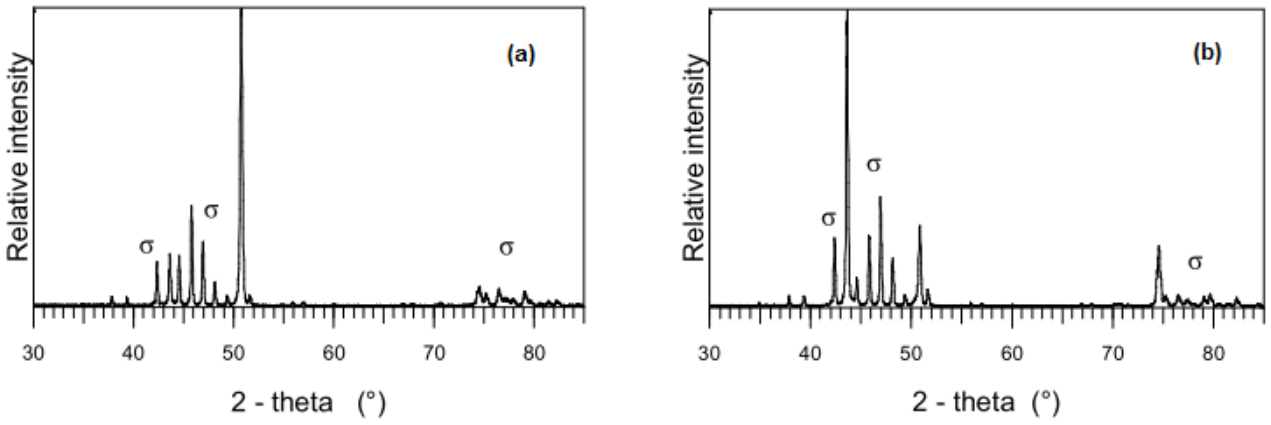

Figure 3.4: (a) XRD pattern of parent alloy (γ: austenite; α: ferrite); and (b) XRD pattern of weldment (HAZ) annealed at 1133 K, 3h (σ: sigma phase). Source: Garin, 2012).

3.3 Pulp and Paper Mill

Carbon steel and 300 series austenitic stainless steels are also used in pulp mill equipment (Wensley, 2005). DSS are also being used in new pulp mill equipment; however, these materials have not yet been studied (Hazlewood, 2006).

The main processes in pulp and paper manufacturing are raw material preparation and handling, pulp manufacturing, pulp washing and screening, chemical recovery, bleaching, stock preparation, and papermaking (Bajpai, 2012; Sheffield, 1993). The UNS S32205 DSS is typically applied in the pulp and paper industry in digester and liquor tanks (NAS, 2010; Wensley, 2004).

Most of the DSS digesters have been constructed using the UNS S32205 stainless steel due to the greater availability of this material compared with other DSS alloys, the current trend is to construct both batch and continuous digesters with this material (Wensley, 2005). UNS S32304 DSS has a slightly superior corrosion resistance than the UNS S32205 and is also a good candidate material of construction for new Kraft digesters. Wensley (2004) studied the application of these materials in batch and continuous process and observed that DSS have excellent corrosion resistance in both digester liquors and that cold formed heads are problematic for large DSS pressure vessels (Wensley, 2004).

DSS for the non-pressurized vessel (pulp storage tower) were evaluated. The calculation covering costs of material and work showed that UNS S32304 might yield cost savings of 8% compared to a tower of carbon steel lined with austenitic stainless steel. Field tests have also shown that the S31803 has a higher corrosion resistance in sulfite digester environments than AISI 316L and 317L (Nordström, 1994).

Chemical pulps are made by cooking (digesting) the raw materials, using the Kraft process (sulfate) and sulfite processes. The Kraft process is the most dominating chemical pulping process worldwide. In the Kraft pulp process, the active cooking chemicals (white liquor) are sodium hydroxide (NaOH) and sodium sulfide (Na_2S) (Bajpai, 2012; Bajpai, 2015), the operation is at high temperature (about 170 °C) and the pressure of 5 to 8.5 bar (72 to 123 psi) is used in delignification during the chip cooking cycle (Russel, 1999; Hazlewood, 2006; Nava, 2008). The sulfide and hydroxide groups are strong nucleophiles and break the polymeric lignin into smaller species (Kannan, 1996).The wood chips are treated with the white liquor at elevated temperature and pressure and form the pulp (Bajpai, 2008). Moreover, the white liquor is considered to be the most aggressive of the alkaline pulping liquors (Bhattacharya, 2011; Wensley, 2005).

Pulp mills can be divided into two major processing steps: fiber and chemical recovery as shown in Figure 3.5. The main goal of the fiber processing line is to remove lignin from wood and to achieve high brightness pulp in the end bleaching sequence. The chemical recovery cycle generated the sub-product, extracted from pulping wood in the digester, called the black liquor, with smaller amounts of wood extractives and residual inorganic pulping salt (Demirbas, 2002, Wensley,

2005).

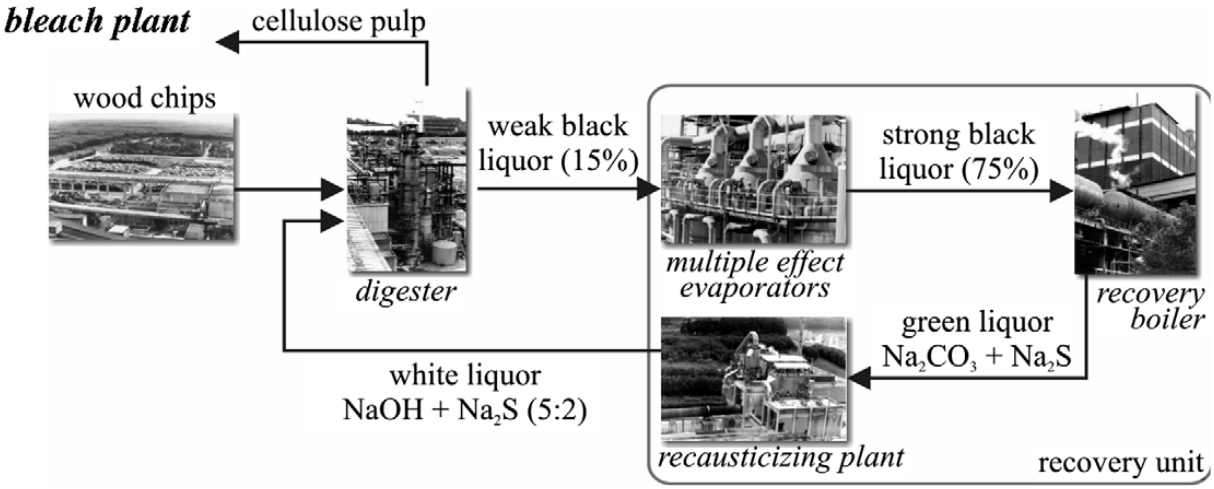

Figure 3.5: Schematic representation of the pulp mill plan (Cardoso *et al.*, 2009).

The black liquor chemical composition depends on the type of the raw material processed and can be considered as a complex aqueous solution constituted by organic materials from wood or fibrous plants (lignin, polysaccharides and resinous compounds of a low molar mass) and inorganic compounds (mainly soluble salt ions) (Cardoso *et al.,* 2009; Singh, 2007).

Black liquor is the waste from the Kraft process and consists of residual inorganic chemicals (sodium sulfide, sulfate, sodium thiosulfate, sodium carbonate, and sodium hydroxide) after pulping process, numerous organic extracts in the wood such as organic acids and aliphatic sulfur, and other constituents are produced due to fragmentation reactions of lignin and its products during the pulping process (Frederick, 1997). The corrosion rate of the equipment in contact with black liquor depends on changes in pulping parameter or wood species (Singh, 2007; Anaya, 2001), for example, hardwoods result in lower corrosion rates than softwoods (Bauer, 1997).

The presence of non-processing elements (NPE) in black liquors (as potassium, chlorine, calcium, aluminum, silicon and iron ions) could cause incrustation on equipment walls, corroding these surfaces (Cardoso *et al.,* 2009).

Black liquor is concentrated by multi-effect evaporation system and burned in the recovery boiler where the combustion of organics provide energy to produce high pressure steam and to carry out the reduction reactions to recover sodium sulfide (Na_2S) and sodium carbonate (Na_2CO_3). The inorganic

product of the boiler recovery is used to regenerate the sodium hydroxide and sodium sulfide needed for pulping (Cardoso *et al.*, 2009).

The combustion of the strong black liquor converts the recovered inorganic chemicals to smelt which is dissolved in water to give the green liquor (which are sodium carbonate (Na_2CO_3) and sodium sulfide (Na_2S) generated during the liquor recovery cycle (Kannan, 1996; Bajpai, 2008). The green liquor is causticized to produce the white liquor (Tuthill, 2002) as showed in Figure 3.6 and is processed in two steps. The recovery boiler is used to burn black liquor from sulfate pulping for recovery of inorganic chemicals as well as for energy production (Bajpai, 2008).

$$CaO + H_2O \rightarrow Ca(OH)_2 \quad (1)$$

$$Ca(OH)_2 + Na_2CO_3 \rightarrow CaCO_{3(s)} + 2NaOH \quad (2)$$

The cyclic recovery processes of inorganic chemical recover the white liquor used to cook or digest the wood chips. The first step is that, the black liquor is evaporated to remove the excess water to be burned. In the second stage, the reduced molten smelt (sodium sulfide and sodium carbonate) produced in the recovery boiler is quenched with water producing the green liquor (Wensley, 2005).The sodium carbonate is transformed in sodium hydroxide by calcium hydroxide to recover the inorganic chemical from white liquor. Organic chemicals dissolved out of the wood are the fuel portion of the black liquor fired in the recovery furnace. This combustion also raises steam for energy generation and for use in the process. The Kraft pulping is economically successful because the used cooking liquor can be recovered and reused in the chemical recovery process (Tuthill, 2002; Ecy, 1998).

Carbon steels and standard austenitic grades of stainless steel were the dominant metals for many years in the pulp and paper industry. However, the use of UNS S32205 duplex and other duplex stainless steels are increasing in the production of new equipment (Wensley, 2001). The reason for the focus on duplex steel is due to cost savings and better corrosion properties than carbon steel (Penn Stainless Products, 2012).

The DSS provide a wide range of corrosion resistance in various environments applications as pulp, pulp digesters, liquor tanks and paper machines. DSSs are an optimum materials choice due to the

competitive price. DSSs have a high resistance to stress corrosion cracking (SCC) and high mechanical strength due to microstructure, and these material are used in the sulfate (Kraft process) pulp digesters that work under highly alkaline and hot conditions. The UNS S32205 steel has mainly been used in continuous digester. Other duplex applications are associated with cooking process are black and white liquors tanks, and circulation systems such as heat exchangers, piping, pumps and valves (Armas, 2009).

Austenitics are still the most commonly used alloys in the pulp and paper industry, but this could change if the price of nickel and molybdenum remains high. A high-strength duplex steel (ferritic-austenitic) was used primarily in the industry in 1988 in Kraft digesters in a New Zealand plant. Duplex production and applications have increased during the last decade and today they are being used in digesters for cooking chips and reactors used in the oxygen delignification and bleaching processes. For example, in the sulfate process, the 316L stainless steel is widely used; however, UNS S32205 duplex, UNS S32101 and UNS S32304 Lean Duplex (LDX) provide a higher corrosion resistance than the 316L steel. In the washing and screening processes, the superior surface hardness of 2304, 2205 and 2101 duplex steels can reduce maintenance costs. Duplex UNS S32205 and LDX 2304 are the most popular material for oxygen reactors because of the protection provided against external stress corrosion cracking (SCC). Duplex grades are also finding increasing use in chemical recovery, mechanical and recycled pulp processing and in the head boxes and suction roll shells of paper machines. The UNS S32205 is common for batch and continuous digesters and also available for oxygen delignification and pressurized peroxide reactors (Chaeter, 2007).

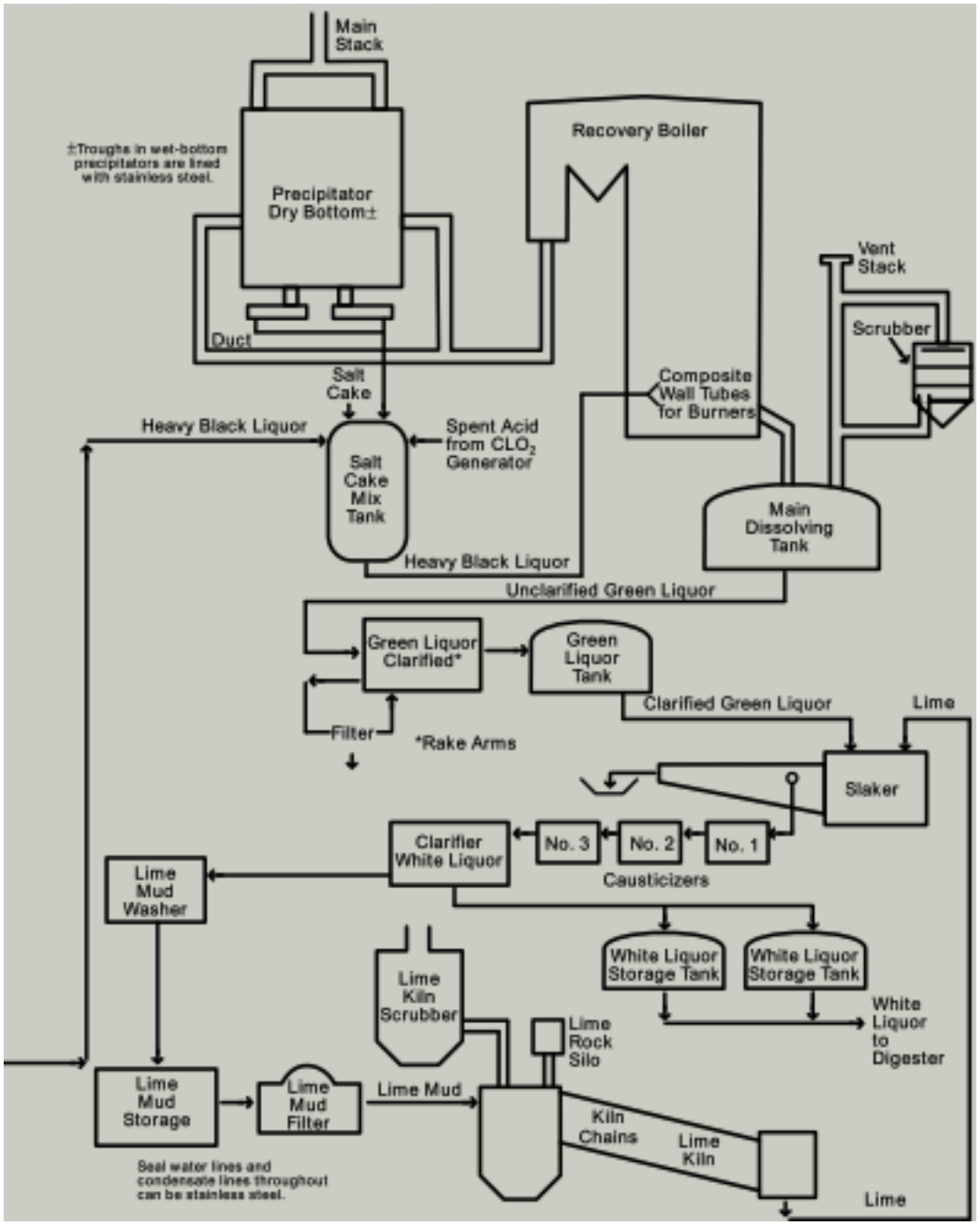

Figure 3.6: Flow Diagram of Black Liquor Recovery Boiler Liquor Tanks–Lime Kiln. Source: Tuthill, 2002.

DSS have several advantages such as superior corrosion resistance in pulping liquors, high mechanical strength, wear and erosion-corrosion resistance and excellent resistance to stress corrosion cracking when related to the austenitic grades (304L, 316L, and 317L) and these materials are less sensitive to price fluctuations of raw materials due to the lower nickel content than austenitic

grades. Bergquist reported two examples of failure cases of duplex stainless steels in the application in paper services such as cracks in a lamellar heat exchanger using UNS S32205 and corrosion damage in heavy black liquor due to cracking (Bergquist, 2009).

Paoliello (2011) studied the influence of cooking process in the continuous digester on steel corrosion and observed that cooking method considerably affects electrochemical potentials, passivation range and the corrosion behavior of continuous digesters (Paoliello *et al.,* 2011).

Bauer (1997) showed the corrosion rates of steels tested at seven different plants in Sweden (Figure 3.7) and observed that carbon steel is not reliable in the digester environment and on the other hand the DSS (SAF 2304 and UNS S32205) showed lower corrosion rates and an excellent resistance to stress corrosion. DSS are mainly used nowadays for building new digesters in the pulp and paper industry. The SAF 2205 (UNS S32205) is a high-alloy austenitic-ferritic stainless steel containing 3%wt. molybdenum, showing resistant to stress corrosion, and the content of molybdenum and nitrogen mean that it is highly resistant to local corrosion attacks, such as pitting (Bauer, 1997; Tuthill, 2002).

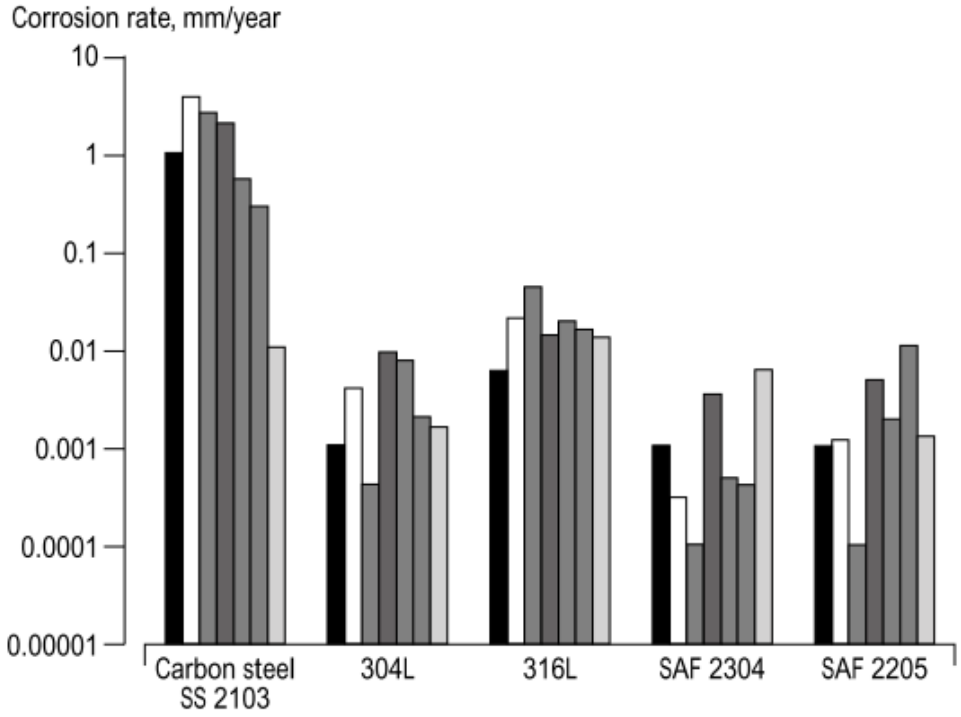

Figure 3.7: Corrosion rates for steel test pieces exposed in a digester of pre-heaters. Observe that the vertical axis has a logarithmic scale. Source: Bauer, 1997.

In the pulp and paper industry, carbon steel pulp mill equipment, like digesters, storage vessels, have shown general corrosion and stress corrosion cracking. The DSS have better resistance to corrosion and stress corrosion cracking in high pH environments in relation to carbon steel and austenitic stainless steels. Therefore these machines are being replaced by DSS (Bhattacharya, 2007; Wang, 2015).

Stress corrosion cracking of three austenitic (S31603, ASTM F138, N08904) and DSS (S31803) was tested at high temperature in caustic solutions under active conditions both in the absence and in presence of sulfide ions. The SCC susceptibility was dramatically increased by the additions of sulfide ions, in this study all the materials tested were subjected to severe SCC even at the highest strain rate (Rondelli, 1997). DSS was evaluated in sulfide-containing caustic solution to simulate the environmental of white liquor (NaOH + Na_2S). Austenite showed more susceptible to SCC than ferrite. However, SCC susceptibility depends on the alloy and environmental conditions (Bhattacharya, 2008).

3.4 Electrochemical Impedance Spectroscopy (EIS)

Electrochemical impedance spectroscopy is a powerful technique to study the coated metals in corrosive environments and provides information about corrosion resistance and mechanisms.

Constant phase elements (CPE) are most often used to describe the frequency dependence of non-ideal capacitive behavior and have become common in fitting procedures of electrochemical impedance to study corroding systems. The dimension of CPE is s^n/Ω, while that of an ideal capacitor (C) is s/Ω (Mansfeld, 2001). And the n exponent $0 < n < 1$ indicates the capacitor-like nature of the CPE: n = 1 for a perfect capacitor and n = 0 for a perfect resistor (Orazem, 2008; Fajardo, 2014).

$$CPE = \frac{S \cdot s^n}{Area} = \frac{A^2 \cdot s^3 \cdot Kg^{-1} \cdot m^{-2} \cdot s^n}{Area}$$

If n = 1

$$C = \frac{S \cdot s^1}{Area} = \frac{A^2 \cdot s^3 \cdot Kg^{-1} \cdot m^{-2} \cdot s^1}{Area} = \frac{F}{Area} = \frac{s}{\Omega}$$

If n = 0

$$CPE = \frac{S \cdot s^0}{Area} = \frac{A^2 \cdot s^3 \cdot Kg^{-1} \cdot m^{-2} \cdot 1}{Area} = \frac{A^2 \cdot s^3 \cdot Kg^{-1} \cdot m^{-2}}{Area} = \frac{\Omega^{-1}}{Area}$$

Impedance representation in terms of magnitude and phase angle as functions of frequency on a logarithmic scale are called bode plots (Orazem, 2008). When the impedance data are plotted in the complex plane (imaginary component *versus* real component) they are called Nyquist plot.

The Kramers-Kroning relationships are applied to evaluate the validity of experimental results, which must satisfy the priori conditions of linearity, stability, causality, continuity and finiteness (Zheng *et al.,* 2014; MacDonald, 2005).

3.5 References

ANAYA, A.; SINGH, P.; **Effect of Wood Species on Corrosivity of Black Liquors.** National Association of Corrosion Engineers.p. 1-16 (2001).

ARMAS, IRIS ALVAREZ; DEGALLAIX-MOREUIL, S.; ARMAS, Iris Alvarez; DEGALAIX, Suzanne Moreuil, **Duplex stainless steels**, 1st. ed. [s.l.]: Wiley, 2009.

ASM. **Introduction to Stainless Steels**. ASM International: The Materials Information Society. p. 1-7 (2000).

BADDOO, N. R.; **Stainless steel in construction: A review of research, applications, challenges and opportunities**. Journal of Construction Steel Research.v. 64 p.1199-1206 (2008).

BAJPAI, P.; **Chemical Recovery in Pulp and Papermaking.** Pira International (2008).

BAJPAI, P.; **Biotechnology for Pulp and Paper Processing.** Springer Science. Chapter 2: Brief Description of the Pulp and Paper Making Process, p. 7-15, 2012.

BAJPAI, Pratima, **Chemistry and Sustainability in Pulp and Paper Industry**, Patiala, India: Springer US, 2015.

BAUER, A.; LUNDBERG, M.; **Choosing materials to solve corrosion problems in the pulp and paper industry.** Anti-Corrosion Methods and Materials.v.44, p. 161-169 (1997).

BHATTACHARYA, A.; SINGH, P.; **Stress corrosion cracking of welded 2205 duplex stainless steel in sulfide-containing caustic solution.** Journal of Failure Analysis and Prevention. V. 7 (5), p. 371-377, (2007).

BHATTACHARYA, A.; **Stress Corrosion Cracking of Duplex Stainless Steels in Caustic Solutions.**Dissertation.Georgia Institute of Technology. December 2008.

BHATTACHARYA, A.; SINGH, P.; **Electrochemical behavior of duplex stainless steels in caustic environment.**Corrosion Science.v.53, p. 71-81 (2011).

BERGQUIST, A.; WEGRELIUS, L.; **Duplex 2205 – Experiences in Pulp and Paper Industry of a 30 Years Old Steel Grade.**TAPPI Engineering, Pulping & Environmental Conference.October, Tennessee (2009).

KAXIRAS, E.; CALLISTER, William D; RETHWISCH, David G, Materials Science, **Computing in Science & Engineering**, v. 3, n. 6, p. 960, 2001.

CARDOSO, M.; OLIVEIRA, E. D.; PASSOS, M.L.; **Chemical composition and physical properties of black liquors and their effects on liquor recovery operation in Brazilian pulp mills.** Fuel. v. 88 p. 756-763 (2009).

CHARLES, J.; **Duplex stainless steels, a review after DSS'07 in Grado**. La Revue de Metallurgie. v. 5 p. 155-171 (2008).

CHAETER, J.; **The pulp and paper ind turns to duplex.** Stainless Steel World.October (2007).

DENG, B.; JIANG, Y.; GONG, J.; ZHONG, C.; GAO, J.; LI, J.; **Critical pitting and repassivation temperatures for duplex stainless steel in chloride solutions**. Electrochimica Acta. v. 53, p.5220-5225 (2008).

DEMIRBAS, A.; **Pyrolysis and steam gasification processes of black liquor.** Energy Conversion and Management. v. 43, p.877-884 (2002).

DUBIEL, S M; CIESLAK, J. Sigma-Phase in Fe-Cr and Fe-V Alloy Systems and its Physical Properties. **Critical Reviews in Solid State and Materials Sciences**, v. 36, n. 4, p. 191–208, 2011.ISI>://WOS:000298164500001\nhttp://www.tandfonline.com/doi/pdf/10.1080/10408436.2011.589232>.

ECY, **Chemical Pulp Mills Kraft (Sulfate) Pulping**, Department of Ecology State of Washington, p. 1–10, 1998.Accessed 28/05/2015 (http://www.ecy.wa.gov/programs/air/pdfs/pulpmil3.pdf).

FAJARDO, S.; BASTIDAS, D. M.; CRIADO, M. BASTIDAS, J. M.; **Electrochemical study on the corrosion behaviour of a new low-nickel stainless steel in carbonated alkaline solution in the presence of chlorides**, **Electrochimica Acta**, v. 129, p. 160–170, 2014.

FEMENIA, M.; PAN, J.; LEYGRAF, C. **Characterization of Ferrrite-Austenite Boundary Region of Duplex Stainless Steels by SAES.** Journal of The Electrochemical Society. v. 151, p. B581-B585 (2004).

FARINA, C.; GRASSINI, U.; **Experiences and NDT Controls with Duplex Stainless Steels in Chemical and Refinery Plants**. Duplex 6th World Conference & Expo, (2000).

FENG, Q.; JIANG, C.; XU, Z.; XIE, L.; VINCENT, J.; **Effect of shot peening on the residual stress and microstructure of duplex stainless steel.** Surface and Coatings Technology. v. 226, p.140-144 (2013).

FONTES, T. F.; **Efeito da fase alfa linha nas propriedades mecânicas e de resistência à corrosão do aço inoxidável dúplex UR 52 N+**. Dissertaçao. Instituto de Pesquisas Energéticas e Nucleares (Autarquia associada à Universidade de São Paulo), (2009).

FREDERICK W.J.; ADAMS, T.N.; GRACE, T.M.; HUPA, M.; LISA, K.; JONES, A.K.; TRAN, H.; **Kraft Recovery Boilers**. TAPPI Press [chapter 3], Atlanta, (1997).

GAGNEPAIN, J.C.; **Duplex Stainless Steels : Success Story and Growth Perspectives**, Stainless Steel World, Dezembro, p. 31–36 (2008).

GARIN, Jorge L; MANNHEIM, Rodolfo L, RIETVELD QUANTITATIVE ANALYSIS OF SUPER DUPLEX STAINLESS STEEL, **JCPDS**, p. 98–105, 2012.

GUNN, R.; **Duplex Stainless Steels - Microstructure, Properties, and Applications**. Abington Publishing: Cambridge England, (1997).

KANNAN, S.; **The Role Of Dihydroxybenzenes And Oxygen On The Corrosion Of Steel In Black Liquor.** Corrosion Science. v. 38 nº. 7, p. 1051-1069 (1996).

KAWAGUCHI, S.; SAKAMOTO, U.; TAKANO, G.; MATSUDA, F.; KIKUCHI, Y.; MRÁZ, L.; **Microstructural changes and fracture behavior of CF8M duplex stainless steels after long-term aging.** Nuclear Engineering and Design. v. 174, p. 273-285 (1997).

KRAUSS, George, **Steel Processing, Structure, and Performance**, 1st. ed. [s.l.]: ASM International, 2005.

HAZLEWOOD, P E; SINGH, P M; HSIEH, J S, Effect of Black Liquor Oxidation on the Stress Corrosion Cracking Susceptibility of Selected Materials, **Corrosion Science**, v. 62, n. 9, p. 765–772, 2006.

INTERNATIONAL ASSOCIATION OF MOLYBDENUM - IMOA. **Practical Guidelines for the Fabrication of Duplex Stainless Steels**. London. Second Edition, (2009).

ITMAN,A. F.; SILVA, R. V.; CARDOSO, W. S.; CASTELETTI, L. C.; **Effect of niobium in the phase transformation and corrosion resistance of one austenitic-ferritic stainless steel**. Materials Research, (2014).

JIMENEZ, J.A.; CARSI M.; RUANO, O.A.; **Characterization of a δ/γ duplex stainless steel.**Journal of Materials Science. v. 35, p. 907-915 (2000).

JONES, Russell H, **Environmental effects on engineered materials**, Richlland, Washington: Marcel Dekker, 2001.

JUAN, BY; NAVA, CARLOS; **The Suitability of Thermal Spray Products in Digester Liquor Environments**, Arcmelt Company, v. 5, n. 5, p. 15, 2008.

LAI, J. K. L.; LO, K. H.; SHEK, C. H.; **Stainless Steels and Introduction and their recent developments**.Bentham Books, (2012).

LO, K. H.; SHEK, C. H.; LAI, J.K.L.; **Recent developments in stainless steels**. Materials Science and Engineering R. v. 65, p.39–104 (2009).

MACDONALD, J. Ross; BARSOUKOV, Evgenij, Impedance Spectroscopy, 2nd. ed. New Jersey, USA: Wiley, 2005.

MARCUS, PHILIPPE MANSFELD, Florian, **Analytical Methods in Corrosion Science and Engineering**, Boca Raton: Taylor &Francis Group, 2006.

MANSFIELD, F.; HSU, C.H.; **Technical Note: Concerning the Conversion of the Constant Phase Element Parameter Y_0 into a Capacitance.** Corrosion Science. v. 57, p. 747-748 (2001).

MICHALSKA, J.; SOZAŃSKA, M.; **Qualitative and quantitative analysis of σ and χ phases in 2205 duplex stainless steel.** Materials Characterization. v. 56, p.355-362 (2006).

NAS, **Flat Products Stainless Steel Grade Sheet**, North American Stainless, p. 9, 2010.

NORDSTRÖM, J; RUNG, B**, Digesters and pulp storage towers of duplex stainless steels saving weight and costs**, ACOM (Sweden), n. 3, p. 1–8, 1994.

ORAZEM, Mark E.; TRIBOLLET, Bernard, **Electrochemical Impedance Spectroscopy**, [s.l.]: John Wiley & Sons, 2008.

PAOLIELLO, F.; LINS, V. F.; CARDOSO, M.; **Influence of cooking conditions on continuous digester corrosion in a Brazilian pulp mill.**TAPPI Journal. P. 51-60. August 2011.

PENN STAINLESS PRODUCTS; **Duplex usage in the Pulp and Paper industry**.www.pennstainless.com. 2012. Web.February (2015).

PIERRE, R, **Handbook of Corrosion Engineering Library of Congress Cataloging-in-Publication Data**, [s.l.: s.n.], 1999.

REED-HILL, Robert E., **Physical Metallurgy Principles**,4th, Cengage Learning, 2009.

RONDELLI, G.; VICENTINI, B.; SIVIERI, E., Stress corrosion cracking of stainless steels in high temperature caustic solutions, **Corrosion Science**, v. 39, n. 6, p. 1037–1049, 1997.

RUSSEL, E. Hodges, Near-infrared spectroscopy for on-line analysis of white and green liquors, **Tappi Journal**, v. 82, n. 9, p. 101–106, 1999.

RUSSEL, S.; LUNDIN, C.; **The development of Qualification Standards for Cast Duplex Stainless Steel**. Material Science and Engineering.The University of Tennessee. v. 2 (2005).

SAHU, J K et al, Effect of 475 ºC embrittlement on the mechanical properties of duplex stainless steel, v. 508, p. 1–14, 2009.

SASTRI, V. S.; GHALI, Edward; ELBOUJDAINI, Mimoun. **Corrosion Prevention and Protection: Practical Solutions**. Canada: John Wiley & Sons, 2012.

SCHWEITZER, P. A. **Fundamentals of Metallic Corrosion Atmosferic and Media Corrosion of Metals**. 2nd. ed. [s.l.]: CRC Press Taylor & Francis Group, 2006.

SENATORE, Marcelo; FINZETTO, Leandro; PEREA, Eduardo. Ligas Inoxidáveis Estudo comparativo entre os aços inoxidáveis dúplex e os inoxidáveis AISI. **Rem: Revista Escola de Minas**, v. 60, n. 1, p. 175–181, 2007.

TALBOT, D.; TALBOT, J., **CORROSSION SCIENCE and TECHNOLOGY**, [s.l.]: CRC Press Materials Science and Technology, 1998.

TUOMI, A.; LOFSTRAND, A.; HARJU, M.; **Increased usage of duplex materials in manufacturing of pulping equipment.**Duplex America 2000 Conference.p. 401-408 (2000).

TUTHILL, H. A., **Stainless Steels and Specialty Alloys for Modern Pulp and Paper Mills**, The Nickel Development Institute Reference Book Series, n. 11, p. 1–22, 2002.

SAHU, J.K.; KRUPP, U.; GHOSH, R.N.; CHRIST, H.J.; **Effect of 475 ◦C embrittlement on the mechanical properties of duplex stainless steel**. Materials Science and Engineering A. v.508, p. 1–14 (2009).

SASTRI, V. S.; GHALI, Edward; ELBOUJDAINI, Mimoun, **Corrosion Prevention and Protection: Practical Solutions**, Canada: John Wiley & Sons, 2012.

SENATORE, Marcelo; FINZETTO, Leandro; PEREA, Eduardo, Ligas Inoxidáveis Estudo comparativo entre os aços inoxidáveis dúplex e os inoxidáveis AISI, **Rem: Revista Escola de Minas**, v. 60, n. 1, p. 175–181, 2007.

SCHULZ, Z.; WHITCRAFT, P.; **Availability and Economics of Using Duplex Stainless Steels**, Corrosion 2014, n. 4345, p. 1–10 (2014).

SCHWEITZER, P. A., **Fundamentals of Metallic Corrosion Atmosferic and Media Corrosion of Metals**, 2nd. ed. [s.l.]: CRC Press Taylor & Francis Group, 2006.

SHEFFIELD, A.; RUNG, B.; **Digesters and Pulp Storage Towers of Duplex Stainless Steels-Saving Weight and Costs.**TAPPI Engineering Conference (1993).

SINGH, P.; **Effect of wood species on corrosion behavior of carbon steel and stainless steels in black liquors.**Corrosion Science.v.49, p. 497-509 (2007).

SOPOUŠEK, J.; KRUML, T., Sigma-phase equilibria and nucleation in Fe-Cr-Ni alloys at high temperature, **Scripta Materialia**, v. 35, n. 6, p. 689–693, 1996.

WANG, Y.; SINGH, P., Corrosion Behavior of Austenitic and Duplex Stainless Steels in Thiosulfate and Chloride Containing Environments, **Corrosion Science**, v. 71, n. 8, p. 1–8, 2015.

WENSLEY, Angela, Corrosion Protection of Kraft Digesters, **Corrosion 2001**, n. 1423, 2001.

WENSLEY, Angela, **Experience With Duplex Stainless Steel Kraft Digesters**, Corrosion, N. 04249, P. 1–16, 2004.

WENSLEY, Angela, **Corrosion in Alkaline Pulping Liquors**, *in*: NACE, New Orleans, LA:, 2004, p. 1–13.

WENSLEY, Angela, **Corrosion And Cracking Of Bottom Scrapers In Continuous Digesters**, National Association of Corrosion Engineers, n. 5199, p. 1–26, 2005.

WESTIN, Elin M, **Microstructure and properties of welds in the lean duplex stainless steel LDX 2101** ®, Royal Institute of Technology, 2010.

YONEKUBO, A. E.; **Caracterização microestrutural do aço inoxidável superdúplex UNS S32520 (UR 52N+) processado por moagem de alta energia**. Dissertação.Universidade Estadual De Ponta Grossa (2010).

ZHENG, Z.J.; GAO, Y.; GUI, Y.; ZHU, M.; **Studying the fine microstructure of the passive film on nanocrystalline 304 stainless steel by EIS, XPS, and AFM.** Journal Solid State Electrochemical.v. 18, p. 2201-2210 (2014).

4 RIETVELD AND IMPEDANCE ANALYSIS OF COLD AND HOT ROLLED DUPLEX AND LEAN DUPLEX STEELS FOR APPLICATION IN PAPER AND PULP INDUSTRY

Luiza Esteves[a*], Paulo R. P. Paiva[b], Adolfo K. N. Viana[c], Vanessa F.C. Lins[a]

Affiliation

[a] Federal University of Minas Gerais, Chemical Engineering, Antônio Carlos Avenue 6627, Brazil, Zip Code 13565-905 Phone Number +553134091781 luizaeq@yahoo.com.br, vlins@deq.ufmg.br

b Federal Center of Technological Education of Minas Gerais (CEFET) Av. Amazonas, 5855 Zip Code 30510-000 paulorenato.paiva@gmail.com

[c] Aperam South America Praça 1º de Maio, 9 Centro , Timóteo, MG Zip Code 35180-018 adolfo.viana@aperam.com

ABSTRACT

In this study, X-Ray Diffraction (XRD) and Rietveld Refinement were performed to identify and quantify the ferrite and austenite phase of cold and hot rolled duplex stainless steels (UNS S31803) and lean duplex stainless steels (UNS S32304). Electrochemical impedance spectroscopy (EIS) was applied to evaluate the chemical behavior of duplex and lean duplex stainless steels in white, green, and black liquors of paper and pulp industry. Rietveld analysis results showed a higher austenite content than the standard limit for duplex steels in the hot rolled condition. The hot rolling condition plays a major role in improving corrosion resistance in white liquor mainly for the lean duplex steel.

Keywords: Duplex stainless steels; Rietveld Refinement; Electrochemical impedance spectroscopy; Pulp and paper industry

DOI: http://dx.doi.org/10.1590/1980-5373-MR-2016-0234

4.1 Introduction

Duplex stainless steels (DSSs) presents a mixed microstructure of about equal proportions of γ-austenite (face-centered cubic, FCC) and α-ferrite (body-centered cubic, BCC)[1], and have existed for more than 70 years. DSSs can be readily hot rolled or cold-rolled. The microstructure depends on the chemical composition of the alloy and thermomechanical treatment[2]. The alloy elements can act as ferrite stabilizers (chromium, silicon, molybdenum, titanium and niobium) or austenite stabilizers (nickel, carbon, copper, nitrogen and manganese)[3]. Hence, the chemical composition of austenite and ferrite are different, resulting in different corrosion resistance in a given environment[4]. Phase fractions and phase chemical compositions associated to the pitting resistance equivalent number (PREN=wt.%Cr+ 3.3 wt.%Mo+ 16 wt.%N)[4] of DSSs are affected significantly by solution-treatment parameters (temperature and time)[4,5]. Tan *et al.*[4] reported that the pitting corrosion resistance of a super duplex stainless steel was determined by the pitting resistance equivalent number of weaker phase. On the other hand, improper heat treatment temperature can result in deleterious secondary phases[4]. Also, DSSs, plastic deformation may induce austenite to martensite transformation[6,7].

The optimal phase balance in order to improve mechanical properties and corrosion resistance can be a range between 45% and 60% austenite. The microstructure is obtained by simultaneous control of the chemical composition and thermomechanical history (manufacturing process)[8,9].

The Rietveld method together with conventional X-ray diffraction (XRD) techniques was used to quantify the microstructural formation such as austenite; ferrite and sigma-phase in the cast super duplex steel after having been submitted to a series of heat-treated weldments[10]. The Rietveld method is a technique for refinement of crystal structures that uses data from X-ray or neutron diffraction[11]. This method is based on a mathematical fit for a real standard (experimental data) with a calculated standard (theoretical model) by minimizing the difference between measured and calculated points, through the method of least squares. The calculated standard is obtained from crystallographic databases such as Inorganic Crystal Structure Database (ICSD), Linus Pauling File (LPF), NIST Atomic Spectra Database, and Cambridge Structural Database (CSD). These databases provide the symmetry of the space group, atomic positions, occupation positions, and network parameters. To

implement the method, XRD data are used exactly as obtained using the diffractometer, without any treatment[11,12].

A major advantage of this method of quantification is that it uses all the points of an XRD spectrum and considers overlapping peaks, which usually make other methods of XRD quantification unfeasible. The parameters related to the diffractogram scanned data, which vary and are calculated during refinement, are as follows: scale factor, baseline (background), peak profile, cell parameters, structure factor, displacement and preferred orientation[11].

In the pulp and paper industry, carbon steel pulp mill equipment such as digesters and storage vessels have shown general corrosion and stress corrosion cracking. The duplex stainless steels have a higher corrosion and stress corrosion cracking resistance in high pH environments at severe conditions of pressure and temperature in relation to carbon steel and austenitic stainless steel. Therefore, digesters and storage vessels are being replaced by duplex stainless steels[13]. The lean duplex steel is a cheaper alternative to duplex steels due to the lower contents of nickel and molybdenum[14].

The Kraft process used in the paper and pulp industry is divided into three steps: firstly, the decomposition of the wood is performed by using active cooking chemicals (white liquor) constituted by sodium hydroxide and sodium sulfide[15]. Secondly, the black liquors consisting of residual inorganic chemicals such as sodium sulfide, sulfate, sodium thiosulfate, sodium carbonate, and sodium hydroxide, and organic extractives in wood are formed due to the fragmentation reactions of lignin[16]. Lastly, there is a chemical recovery by combustion of strong black liquor which converts the recovered inorganic chemicals in melting which is dissolved in water, and the green liquor (sodium carbonate (Na_2CO_3) and sodium sulfide (Na_2S))[17] are produced. Furthermore, the white liquor is the most aggressive of pulping liquors[18].

The application of the Rietveld method of quantitative analysis for UNS S31803 and UNS S32304 is not found in the literature. This study has also investigated the influence of microstructure of cold and hot rolled duplex steels on electrochemical properties of duplex and lean duplex steels in white, green, and black liquors from Pine and southern hardwood mix of an American pulp and paper industry.

4.2 Materials and Methods

4.2.1 Material and Sample Preparation

The duplex stainless steels, designated by Unified Numbering System (UNS) are UNS 31803 and UNS S32304 (lean Duplex), were supplied by APERAM South America (Brazil) in hot-rolled and cold-rolled conditions. The steels were examined as-received: hot rolled coils, annealed at 1075 ± 25°C with 4 mm of thickness and cold rolled coils, annealed at 1070 ± 25 °C, with a thickness of 1.8 mm. The steel sheets were cut in dimensions of 1 cm x 1 cm and the lengths were maintained parallel to the rolling direction. The chemical composition of these DSSs used in this work is shown in Table 4.1.

Table 4.1: Chemical composition of the DSSs investigated (wt%).

Steel	Rolling	Cr	Ni	Mo	N	C	Si	Mn	S
S31803	Cold	22.43	5.34	2.67	0.11	0.012	0.29	1.85	0.0004
S31803	Hot	22.45	5.31	2.63	0.11	0.013	0.38	1.81	0.0005
S32304	Cold	22.40	4.10	0.29	0.14	0.015	0.46	1.55	0.0002
S32304	Hot	22.87	4.20	0.27	0.15	0.011	0.20	1.45	0.0004

4.2.2 Metallographic Analysis

The samples were immersed in a modified Behara reagent, which consists of 80 mL distilled and deionized water, 20 mL of hydrochloric acid (HCl), and 1 g potassium metabisulphite ($K_2S_2O_5$); 2 g of ammonium difluoride (NH_4H HF) was added to this stock solution just before the etching[19]. The microstructure analyses were carried out using a Leitz Metalloplan optical microscope (OM).

4.2.3 X-Ray Diffraction (XRD)

XRD analyses were performed to identify the phases present in the samples, using a Shimadzu 7000 equipment under the following operating conditions: CuKα radiation (35 KV/40 mA), goniometer speed

of 0.02° per step 2θ, with counting time of 5 seconds per step and collected from 30° to 100° 2θ. Spectra interpretation was carried out by comparing standards contained in the database (PDF 02 International Centre for Diffraction Data, ICDD, 2003).

The Rietveld refinement was performed using the GSAS and interface EXPGUI program[20]. The *Thompson-Cox-Hastings pseudo-Voigt profile function* was used, and the background was adjusted by Chebyschev polynomial. Scale factor, unit cell, background radiation, profile asymmetry, the full width at half height from the instrumental broadening parameters obtained with a standard, atomic position, isotropic atomic displacements, and cations occupational factors were refined. The values for R_p (profile factor), R_{Bragg} (Bragg's index), R_{wp} (weighed profile factor), χ^2 and the graphs obtained at every 3 cycles of refinement were measured to check the quality of refinement and to better monitoring the results.

4.2.4 Electrochemical Analysis

Electrochemical impedance spectroscopy (EIS) was performed using a Gamry potentiostat. A three-electrode electrochemical cell was used with a saturated calomel electrode (SCE) as the reference with Luggin capillary and platinum (Pt) wire as a counter electrode, and the duplex stainless steel as the working electrode. The open circuit potential measurements were performed for 1 h or until to obtain a stable open circuit potential value. The amplitude sine-wave of the applied potential is 10 mV from 100 kHz to 5 mHz with 7 points per decade. The measurements were performed in triplicate to ensure the reproducibility. The experimental impedance spectra were fitted using Z-View software version 3.4d. The electrochemical tests were performed in white, green and black liquors, supplied by Mead Westvaco Corporation - MWV. Parameters were white liquor (WL): 88 g/L effective alkali (EA) as Na_2O, green liquor (GL): 117 g/L total titratable alkali (TTA) as Na_2O and weak black liquor (BL): 15% solids. These electrolytes, such as BL, were originated by southern hardwood mix and GL and WL were originated by Pine mix and hardwood mix.

4.3 Results and Discussion

4.3.1 Microstructure Characterization

Figure 4.1 shows typical microstructures found in as-received duplex stainless (a) UNS 31803 steel cold rolled, (b) UNS 31803 steel hot rolled. Figure 4.2 shows (a) 2304 steel cold rolled and (b) 2304 steel hot rolled, respectively, containing only austenite (lighter) and ferrite phases (dark). Furthermore, secondary phases, such as sigma and chi were not observed. The phases observed are elongated in the rolling direction as reported in literature[21].

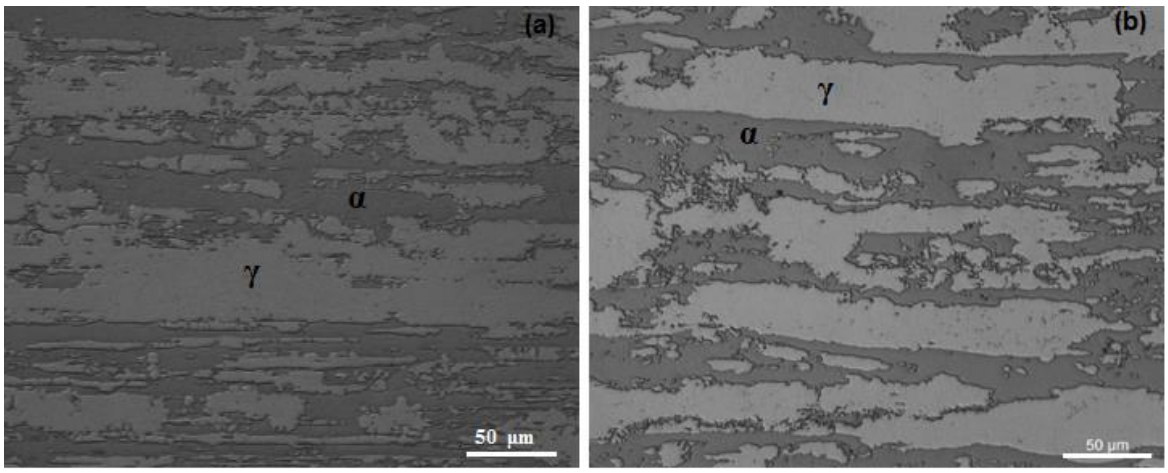

Figure 4.1: Typical microstructures found in the (a) UNS 31803 cold and (b) UNS 31803 hot rolling containing only austenite (clear) and ferrite (dark). Modified Behara Etching.

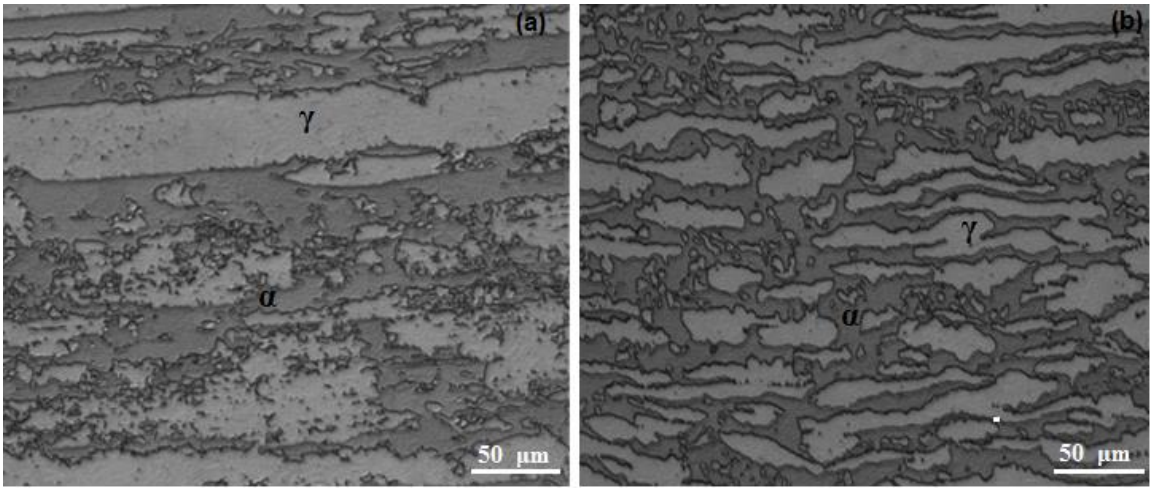

Figure 4.2: Typical microstructures found in the (a) 2304 cold and (b) 2304 hot rolling containing only austenite (clear) and ferrite (dark). Modified Behara Etching.

4.3.2 Quantitative XRD analysis

Austenite and ferrite phases were identified in duplex and lean duplex steels, and secondary phases such as sigma (σ) or chi (χ) phase were not observed in the steel microstructure. Visual evaluation of the graphic setting for both observed and calculated diffractograms is extremely important in assessing quality of refinement as shown in Figures 4.3 and 4.4. For refinement to be considered accurate, the line representing the calculated diffractogram should overlap the line that represents the observed diffractogram, and the difference line should be equal to a straight line[22]. Quality of the Rietveld refinement is verified through statistical numerical parameters (indicators) which are used during and after refinement in order to verify if it is occurring satisfactorily[12]. The most commonly used statistical parameters for the GSAS program are R_p (profile factor), R_{wp} weighed profile factor), $R_{Bragg's}$ (Bragg's index: this index compares the peaks' integrated intensities) and $\chi 2$ (Goodness of Fit = GOF = S).

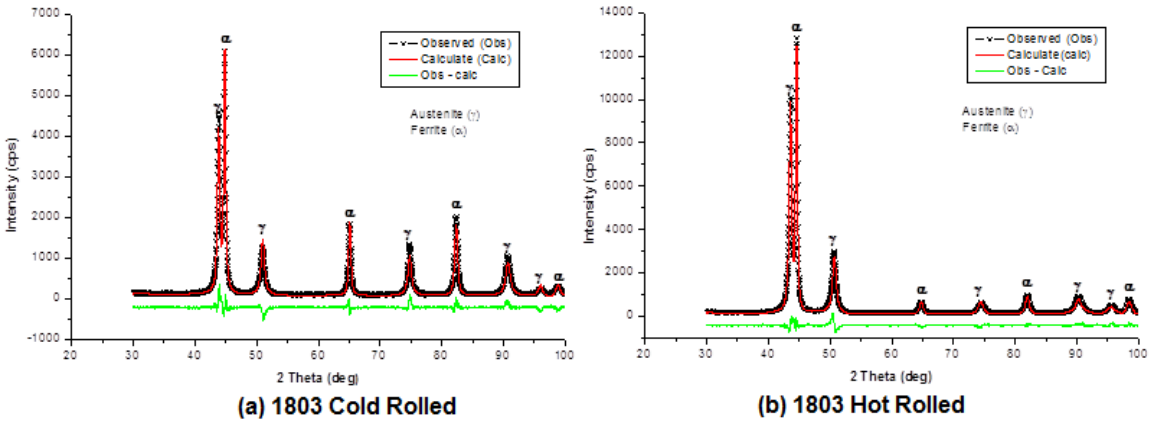

Figure 4.3: Observed (pluses) and calculated (line) diffraction pattern for the (a) UNS 31803 Cold and (b) UNS 31803 Hot rolling. The lower curve shows the difference between observed and calculated patterns.

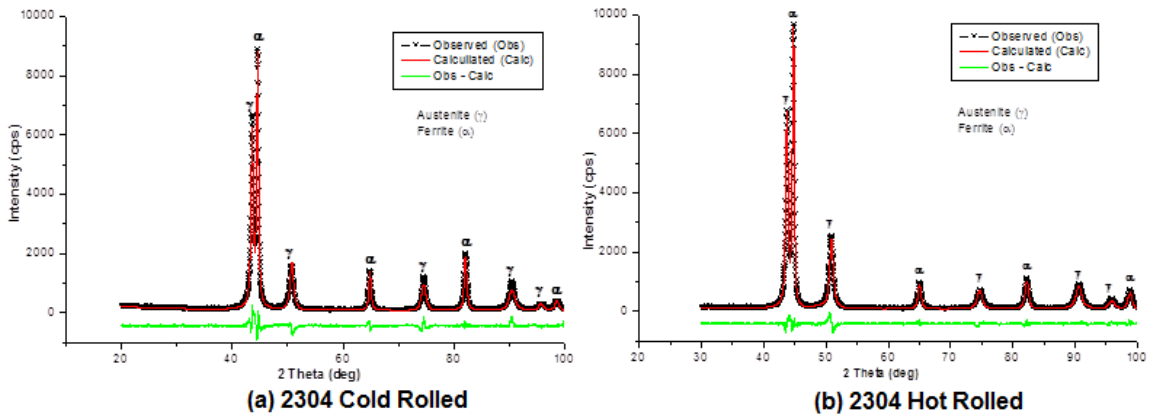

Figure 4.4: Observed (pluses) and calculated (line) diffraction pattern for the (a) 2304 cold and (b) 2304 hot rolling. The lower curve shows the difference between observed and calculated patterns.

The χ^2 parameter values found for the UNS 31803 cold and hot rolled steels and the lean duplex cold and hot rolled steels were 3.5%, 3.4%, 3.6% and 2.4%, respectively (Table 4.2). The χ^2 parameter value should be equivalent to 1.0% in a perfect refinement. In practice, values below 5.0% refer to an optimized refinement[22]. The $R_{Bragg's}$, R_p and R_{wp} (Table 4.2) for the samples are somewhat higher than those normally obtained for refinement of simple phases[12]. This mismatch is due to the displacement of 2θ and peaks'symmetry[23].

Table 4.2: Rietveld quantitative analysis results for DSSs samples.

	Weight percent		**R_{Braag}**	**R_{wp}**	**R_p**	**χ_2**
	Austenite (γ)	**Ferrite (α)**				
S31803 Cold	49.9	50.1	5.9%	8.7%	8.7%	3.5%
S31803 Hot	62.7	37.3	3.0%	9.3%	6.1%	3.4%
S32304 Cold	54.3	45.7	4.0%	10.7%	8.2%	3.6%
S32304 Hot	57.2	42.8	2.1%	8.6%	6.3%	2.4%

According to the XRD results shown in Table 4.2, the hot rolled steels exhibited a higher difference between the austenite and ferrite content. Consequently, amounts of ferrite and austenite formed during hot working or annealing are dependent on temperature. Thus, the hot working temperature must be controlled to obtain the balance between the phases in the duplex stainless steel[24]. The hot rolled duplex stainless steel showed a high content of austenite than the standard limit for duplex steels, which can be associated with a limitation of Rietveld refinement, because this technique is usually applied for powder diffraction data[23]. Data collection might have promoted errors to justify the higher content of austenite than the standard limit of concentration. In the other hand, Table 4.3 shows the contents of austenite and ferrite obtained using a conventional technique, the Image pro software by an optical microscope. In summary, the conventional method after etching with a modified Behara reagent was more reliable to quantify the content of austenite in duplex stainless steels. The main weakness of the Rietveld refinement is that it is usually performed for powder measurements and strengths of this technique are the lower time for analysis than the image analysis and the possibility of phase quantification if the lattice parameters are well defined and the diffraction peaks are not overlapping.

Table 4.3: Austenite and ferrite contents obtained using Image pro software.

Samples	Weight percent	
	Austenite (γ)	**Ferrite (Fe-α)**
UNS S31803 Cold Rolled	48	52
UNS S31803 Hot Rolled	50	50
UNS S32304 Cold Rolled	47	53
UNS S32304 Hot Rolled	46	54

4.3.3 Electrochemical Measurements

Figures 4.5, 4.6 and 4.7 show the (a) Nyquist and (b) Bode diagrams of cold and hot rolled duplex stainless steels in white, green, and black liquors. Electrochemical impedance spectroscopy was used to evaluate the polarization resistance (Rp) of steels in liquors of pulp and paper industry. The EIS spectra were fitted using a simplified Randles circuit as an equivalent electrical circuit (EEC), which consisted of an electrolyte resistance (Re) in series with a parallel combination of a constant phase

element and a polarization resistance as shown in Figure 4.8. Furthermore, Bode diagrams (Figures 4.5b, 4.6b, and 4.7b) suggest the presence of one time constant. A second maximum identified in Bode curves of hot rolled UNS 31803 steel in white and green liquors occurred at higher frequencies above 10^4 Hz and was not associated with a corrosive process. Constant phase elements (CPE) are used to describe the frequency dependence of non-ideal capacitive behavior (Table 4.4). The dimension of CPE is s^n/Ω, while that of an ideal capacitor (C) is s/Ω. When n is equal to 1, a CPE simplifies to a capacitor; when n equals 0 a CPE represents a pure resistor[25]. Low χ^2 values were considered. The average of polarization resistance between the measurements in each solution is shown in Figure 4.9.

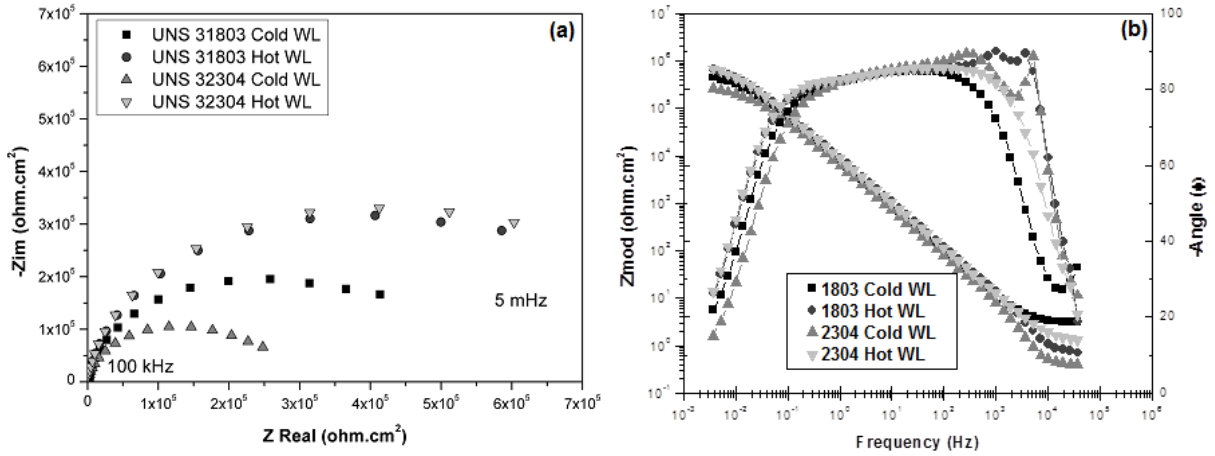

Figure 4.5: (a) Nyquist plot, (b) Bode plot of impedance spectra of UNS 31803 Cold, UNS 31803 Hot, 2304 Cold, and 2304 Hot rolling in white liquor.

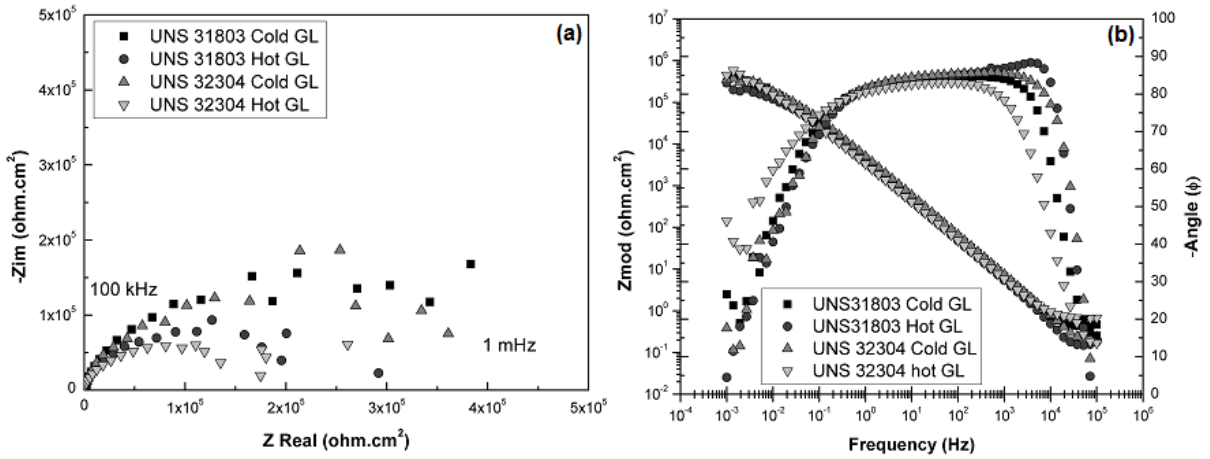

Figure 4.6: (a) Nyquist plot, (b) Bode plot of impedance spectra of UNS 31803 Cold, 1803 Hot, 2304 Cold, and 2304 Hot rolling in green liquor.

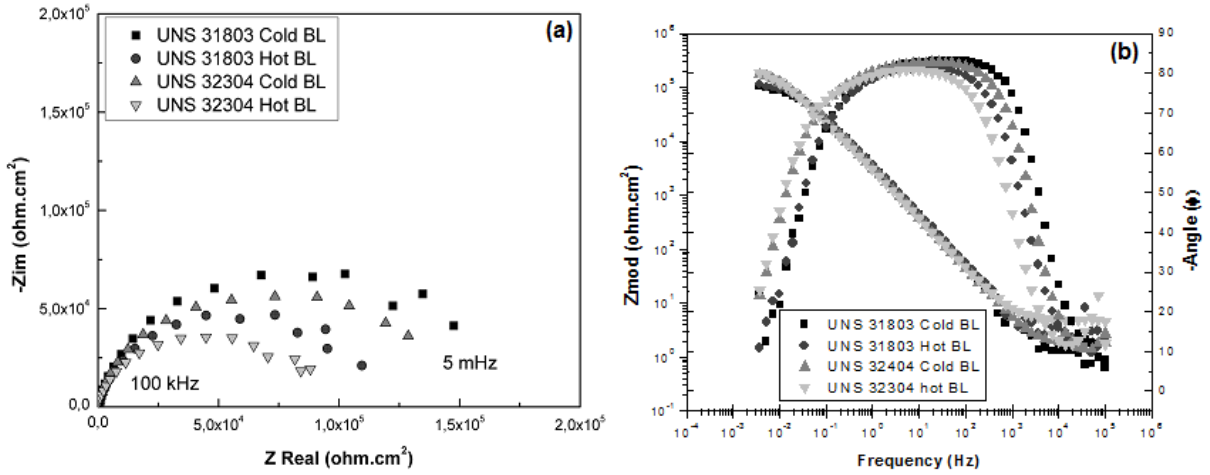

Figure 4.7: (a) Nyquist plot, (b) Bode plot of impedance spectra of UNS 31803 Cold, UNS 31803 Hot, 2304 Cold, and 2304 Hot rolling in black liquor.

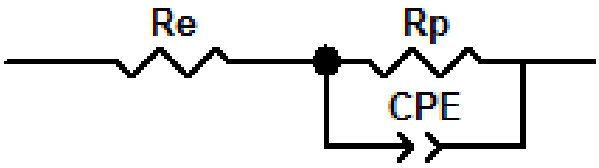

Figure 4.8: Electrical equivalent circuit (EEC) used for EIS experimental data fitting for the DSS 1803 and the DSS 2304 in pulp mill liquor.

Table 4.4: Fitting results EIS Experimental Data in green liquor (GL), white liquor (WL), and black liquor (BL).

DSS	OCP (mV_{SCE})	SD (mV_{SCE})	CPE ($F.s^n.cm^{-2}$)	n
31803 Cold Rolled GL	-701.4	13.5	$5.93x10^{-5}$	0.93
31803 Hot Rolled GL	-714.9	46.3	$6.79\ x10^{-5}$	0.91
32304 Cold Rolled GL	-727.0	16.3	$4.89\ x10^{-5}$	0.93
32304 Hot Rolled GL	-693.0	27.9	$6.73\ x10^{-5}$	0.92
31803 Cold Rolled WL	-345.0	27.6	$2.53\ x10^{-5}$	0.95
31803 Hot Rolled WL	-339.4	8.3	$2.18\ x10^{-5}$	0.95
2304 Cold Rolled WL	-345.0	23.6	$2.76\ x10^{-5}$	0.95
2304 Hot Rolled WL	-338.6	7.7	$2.68\ x10^{-5}$	0.94
31803 Cold Rolled BL	-673.2	21.7	$5.77\ x10^{-5}$	0.93
31803 Hot Rolled BL	-678.1	19.5	$4.52\ x10^{-5}$	0.90
32304 Cold Rolled BL	-675.2	19.5	$6.41\ x10^{-5}$	0.92
32304 Hot Rolled BL	-658.2	50.9	$6.18\ x10^{-5}$	0.91

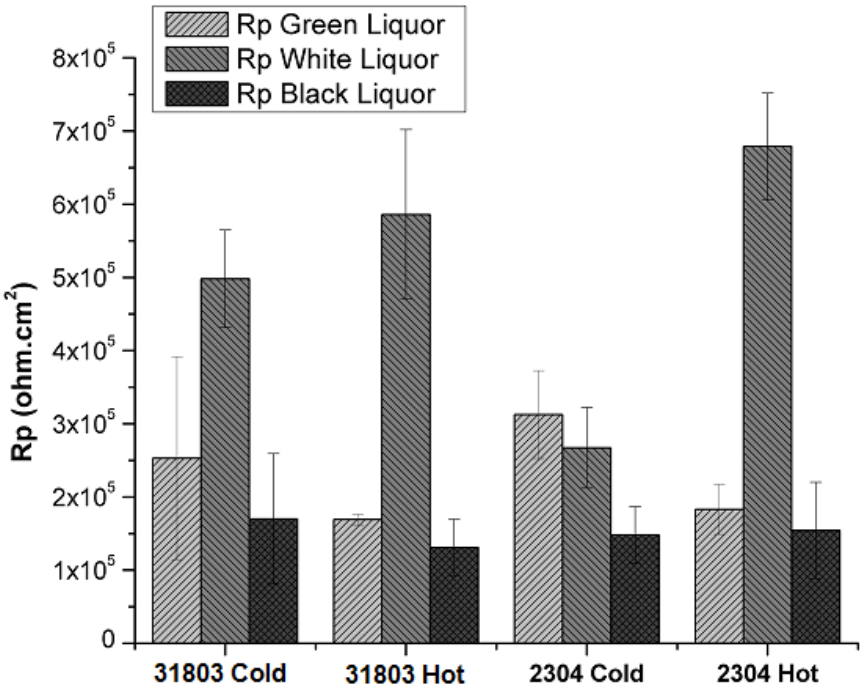

Figure 4.9: Experimental data for UNS 31803 Cold, UNS 31803 Hot, UNS 32304 Cold, UNS 32304 Hot in green liquor, white liquor, and black liquor.

Furthermore, the steels in black liquor showed a similar electrochemical behavior and exhibited the lowest polarization resistance compared to other environments. This effect could be associated with the presence of solid particles in black liquor which contains 15% of solids and, during the test, the

solid particles can deposit on the steel surface generating regions of different potentials, and creating anodic and cathodic areas (and electrochemical cells). The deposition of solids on the steel surface should generate aeration cells where the region under the deposit is the anodic region (lower oxygen concentration). The solid particles deposited on the steel surface also can act as a cathodic region, reducing the active area and enhancing corrosion of steel. In addition, an industrial solution was used with a heterogeneous composition dependent of the type of wood and process conditions, which contributes to the variability during the measurements. Literature reports that the organic compounds in black liquor can act as steel corrosion inhibitors[16]. However, in this work, in the black liquor, the steels showed the lowest values of corrosion potential and polarization resistance.

The medium of green liquor contains sodium sulfide and sodium carbonate, which precipitated on the steel surface. The carbonate deposits generated aeration electrochemical cells and potential gradients on the steel surface. The surface area under the carbonate can act as an anodic region due to the lowest oxygen concentration. The carbonate precipitation can also reduce the anodic region on the steel surface and acts as a cathodic region where the cathodic reaction occurs. This condition contributes to enhance the corrosion of steels. The values of polarization resistance of steels in green liquor were similar and higher than in black liquor but lower than in white liquor. In summary, particles in solution that allowed deposition on the surface of the working electrode showed more influence on the polarization resistance than microstructure of duplex.

The hot rolled steels showed a higher corrosion resistance in white liquor than the cold rolled steels. The cold rolled steel presented a more heterogeneous surface with elongated phases[26] (Figures 5.1 and 5.2), and a higher dislocation concentration generating several active sites to process corrosion. In white liquor, the standard duplex steels, which showed the highest PREN number and highest contents of nickel and molybdenum, showed a higher corrosion resistance than the lean duplex steels[8] for cold working. However, the effect of molybdenum in caustic environments is not significant to improve the corrosion resistance of duplex steels[18]. The hot rolling condition plays a major role in improving corrosion resistance in white liquor mainly for the lean duplex steel. The microstructure containing lower dislocation concentration contributes to enhance corrosion resistance of hot-rolled steels in relation to the cold rolled condition.

The medium of white liquor was the less aggressive medium for both steels. In medium of white liquor, no precipitation of solids or compounds occurred on the steel surface. The white liquor contains sodium hydroxide, which is beneficial to steel passivation, but contains sodium sulfide, which is detrimental on the passivation behavior[18].

4.4 Conclusions

Rietveld analysis was not efficient to determine the amount of austenite and ferrite in duplex and lean duplex steels and the influence of the rolling condition on the phase contents was identified.

The medium of white liquor was the less aggressive medium for both steels. The hot rolling condition plays a major role in improving corrosion resistance in white liquor mainly for the lean duplex steel.

The steels showed the lowest values of corrosion potential and polarization resistance in black liquor. Depositions of solids and carbonates on the steel surface in black and green liquors, respectively, contributed to reduce the corrosion resistance of duplex and lean duplex steels.

Acknowledgements

The authors are grateful to the Brazilian government agencies — CNPq, CAPES, and FAPEMIG.

4.5 References

1 Lai JKL, Shek CH, Lo KH. Stainless Steels: An Introduction and Their Recent Developments. Bentham Science Publishers. (2012).

2 Silva RV, Casteletti LC. Effect of Niobium in the Phase Transformation and Corrosion Resistance of One Austenitic-ferritic Stainless Steel 2 . Experimental Procedures, Mater. Res. 17 (2014) 801–806. doi:http://dx.doi.org/10.1590/1516-1439.190113 ©.

3 Michalska J, Sozańska M. Qualitative and quantitative analysis of σ and χ phases in 2205 duplex stainless steel, Mater. Charact. 56 (2006) 355–362. doi:10.1016/j.matchar.2005.11.003.

4 Tan H, Jiang Y, Deng B, Sun T, Xu J, Li J. Effect of annealing temperature on the pitting corrosion resistance of super duplex stainless steel UNS S32750, Mater. Charact. 60 (2009) 1049–1054. doi:10.1016/j.matchar.2009.04.009.

5 Lo KH, Lai JKL, Shek CH, Li DJ. Effects of pre-treatment on the ac magnetic susceptibility and ageing behaviour of duplex stainless steels, Mater. Sci. Eng. A. 452–453 (2007) 78–86. doi:10.1016/j.msea.2006.10.120.

6 Tavares SSM, Pardal JM, Silva MR, de Oliveira CAS. Martensitic Transformation Induced by Cold Deformation of Lean Duplex Stainless Steel UNS S32304, Materials Research. 17 (2014) 381–385.

7 Tavares SSM, Silva MR , JM Pardal, HFG Abreu, AM Gomes. Influence of microstructure on the corrosion resistance of the duplex stainless steel UNS S31803, Mater. Charact. 59 (2008) 1127–1132. doi:10.1016/j.matchar.2007.09.002.

8 Gunn RN. Duplex Stainless Steel: Microstructure, properties amd applications, Abington Publishing, 1997.

9 Jones RH. Environmental effects on engineered materials, marcel Dekker, Richlland, Washington, 2001. doi:10.1201/9780203908129.

10 Garin JL, Mannheim RL. Rietveld Quantitative Analysis Of Super Duplex Stainless Steel, JCPDS. (2012) 98–105.

11 Rietveld HM. A profile refinement method for nuclear and magnetic structures, J. Appl. Crystallogr. 2 (1969) 65–71. doi:10.1107/S0021889869006558.

12 Young RA. *The Rietveld Method*, (1993). Oxford University Press: Atlanta.

13 Bhattacharya A, Singh PM. Stress corrosion cracking of welded 2205 duplex stainless steel in sulfide-containing caustic solution, J. Fail. Anal. Prev. 7 (2007) 371–377. doi:10.1007/s11668-007-9069-6.

14 Westin, EM, Microstructure and properties of welds in the lean duplex stainless steel LDX 2101. PhD Thesis, Royal Institute of Technology, 2010.

15 Bajpai P. *Biotechnology for Pulp and Paper Processing*, (2012) 7–15. Springer: Boston, MA. doi:10.1007/978-1-4614-1409-4.

16 Singh PM, Anaya A. Effect of wood species on corrosion behavior of carbon steel and stainless steels in black liquors, Corrosion Science. 49 (2007) 497–509. doi:10.1016/j.corsci.2006.04.020.

17 Bajpai P. *Chemical Recovery in Pulp and Papermaking*, (2008). Pira International Ltd: Surrey, UK.

18 Bhattacharya A, Singh PM. Electrochemical behaviour of duplex stainless steels in caustic environment, Corros. Sci. 53 (2011) 71–81. doi:10.1016/j.corsci.2010.09.024.

19 Magnabosco R. Kinetics of Sigma Phase Formation In a Duplex Stainless Steel 2 . Experimental Procedure, Mater. Res. 12 (2009) 321–327.

20 Toby BH. EXPGUI , a graphical user interface for GSAS EXPGUI , a graphical user interface for GSAS, (2001) 210–213.

21 Revie HH, Uhlig RW. *Corrosion and Corrosion Control: An introduction to corrosion science and engineering*, 4th ed., John Wiley & Sons, New Jersey, USA. (2008). doi:10.1179/000705972798323134.

22 Deysel K. Leucoxene Study - A Mineral Liberation Analysis (MLA) Investigation, (2007) 167–172. www.onemine.org.

23 McCusker LB, Von Dreele RB, Cox DE, Louër D, Scardi P. Rietveld refinement guidelines, J. Appl. Crystallogr. 32 (1999) 36–50. doi:10.1107/S0021889898009856.

24 Krauss G. *Steel Processing, Structure, and Performance*, 1st ed., ASM International, 2005. doi:10.1038/129356a0.

25 Hsu CH, Mansfeld F. Technical Note: Concerning the Conversion of the Constant Phase Element Parameter Y 0 into a Capacitance, Corrosion. 57 (2001) 747–748. doi:10.5006/1.3280607.

26 Jimenez, JA, Carsi M, Ruano, OA. Characterization of a δ/γ duplex stainless steel. Journal of Materials Science. v. 35, p. 907-915 (2000).

5 SCANNING KELVIN PROBE FORCE, MAGNETIC FORCE MICROSCOPY AND ELECTROCHEMICAL CHARACTERIZATION OF STANDARD AND LEAN DUPLEX STAINLESS STEEL

Luiza Esteves[a*], W. R. C. Campos[b], M. M. A. M. Schvartzman[b], Vanessa F.C. Lins[a]

Affiliation

[a] Federal University of Minas Gerais, Chemical Engineering, Antônio Carlos Avenue 6627, Brazil, Zip Code 31270-901 Phone Number +553134091781 luizaeq@yahoo.com.br

[b] Comissão Nacional de Energia Nuclear, Centro de Desenvolvimento da Tecnologia Nuclear, Antônio Carlos Avenue 6627, Brazil, Zip Code 31270-901

ABSTRACT

This work aimed at characterizing the duplex stainless steel (DSS) relating to microstructure and electrochemical behavior in industrial white liquor (WL) from a pulp and paper mill. Microstructure was analyzed using magnetic force microscopy (MFM) and scanning Kelvin probe microscopy (SKPFM). MFM/SKPFM technique showed to be a powerful tool to study the phases in DSS without surface etching. Austenite phase exhibits the highest Volta Potential. MFM was used to distinguish the phases in the DSS due to magnetic features (ferrite is ferromagnetic and austenite is paramagnetic). Difference of chemical composition of austenite and ferrite causes selective dissolution in industrial WL.

Keywords: Duplex stainless steels; SKPFM/MFM; Electrochemical impedance spectroscopy; Pulp and paper industry.

5.1 Introduction

Duplex stainless steel (DSS) is a dual phase, containing equal proportions of γ-austenite (face centered cubic - FCC) and α-ferrite (body centered cubic - BCC); have existed for more than 70 years [1, 2]. Both constituent phases contain at least about 11wt% chromium [3]. The ferrite phase has been known by a lower content of nickel and a higher content of molybdenum compared to the austenite phase [4]. In DSSs, Cr, Mo, Ni and N are not uniformly distributed between ferrite and austenite phase and this heterogeneity may lead to galvanic interactions, which may result in a difference in corrosion behavior between these phases [5].

Gheno (2008) differentiated by magnetic force microscopy (MFM) the ferromagnetic phase (ferrite) and paramagnetic phase (austenite) in annealed and aged UNS 32205 DSS and obtained images of the phase distribution in DSS without requiring the surface etching. These images were obtained using the principle of force gradient detection [6].

The Electrochemical Scanning Probe Microscopy (ECSPM) has been used to observe, *in situ* and in real time, the early stages of corrosion [7]. Scanning Probe Microscopy (SPM) techniques such as Magnetic Force Microscopy (MFM), Scanning Kelvin Probe Force Microscopy (SKPFM) and current-sensing atomic force microscopy (CSAFM) measurements were used to distinguish and identify the ferrite and austenite phases in electrochemical polished (HNO_3:H_2O = 1:1 for 20 s at 1.2 V applied voltage) DSS and in the conventional UNS 32507. The analysis is related as a result of high nickel content in austenite, which has a higher Volta potential, compared with ferrite enriched with chromium and the difference in topography heights between the phases can be attributed to the different etching rating in electrochemical polishing. This difference could be explained by the hardness difference of the two phases [8].

The furnace-cooled UNS 32205 DSS was employed to distinguish between the two phases. To analyze the microstructure, the MFM was used to study magnetic domain distribution and SKPFM was applied to evaluate the variation of Volta potential between austenite (γ) and ferrite (α). The MFM/SKPFM technique showed to be a powerful tool to study the phases in DSS without surface etching [4].

DSS 2205 in acidic chloride solutions was studied in situ by electrochemical scanning tunneling microscopy (STM) to evaluate selective dissolution of phases. The ferrite dissolution rate decreased with the distance to austenite and ferrite dissolves preferentially than austenite phase. Potentiodynamic measurement was carried out in the mild solution (0.05 M H_2SO_4 + 1 M NaCl) and in aggressive solution (4 M H_2SO_4 + 1 M HCL). In the mild solution, a wide passive region and a sharp increase in current at high anodic potentials could be explained due to localized corrosion, oxidation of Cr^{3+} in the passive film into Cr^{6+} species, oxygen evolution, or combination of these factors and the potential difference can be due a pH-dependence of the reaction [9].

The UNS S32750, UNS 32304 and UNS 32205 DSSs were characterized using SKFM and MFM, the ferrite phase was associated with regions of lower potential indicating a higher tendency to corrosion. Due to the high lateral resolution of SKFM, this technique can be compared with other localized techniques to study local corrosion process [10].

Atomic and magnetic force microscopy, AFM and MFM, were simultaneously employed to study the topographic and magnetic properties in DSS. Different tip–surface separations were studied and values up 30 nm cannot see more evidence of topography, and only magnetic domains can be visualized; also, magnetic tips coated with high coercivity and low magnetization films were employed to the characterization of the magnetic domains in the DSS samples studied, which the low magnetization tips demonstrated to be more appropriate [11].

Femenia (2002) investigated local dissolution behavior of three DSSs (UNS S32304, UNS S32205, and UNS S32750) in a solution of 1M H_2SO_4 plus 1 M NaCl by using *in situ* electrochemical scanning tunnelling microscopy (STM). The UNS S32205 has a higher content of Mo and N compared to UNS S32304, and therefore a better resistance to localized corrosion. It has as well a better resistance against general corrosion and is resistant to an aqueous solution of 1 M sulfuric acid at room temperature. The UNS S32304 showed severe local dissolution in the form of both pitting-like dissolution occurring at the active potential region, and selective dissolution of ferrite phase that already started at the corrosion potential. No pitting-like corrosion was observed on UNS 31802, but a small amount of selective dissolution occurred at anodic potentials in the active region. No local dissolution was observed on UNS S32750 surface in this solution in active and passive potential

regions. It was possible to observe multi-peaks in the active region for the UNS S32304 and analysis of UNS S32205 DSS suggests certain heterogeneity in their dissolution behavior [12].

Secondary phases in DSS were identified by magnetic force microscopy and Scanning Kelvin probe force microscope [13]. Volta potential indicated that nitride and sigma phase were more active than ferrite, while austenite showed a nobler potential [13].

In this work, standard DSS (UNS 31803) and LDSS lean (UNS 32304) DSS was studied using MFM/SKPFM to correlate the difference of Volta potential and corrosion behavior. The electrolyte used was industrial white liquors (WL) supplied by a Brazilian pulp and paper mill, aiming application of DSS in digester equipment of pulp and paper industries.

5.2 Materials and Methods

5.2.1 Material and Sample Preparation

The DSSs, designated by Unified Numbering System (UNS) are UNS S31803 and UNS S32304 (lean Duplex), were supplied by APERAM South America (Brazil) in cold-rolled conditions. The steels were examined as received: cold rolled coils, annealed at 1070 ± 25 °C, with a thickness of 1.8 mm. The chemical composition of these DSSs used in this work is shown in Table 5.1.

Table 5.1: Chemical composition of the investigated DSS ((wt. (%)).

Steel	Rolling	Cr	Ni	Mo	N	C	Si	Mn	S
31803	**Cold**	22.43	5.34	2.67	0.11	0.012	0.29	1.85	0.0004
32304	**Cold**	22.40	4.10	0.29	0.14	0.015	0.46	1.55	0.0002

5.2.2 Metallographic Analysis

The samples were immersed in a modified Behara reagent, which consists of 80 mL distilled and deionized water, 20 mL of hydrochloric acid (HCl), and 1 g potassium metabisulfite ($K_2S_2O_5$); 2 g of ammonium difluoride (NH_4H HF) was added to this stock solution just before the etching [14]. The microstructure analyses were carried out using a Leitz Metalloplan light optical microscope (LOM).

5.2.3 MFM and SKPFM measurements

SKPFM provides a map of Volta Potential ($\Delta\Psi$) with high spatial resolution [4-6, 11, 15; 16, 17] Atomic force microscope (AFM) from MFP-3D-SA Asylum Research was used; and. the tip was a nonmagnetic probe with standard silicon cantilevers (type AC240TM) with Ti/Pt (5/20) coating (2 N/m force constant). The resonant frequency of 45 - 95 kHz was employed for Volta potential ($\Delta\psi$) measurements. The MFM/SKPFM scan size was 80 x 80 μm^2. The topography of the sample surface was obtained in the first pass in tapping mode (contact mode). In the second pass, the cantilever was lifted up from the surface between 50 and 100 nm where the Volta potential was independent of the tip-sample distance. Prior to MFM measurements, the CoCr-coated cantilever was magnetized in the direction perpendicular to the DSS surface (2 N/m constant force, 40-100 kHz resonant frequency). Data analysis was performed with the software Gwyddion. Data acquisition was carried out with 512 x 512 pixel resolution.

5.2.4 Electrochemical Analysis

Electrochemical impedance spectroscopy (EIS) was performed using an Autolab PGSTAT 100 potentiostat. A three-electrode electrochemical cell was used with a saturated calomel electrode (SCE) as the reference using a salt bridge, platinum (Pt) wire as a counter electrode, and the DSS as the working electrode. The open circuit potential measurements were performed for 1 h or until stabilization. The amplitude sine-wave of the applied potential is 10 mV from 100 kHz to 5 mHz with 10 points per decade. The measurements were performed in triplicate to ensure the reproducibility. The experimental impedance spectra were fitted using Z-View software version 3.4d. The electrochemical tests were performed in white liquors supplied by a Brazilian pulp and paper mill. According to Brazilian standards to white liquor: TTA (total titratable alkali): 140 ± 10 g/L (as NaOH), EA (effective alkali): 110 ± 10 g/L (as NaOH), sulfidity: 25 ± 2%, causticizing efficiency: 82 ± 2%, total suspended solids <100 mg/L, and pH > 13. Subsequently, potentiodynamic polarization was carried out using an Autolab PGSTAT 100 N potentiostat. The polarization curves were collected by scanning to the anodic direction at 0.167 mV/s from the corrosion potential (Ecorr). Transpassivity was observed

in all cases, and the scan was until the current reached 3 mA/cm^2. All the electrochemical measurements were repeated at least three times to ensure the reproducibility.

5.3 Results and Discussion

5.3.1 Microstructure Characterization

Figure 5.1 shows typical microstructure found in the DSS as received. Lighter austenite (γ) islands are embedded in the darker etched ferrite (α). In a previous work [18], the contents of austenite and ferrite were evaluated by using image analysis and the contents of ferrite were 52% and 53%, for the cold-rolled UNS 31803 and UNS 32304. Secondary phases such as sigma (σ) or chi (χ) phases were not observed in the steel microstructure [18].

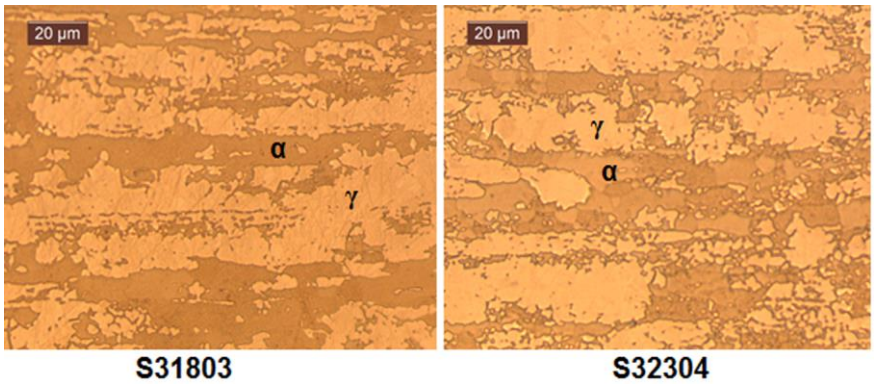

Figure 5.1: Typical microstructures of a) hot rolled UNS S31803 DSS and b) hot rolled UNS 32304, showing ferrite (darker) and austenite (lighter).

5.3.2 SKPFM/MFM

Figure 5.2 shows the Volta potential map (Fig. 5.2a), and Volta potential profile (Fig. 5.2b) for the S32304 steel. Figure 5.3 shows, for the S31803 steel, the Volta potential map (Fig. 5.3a), and Volta potential profile (Fig. 5.3b). The austenite exhibits the highest Volta Potential between austenite and ferrite phases [4, 8, 10] This difference of potential between the phases can promote galvanic interaction and also predict corrosion behavior [9, 10, 15]. Moreover, results may help to explain selective dissolution behavior of the two DSSs in caustic sulfide containing solution [9, 12].

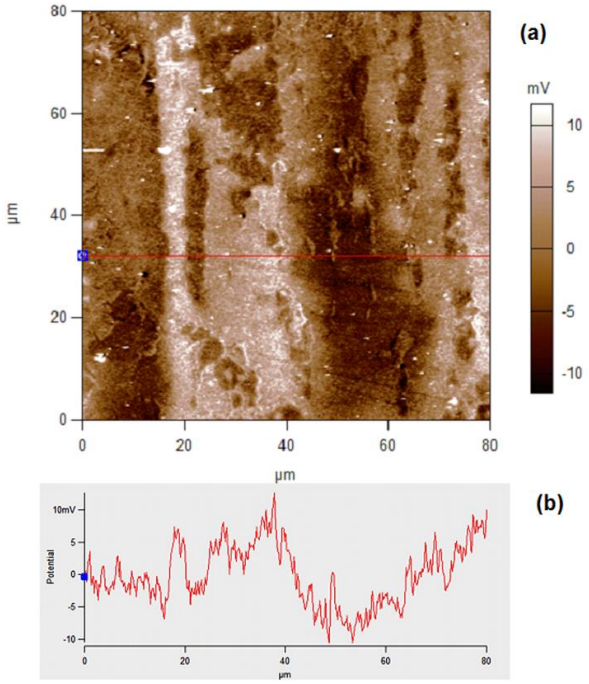

Figure 5.2: Cold rolled UNS 32304 steel, scanned area 80 x 80 µm. (a) Volta potential distribution and (b) Volta potential profile along the section marked.

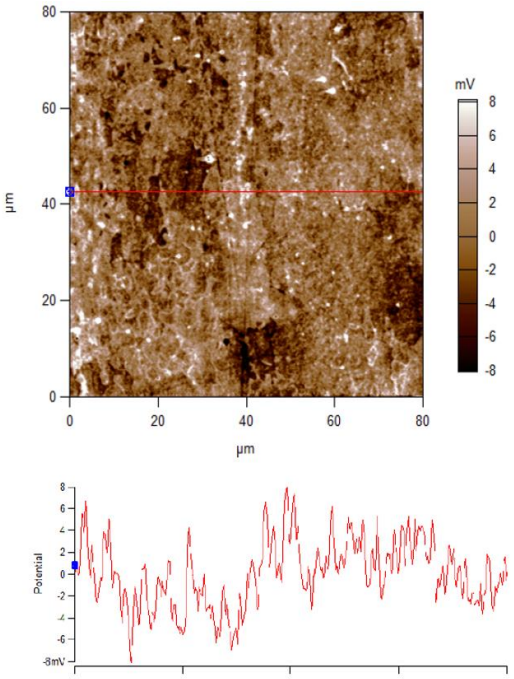

Figure 5.3: Cold rolled UNS 31803 sample, scanned area 80 x 80 µm. (a) Volta potential distribution and (b) Volta potential profile along the section marked.

Ferromagnetic ferrite shows a striped appearance due to magnetic domains, while austenite is paramagnetic showing a uniform structure (non-magnetic) as shown for the S32304 steel in Figure 5.4 and for the S31803 steel in Figure 5.5.

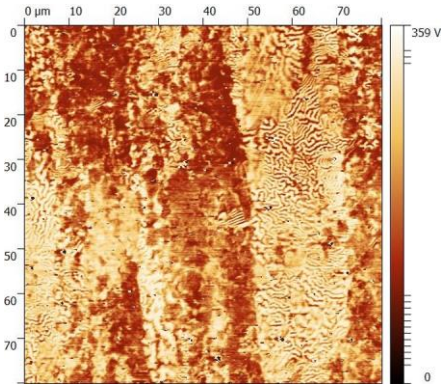

Figure 5.4: Cold rolled UNS 32304 steel, scanned area 80 x 80 µm. Magnetic domain distribution.

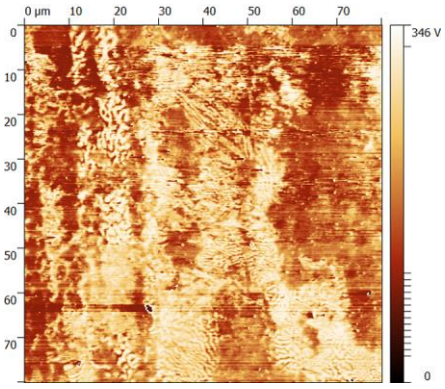

Figure 5.5: Cold rolled UNS 31803 steel, scanned area 80 x 80 µm. Magnetic domain distribution.

5.3.3 Electrochemical Measurements

The Nyquist diagrams of the two DSSs are illustrated in Figure 5.6, which presented similarly incomplete capacitive reactance arcs. In a Bode plot, log |Z| and Φ are both plotted against log ω [19]. It seems the two DSS showed similar corrosion resistance, which also was observed in Bode plots (Figure 5.7) showing equal modulus of impedance (|Z|). In this case, as a substitute of the non-ideal capacitor, constant phase element (CPE) was used to describe the deviation from actual capacitive behavior. Its impedance is expressed as:

$$Z_{CPE} = \frac{1}{Y_0 (j\omega)^{\alpha}} \quad (1)$$

Where Y_0 is the capacitance (Fs $\alpha^{-1}m^{-2}$), ω is the angular frequency (in rad/s), $j^2 = -1$ is the imaginary number and α is the CPE exponent that represents the degree of deviation from a pure capacitor. CPE magnitude is $\Omega^{-1}cm^{-2}s^{\alpha}$ and the alpha exponent, $0 < \alpha < 1$, indicates the capacitor-like nature of the CPE: $\alpha = 1$ for a perfect capacitor and $\alpha = 0$ for a perfect resistor [20].

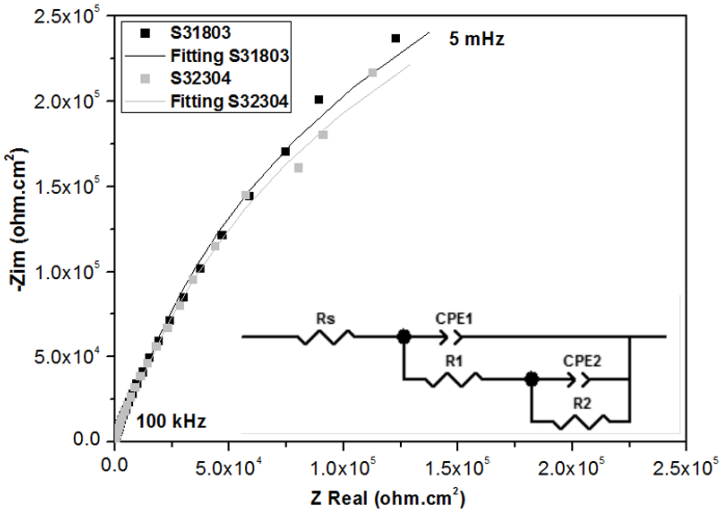

Figure 5.6: Nyquist diagram for S31803 and S32304 steels in industrial white liquor. Solid lines are the fitting results.

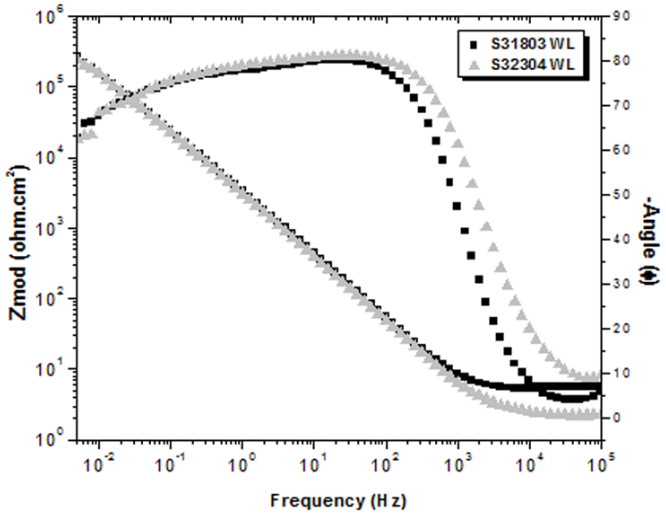

Figure 5.7: Bode plots for DSS S31803 and S32304 in industrial white liquor at room temperature.

From Bode plots, the maximum phase angles are lower than 90 degrees, indicating a deviation as mentioned before from an ideal capacitive behavior. It is well known that impedance modulus at high frequency represents the Rs. Instead, low frequency is related to the polarization resistance, which is

related to the phenomenon that occurs on the metal surface. There are two-time constants that suggest the following equivalent circuit (EC), solution resistance (R_s), porous resistance (R_1) and charger transfer (R_2) [21] for the bilayer oxide film on DSS in industrial WL. The pore electrical resistance is associated to the ionic conduction paths through the passive layer [22].

An important result is that the polarization resistance was higher for the S31803 steel than to the S32304 steel (Figure 5.8), which can be correlated with the higher content of Cr and Ni of the UNS 31803 than of the lean duplex steel (UNS 32304).

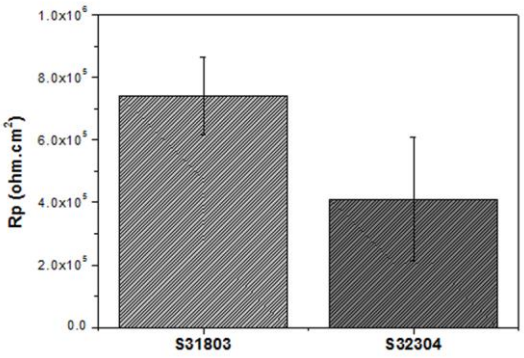

Figure 5.8: Polarization resistance (Rp) of EIS experimental data of S31803 and S32304 in industrial white liquor.

Figure 5.9 shows the polarization curves for the two duplex steel in industrial white liquor at room temperature. It was possible to observe that S31803 steel showed lower current density compared to S32304 steel, there are a wide passive region (-800 mV_{SCE} to 0 mV_{SCE}) for both steels. For the most part of the polarization curve, the electrochemical behavior between the 31803 and 32304 are very similar. However, there is a difference in the Volta Potential between ferrite and austenite phases for UNS 31803 and UNS 32304. This potential difference might result in selective corrosion on the DSS in white liquor after polarization tests (Figure 5.9), revealing the boundaries between austenite and ferrite [9, 23-26] as shown in Figure 5.10. Chromium, silicon, molybdenum, titanium and niobium are ferrite stabilizers and nickel, carbon, copper, nitrogen, and manganese are austenite stabilizers [27, 28]; this heterogeneity may cause a selective corrosion of the less noble areas, which could explain the selective etching shown in Figure 5.10. The heterogeneity in phase composition plays an important role in corrosion behavior of the DSS [12, 29-31]. The WL used in Kraft pulping process are mainly

sodium hydroxide (NaOH) and sodium sulfide (Na_2S) [32, 33], the selective corrosion can be attributed to higher concentration of caustic and sulfur species that could generate a preferential dissolution of the weaker phase. In this medium the cathodic reaction is the reduction of oxygen generating hydroxyl anions, contributing to increase the alkalinity near the steel surface. Hence, due to a highly caustic medium and the presence of S^{2-} ions [34-36], WL is considered the most aggressive among the pulping liquors [37].

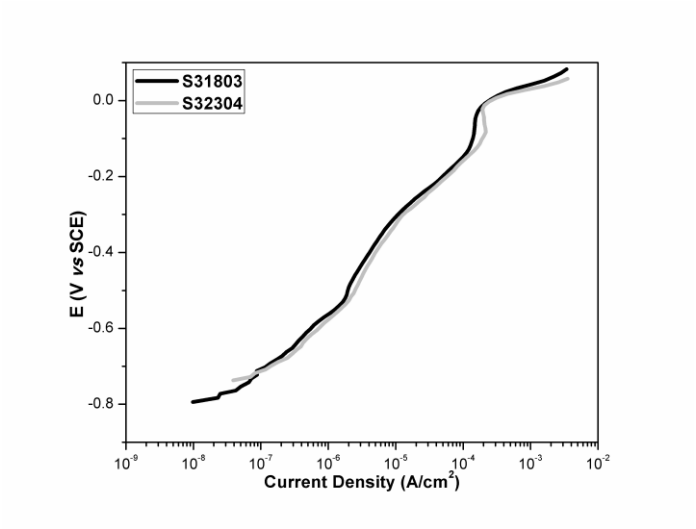

Figure 5.9: Polarization curve of S31803 DSS and S32304 LDSS in industrial white liquor at room temperature.

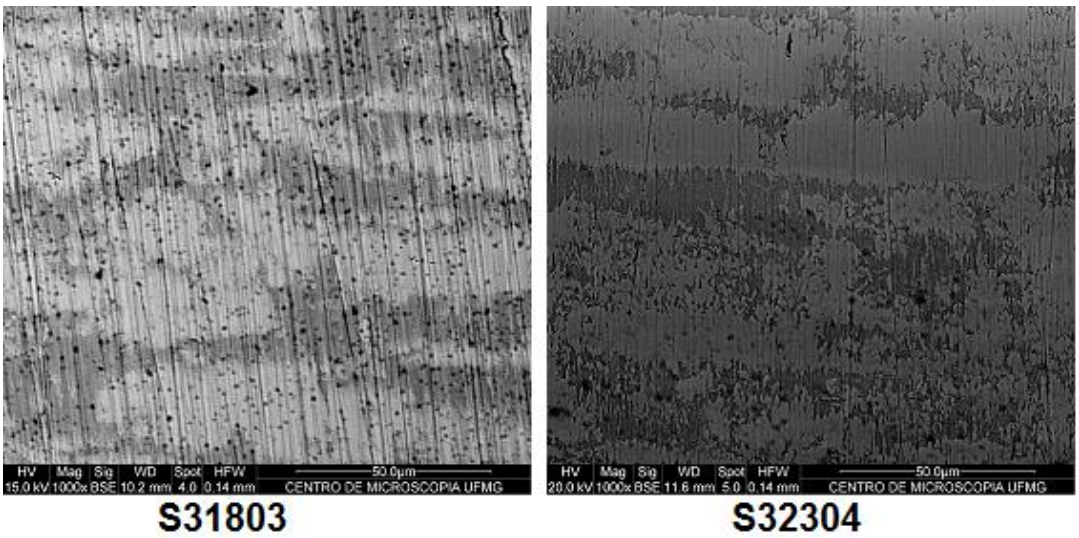

Figure 5.10: SEM micrographs of DSSs after electrochemical tests in industrial white liquor.

5.4 Conclusions

- The MFM/SKPFM technique showed to be a powerful tool to study the phases in duplex stainless steels without the need of surface etching;
- The paramagnetic austenite exhibits the highest Volta Potential between austenite and ferrite phases;
- The difference of the chemical composition of the DSS phases causes selective dissolution of less noble regions, revealing the phases, after electrochemical testing in industrial white liquor.

Acknowledgements

The authors are grateful to the Brazilian government agencies — CNPq, CAPES, and FAPEMIG. They also thank the Centro de Microscopia (UFMG).

5.5 References

[1] J. Olsson, M. Liljas. 60 years of DSS applications. In: NACE Corrosion 94 Conf, paper no. 395, Baltimore, MD, 1994.

[2] I. Alvarez-armas, Duplex Stainless Steels: Brief History and Some Recent Alloys, Recent Patents Mech. Eng. 1 (2008) 51–57. doi:10.2174/2212797610801010051.

[3] J.K.L. Lai, C.H. Shek, K.H. Lo, Stainless Steels : An Introduction and Their Recent Developments, Bentham eBooks, 2012

[4] N. Sathirachinda, R. Gubner, J. Pan, U. Kivisäkk, U. Kivisakk, Characterization of Phases in Duplex Stainless Steel by Magnetic Force Microscopy/Scanning Kelvin Probe Force Microscopy, Electrochem. Solid-State Lett. 11 (2008) C41. doi:10.1149/1.2912601.

[1] A. Bhattacharya, P.M. Singh, Electrochemical behaviour of duplex stainless steels in caustic environment, Corros. Sci. 53 (2011) 71–81. doi:10.1016/j.corsci.2010.09.024.

[2] P. Wensley, Angela; Champagne, Effect of Sulfidity on the corrosivity of white, green, and black liquors, in: Corros. 99, San Antonio, Texas, 1999: pp. 1–5.

[24] J.-O. Nilsson, Super duplex stainless steels, Mater. Sci. Technol. 8 (1992) 685–700. doi:http://dx.doi.org/10.1179/mst.1992.8.8.685.

[25] P.E. Manning, D.J. Duquette, W.F. Savage, Effect of Test Method and Surface Condition on Pitting Potential of Single and Duplex Phase 304L Stainless Steel., Corrosion. 35 (1979) 151–157.

[26] P. Hronsky, D.J. Duquette, Pitting Behavior of Duplex 308L Stainless Steel in Methanol/Water/Hci Solutions., Corrosion. 38 (1982) 63–69.

[27] R. Lai, Y. Cai, Y. Wua, F. Li, X. Hua, Influence of absorbed nitrogen on microstructure and

corrosion resistance of 2205 duplex stainless steel joint processed by fiber laser welding, J. Mater. Process. Technol. 231 (2016) 397–405. doi:10.1016/j.jmatprotec.2016.01.016.

[28] J. Michalska, B. Chmiela, Phase analysis in duplex stainless steel: comparison of EBSD and quantitative metallography methods, IOP Conf. Ser. Mater. Sci. Eng. 55 (2014) 12010. doi:10.1088/1757-899X/55/1/012010.

[29] E. Symniotis, Galvanic effects on the active dissolution of duplex stainless steels, Corrosion. 46 (1990) 2–12.

[30] C.O.A. Olsson, The influence of nitrogen and molybdenum on passive films formed on the austenoferritic stainless steel 2205 studied by AES and XPS, Corros. Sci. 37 (1995) 467–479. doi:10.1016/0010-938X(94)00148-Y.

[31] E. Symniotis, Dissolution mechanism of duplex stainless steels in the active-to-passive transition range and the role of microstructure, Corrosion. 51 (1995) 571–580.

[32] P. Bajpai, Biotechnology for Pulp and Paper Processing, Springer US, Boston, MA, 2012. doi:10.1007/978-1-4614-1409-4.

[33] P. Bajpai, Chemistry and Sustainability in Pulp and Paper Industry, Springer US, Patiala, India, 2015. doi:10.1007/978-3-319-18744-0.

[34] P. Wensley, Angela; Champagne, Effect of Sulfidity on the corrosivity of white, green, and black liquors, in: Corros. 99, San Antonio, Texas, 1999: pp. 1–5.

[35] A. Wensley, Corrosion in Alkaline Pulping Liquors, in: NACE, New Orleans, LA, 2004: pp. 1–13.

[36] D.C. Crowe, D. Tromans, High-Temperature Polarization Behavior of Carbon Steel in Alkaline Sulfide Solution., in: Corrosion, 1988: pp. 142–148.

[37] A. Bhattacharya, P.M. Singh, Electrochemical behaviour of duplex stainless steels in caustic environment, Corros. Sci. 53 (2011) 71–81. doi:10.1016/j.corsci.2010.09.024.

6 ELECTROCHEMICAL BEHAVIOR OF DUPLEX STAINLESS STEELS IN LIQUOR FROM PAPER MILL

Potentiostatic polarization behavior of mild steel was investigated in alkaline electrolytes with additions of sulfur containing compounds to determine the effect of the different species of sulfur in white liquor. Sulfide and thiosulfate ions were corrosion activators. Sulfite and sulfate ions had no effect. Corrosion potential was controlled by polysulfide (Wensley, 1980).

The corrosion of carbon steel was investigated in simulated kraft liquor via polarization testing, mass loss, and corrosion potential measurements to determine the effects of liquor components. Accelerated corrosion was attributed to the occurrence of alternative cathodic reactions involving direct reduction of thiosulfate ions (Peterman and Yeske, 1986).

Some researchers have investigated the effect of organic species including the addition of catechol may play an important role in general corrosion (Wensley, 2005; Anaya, 2001; Singh, 2007; Hazlewood, 2006; Kannan, 1996; Hazlewood *et al.*, 2006). Singh evaluated the corrosion behavior of carbon steel (A 516-Gr 70) and two stainless steels (316, 304), and two duplex stainless steels (DSS) (S32304, S32205) in contact with black liquor produced by pulping five wood species (hardwood and softwood). The potentiodynamic polarization tests were conducted in synthetic liquors at room temperature, with and without the addition of catechol. Moreover, the results of electrochemical tests demonstrated that the organic compounds in the black liquor play the major role in steel corrosion and DSS have shown a good corrosion behavior in all tested black liquors (Anaya, 2001, Singh, 2007).

Bhattacharya (2011) investigated the corrosion properties and electrochemical behavior of different DSS such as S32304, S32205 and S32101 in high pH caustic and alkaline sulfide solutions at different temperatures. The reference electrode used was a saturated calomel saturated (SCE) with luggin capillary, the counter electrode was used was a platinum foil. Tests carried out at higher temperature (170°C) was used the pressure balanced Ag/AgCl external reference electrode as reference electrode. In addition, the role of alloying elements in DSS in these environmental was studied analyzing the polarization measurements of pure Fe, Cr, Ni and Mo and DSS S32205. The increase in corrosion rates of DSS with sulfide addition could be related to the presence of sulfur on

the passivation layer and corrosion susceptibility due to the formation of metal–sulfur compounds, which are less protective than the oxide film. S32205 was found to be most susceptible to general corrosion and S32304 had the lowest corrosion rates in sulfide caustic environmental. Magnetite and awaruite ($FeNi_3$) detected by XRD can develop a more stable passive film in S32304 resulting in lower corrosion rates (Bhattacharya, 2011).

The effect of five type wood species (softwood and hardwood) on the corrosiveness of black liquors was studied selecting one carbon steel (A516-G70), two austenitic stainless steels (SS316, SS304), and two DSS (S32304, S32205). The metal coupons were placed in a S32205 stainless steel 3 L autoclave and submerged in the black liquor. The autoclaves were closed and heated with electric jackets and the specimens were exposed in the black liquor at 170°C for 2 weeks, after which the coupons were removed, weighed, and examined for general and localized corrosion under the microscope. Results from this study shown that corrosion rate is not correlated with their inorganic composition. On the other hand, the organic constituents have very important role in the corrosivity of black liquors. In addition, DSS specimens, in general, have performed very well in all tested black liquors (Anaya, 2001).

Steel tanks are used to store synthetic black liquor at various stages of the process pulp, and show a range of corrosivity for the steel and to elucidate the corrosion mechanisms of steel in black liquor. Kannan (1996) evaluate the effects of substituted phenols on the electrochemical behavior of A-283 Gr C steel in alkaline solutions at 65°C to determine the corrosion of steel storage tanks in the pulp and paper industry. The results indicated that sodium sulfite, dimethyl sulfide, pinene, sodium thiosulfate, and pyrogallol are the chemicals that most contributed to the corrosion of A283 carbon steel in synthetic liquor (Kannan, 1996; Singh, 2007).

Crevice occurs when small quantities of stagnant solutions inside crevices and under shielded areas on a passivated metal surface are selectively depleted of dissolved oxygen. If the oxygen content reaches a critical concentration in this area, the passivity will not support, establishing an active/passive cell, promoting an intense attack due to the high difference of area between the anode (very small) and cathode (Talbot, 1998).

6.1 Experimental procedure

6.1.1 Preparation of the working electrode

The samples were embedded in epoxy resin. The electrical connections necessary for the tests were made by welding a copper wire on the sample surface. The surface samples were wet ground consecutively using 320, 600, 80 and 1200 grit on abrasive papers (silicon carbide papers (SiC)), polished using 3 μm, 1 and 0.25 μm diamond paste, and ultrasonically cleaned in ethanol. In orders to avoid crevices, the samples were masked with black wax (Apiezon Wax W) (Frankel *et al.,* 1992) at least 12 h before the measurements as shown in Figure 6.1 and stored in desiccators. The black wax was previously dissolved in trichloroethylene. Sample preparation was carried out in the Corrosion and Surface Engineering Laboratory at the Department of Chemical Engineering, Federal University of Minas Gerais, Brazil and Department of Materials Science and Engineering at Ohio State University.

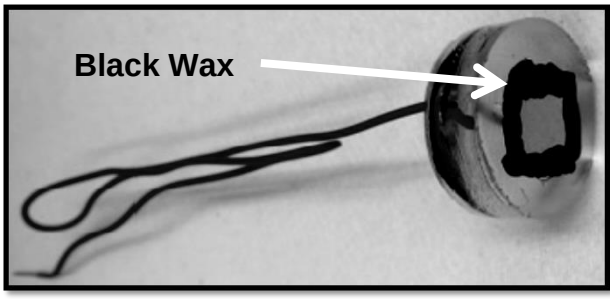

Figure 6.1: Specimens for the electrochemical measurements masked in black wax to avoid crevice.

6.1.2 Conductivity

Conductivity was measured using a LUCADEMA Model mCA 150 conductivity meter.

6.1.3 Electrochemical tests - North American Liquors (White, Weak Black, and Green Liquors)

Mead Westvaco Corporation - MWV (Covington, VA), supplied the white, green and black liquors. In detail the active cooking chemical the white liquor contain sodium hydroxide (NaOH) and sodium sulfide (Na_2S) with high pH (pH > 13), the green liquor Sodium Carbonate (Na_2CO_3) and Sodium Sulfide (Na_2S) with pH >10, and black liquor (residual inorganic chemicals (sodium sulfide, sulfate,

sodium thiosulfate, sodium carbonate, and sodium hydroxide) and organic extractives in wood, and other constituents due to fragmentation reactions of lignin) with pH >13.

In North America, all sodium components based on the equivalent amount of sodium oxide (Na_2O). The concentration unit used is grams per liter (g/L). Some definitions based on TAPPI (United States) as effective alkali (EA) (NaOH +1/2 Na_2S, expressed as Na_2O), total alkali (NaOH + Na_2S + Na_2CO_3 + ½ Na_sCO_3, all expressed as Na_2O (Wensley, 2004). The sulphide-containing caustic solution used were White liquor (WL): 88g/L Effective alkali (EA) as Na_2O, Green liquor (GL): 117g/L total titratable alkali (TTA) as Na_2O and Weak Black liquor (BL): 15% solids. And the BL was originated by southern hardwood mix and GL and WL was originated by Pine mix and hardwood mix. The solutions were filtrated as shown in Figure 6.2.

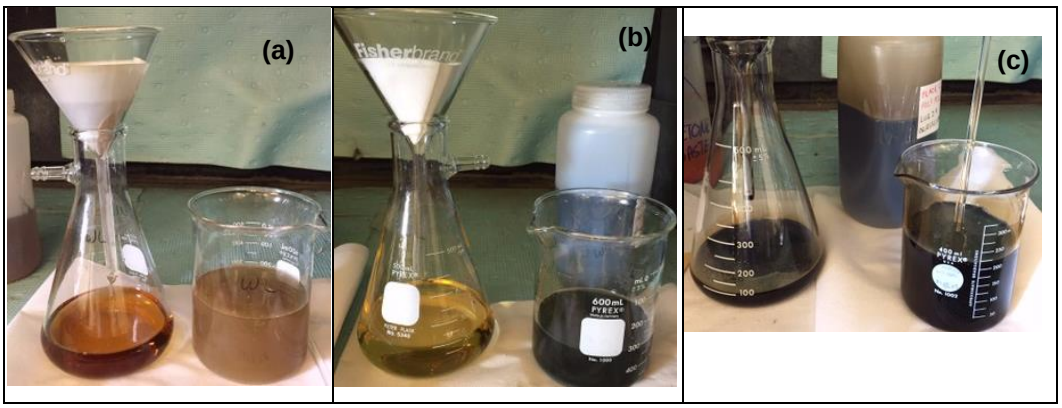

Figure 6.2: Filtration of Liquors (a) White Liquor, (b) Green Liquor and (c) Black Liquor inside the hood.

6.2 Results and Discussion

6.2.1 Cyclic Anodic Potentiodynamic Polarization – North American Liquors

In this study, different set ups to the probe such as flat cell were tested and features like crevice were observed (Figure 6.3), due to different oxygen concentration below the O-ring, which could promote more active area susceptible to corrosion phenomenon. Furthermore, the set up by flat cell has the disadvantage solids deposition above the electrode surface increasing interferences for the measurements, especially because in this study a solution supplied by paper and pulp industry was

used, even though the solutions were filtered before the electrochemical tests. The black wax was applied around the O-ring to avoid crevices, but the upper support of the flat cell pressed the O-ring promoting some defects causing crevice. Consequently, the polarization curve was similar to the previous, for this reason, a conventional cell of three electrodes: working electrode (embedded in epoxy), a counter electrode, and a reference electrode) inside a becher (Figure 6.3).

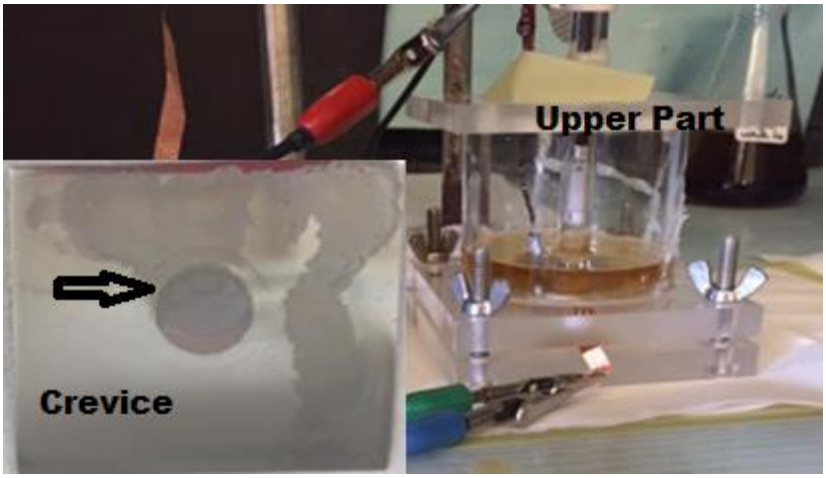

Figure 6.3: Set up of the flat cell and the aspect of the sample after of the polarization measurement in white liquor.

Figure 6.4 shows the different approaches were used to carry out the electrochemical tests in white liquor at room temperature, 60°C, and green liquor for example; the reference electrode was used in the electrolyte. On the other hand, the Luggin capillary was used in green liquor to get closer steel surface and to avoid the contamination of chloride from RE. In black liquor was used a salt bridge, due to the difficult visibility of steel surface.

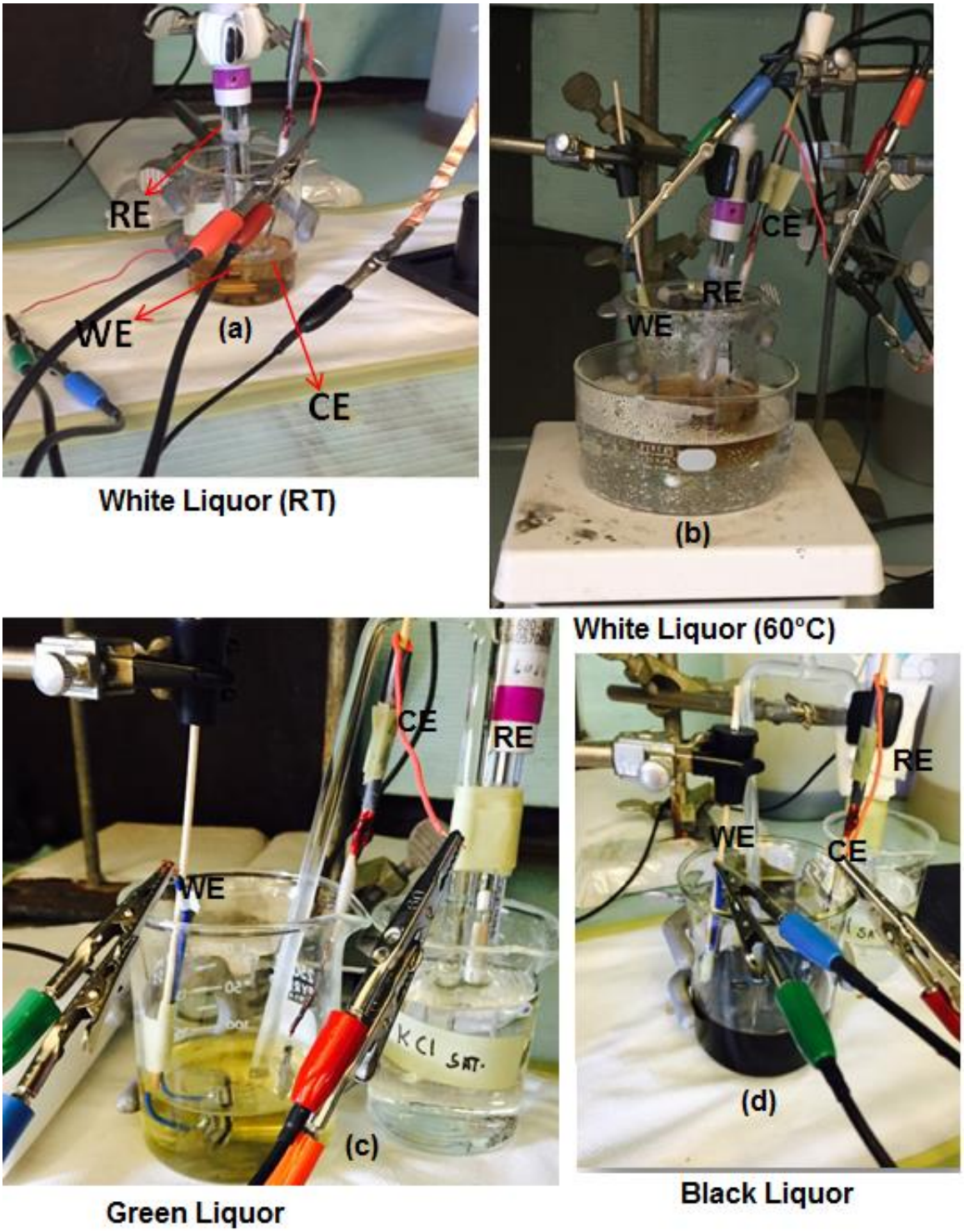

Figure 6.4: Set up for cyclic polarization in: (a) WL at RT, (b) WL at 60 ºC, (c) GL, and (d) BL.

6.2.2 Electrochemical Tests – Brazilian Liquors

Cenibra (Belo Oriente, MG) supplied the white and green liquors. According to Brazilian standards to green Liquor: TTA (total titratable alkali):150 ± 10 g/L (as NaOH), reduction efficiency > 93% ($Na_2S/(Na_2S + Na_2SO_4)$, total suspended solids <200 mg/L, and pH >13. In addition, characterization of white liquor: TTA (total titratable alkali): 140 ± 10 g/L (as NaOH), EA (effective alkali): 110 ± 10 g/L (as NaOH), sulfidity: 25 ± 2%, causticizing efficiency: 82 ± 2%, total suspended solids <100 mg/L, and pH > 13. Table 6.1 shows the conductivity to white and green liquors.

Table 6.1: Conductivity measurements in Brazilian liquors.

	Measured Conductivity (mS/cm) at 25°C
White Liquor	360.4
Green Liquor	196.4

6.3 References

ANAYA, A.; SINGH, P., Effect of Wood Species on Corrosivity of Black Liquors, **Corrosion 2001**, n. 885, p. 1–16, 2001.

BHATTACHARYA, Ananya; SINGH, Preet M., Electrochemical behaviour of duplex stainless steels in caustic environment, **Corrosion Science**, v. 53, p. 71–81, 2011.

HAZLEWOOD, Patrick Evan, **FACTORS AFFECTING THE CORROSIVITY OF PULPING LIQUORS**, Georgia Institute of Technology, 2006.

HAZLEWOOD, P. E.; SINGH, P. M.; HSIEH, J. S., Role of Wood Extractives in Black Liquor Corrosiveness, **Corrosion Engineering**, v. 62, n. 10, p. 911–917, 2006.

KANNAN, S; R.G., Kelly, THE ROLE OF DIHYDROXYBENZENES AND OXYGEN ON THE CORROSION OF STEEL IN BLACK LIQUOR, **Corrosion Science**, v. 38, n. 7, p. 1051–1069, 1996.

PETERMAN, Lee; YESKE, Ronald A, **THIOSULFATE EFFECTS ON CORROSION IN KRAFT WHITE LIQUOR**, The Institute of paper Chamistry, 1986.

TALBOT, D.; TALBOT, J., **CORROSSION SCIENCE and TECHNOLOGY**, [s.l.]: CRC Press Materials Science and Technology, 1998.

WENSLEY, A. AND CHARLTON, R.S., **Corrosion Studies in Kraft White Liquor: Potentiostatic polarization of Mild Sttel in Caustic Solutions Containing Sulfur Species**, National Association of Corrosion Engineers, p. 1–5, 1980.

WENSLEY, Angela, Pulp and Paper, *in*: SCULLY, Robert Baboian; Sheldon W. Dean Jr; Harvey P. Hack; Edward L. Hibner; John R. (Org.), **Corrosion Tests and Standards : Application and Interpretation**, 2nd Editio. West Conshohocken, PA: ASM International, 2005, p. 795–811.

7 CORROSION BEHAVIOR OF DUPLEX AND LEAN DUPLEX STAINLESS STEELS IN PULP MILL

Luiza Esteves[a]*, Marcelo Cardoso[a], Vanessa F.C. Lins[a]

[a] Federal University of Minas Gerais, Department of Chemical Engineering, Antônio Carlos Avenue 6627, Brazil, Zip Code 13565-905 Phone Number +553134091781

luizaeq@yahoo.com.br

Abstract

The cyclic potentiodynamic polarization behavior of duplex stainless steel (DSS) and lean duplex stainless steel (LDSS) was studied in white and green liquors from a pulp processing plant. The corrosion behavior in industrial and synthetic liquor was compared. The polarization curves of the duplex steels in synthetic white liquor were shifted to lower potentials and higher current densities in relation to the steel in industrial white liquor, which proved to be less aggressive to the duplex steel. The duplex steels also showed the highest values of transpassive potential in industrial white liquor compared to synthetic liquor. Cold and hot rolled duplex and lean duplex steels in green liquor showed the lowest values of transpassive potential.

Keywords: Duplex stainless steels; Polarization, Alkaline corrosion; Pulp and paper industry

7.1 Introduction

Chemical pulps are made by cooking (digesting) the raw materials, using the Kraft process (sulfate) and sulfite processes. The Kraft process is the most dominating chemical pulping process worldwide. In the Kraft pulp process, the active cooking chemicals (white liquor) are mainly sodium hydroxide (NaOH) and sodium sulfide (Na_2S)[1, 2], the operation is at high temperature (about 170 °C) and the pressure of 6.5 to 8.5 bar is used in delignification during the chip cooking cycle[3-5]. The chemical recovery cycle is generated the sub-product, extracted from pulping wood in the digester, called the black liquor, with smaller amounts of wood extractives and residual inorganic pulping salt[6, 7]. The combustion of the strong black liquor converts the recovered inorganic chemicals to smelt which is dissolved in water to give the green liquor, which are mainly sodium carbonate (Na_2CO_3), and sodium sulfide (Na_2S) generated during the liquor recovery cycle. The green liquor is causticized to regenerate the white liquor[8-13]. The scheme of the main operation of the chemical recovery cycle is shown in Figure 7.1. Moreover, the white liquor is considered the most aggressive of the alkaline pulping liquors[14].

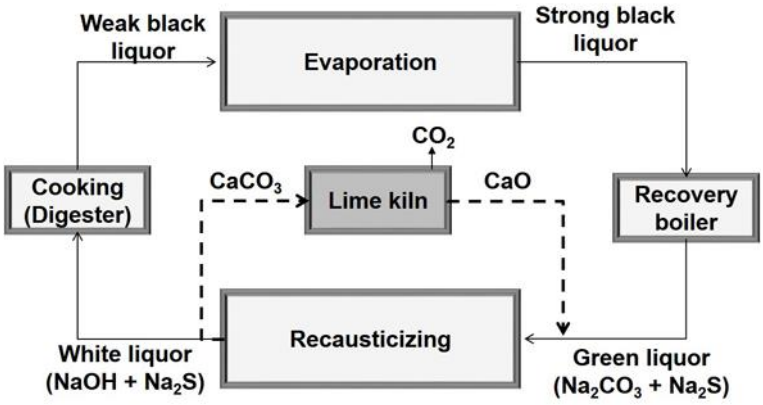

Figure 7.1: Schematic representation of the paper and pulp mill (Kraft process).

Duplex stainless steel (DSS) has been used as a material of construction in the pulp and paper industry for the past 35 years due to its excellent corrosion resistance and high mechanical strength allowing for thickness reduction in equipment. Lean DSS (LDSS) is a DSS with a lower content of molybdenum and nickel and thus a lower cost. Nitrogen addition is used in LDSS to provide the austenite content in alloys with a lower nickel concentration[15-17]. Currently, the materials commonly

selected for the construction of pulp digesters are lean duplex (UNS S32304) or standard duplex (UNS S32205). Older facilities were constructed from AISI 316 austenitic stainless steel coupled to an anodic protection system[18-22]. DSSs combine low nickel content with high mechanical strength, which makes them an efficient and cost alternative to austenitic stainless steel grades.

In the pulp and paper industry, carbon steel pulp mill equipment, like digesters, storage vessels, have been showed general corrosion and stress corrosion cracking[14, 23- 25]. Singh and Anaya evaluated the corrosion behavior of carbon steel (A 516-Gr 70), AISI 304 and 316 stainless steels, and two DSSs (UNS S32304, UNS S32205) in black liquor produced by pulping five wood species in a synthetic liquor. The potentiodynamic polarization tests were performed at room temperature, with and without the addition of catechols. The organic compounds in the black liquor were found to play a major role in steel corrosion, and the DSSs showed a high corrosion resistance in all tested black liquors[22].

Corrosion resistance of DSS in white liquor has been widely studied[14, 21-23]. Bhattacharya and Singh[14] investigated the corrosion properties and electrochemical behavior of different DSSs (UNS S32304, UNS S32205, and UNS S32101) in high pH caustic and alkaline sulfide solutions at different temperatures. They studied the role of alloying elements in DSS in these environments by analyzing the polarization behavior of pure Fe, Cr, Ni and Mo, and DSS UNS S32205. The increase in corrosion rates of DSS with sulfide addition can be related to the presence of sulfur in the passive layer and the formation of metal–sulfur compounds that are less protective than the oxide film[14]. The S32205 steel was found to be most susceptible to general corrosion and the S32304 steel had the lowest corrosion rates in a sulfide caustic environment. A more stable passive film containing magnetite and awaruite ($FeNi_3$) developed on UNS S32304 steel, resulting in lower corrosion rates[14].

Wensley and Champagne evaluated the effect of sulfide concentration on the corrosion resistance of carbon steel specimens with different silicon contents (low-silicon A285-Grade C and medium-silicon A516-Grade 70), austenitic stainless steel (ASI04) and two DSS (UNS S32304 and UNS S32205) in white, green, weak black, strong black, and flash tank liquors. All of the stainless steels (UNS S30403, UNS S32304, and UNS S32205) were highly resistant to corrosion in all the liquors tested, regardless of sulfide content[23, 26, 27].

The aim of this work is to evaluate the corrosion behavior of DSS with two processing conditions, hot and cold rolling is assessed in liquors provided by a pulp and paper producer. In addition, the corrosion resistance of DSS and LDSS in synthetic and industrial white liquor (WL) is compared. To the best of our knowledge, literature on corrosion behavior of LDSS and DSS in industrial liquors from pulp and paper industry is not reported and the mechanisms involved are not fully understood.

7.2 Materials and Methods

7.2.1 Steel characterization

Aperam South America (Brazil) supplied the duplex stainless steels in hot rolled and cold rolled conditions and the chemical compositions of the steels are shown in Table 7.1. The DSS studied is 31803 with 5%wt. Ni and 2.6%wt. Mo and the LDSS is 32304 with a lower content of Ni (4%wt.) and Mo (0.3%wt.). The steels were examined as-received: hot rolled coils annealed at 1075 ± 25°C with a thickness of 4 mm, and cold rolled coils annealed at 1070 ± 25 °C, with a thickness of 1.8 mm. Table 7.2 shows the mechanical properties of the cold rolled and hot rolled steels provided by the manufacturer[28].

Table 7.1: Chemical composition of the DSSs investigated (wt%).

Steel	Rolling	Cr	Ni	Mo	N	C	Si	Mn	S	Fe
31803	Cold	22.43	5.34	2.67	0.11	0.012	0.29	1.85	0.0004	Balance
31803	Hot	22.45	5.31	2.63	0.11	0.013	0.38	1.81	0.0005	Balance
32304	Cold	22.40	4.10	0.29	0.14	0.015	0.46	1.55	0.0002	Balance
32304	Hot	22.87	4.20	0.27	0.15	0.011	0.20	1.45	0.0004	Balance

Table 7.2: Mechanical properties of duplex steels.

Steel samples	Hardness (Rockwell C)	Elongation (%)	Yield Strength (MPa)	Tensile strength (MPa)
DSS Cold rolled S31803	23	28	700	855
DSS Hot rolled S31803	22	30	648	784
LDSS Cold rolled S32304	19	31	604	764
LDSS Hot rolled S32304	18	33	557	691

The metallographic analysis was performed after etching the steel samples in modified Behara reagent [80 mL distilled and deionized water, 20 mL hydrochloric acid (HCl), and 1 g of potassium metabisulfite ($K_2S_2O_5$)]; 2 g of ammonium bifluoride (NH_4H HF) were added to this stock solution just before the etching[29]. The microstructure analyses were carried out using an optical light microscope (LOM, Leitz Metalloplan) with Image Pro software.

7.2.2 Electrochemical Tests

The steel sheets were cut in dimensions of 1 cm x 1 cm with the exposed surface being the rolling surface. The samples were embedded in epoxy resin and electrical connections necessary for the tests were made by welding a copper wire to the back of the sample, which was not in contact with the electrolyte. The samples were wet ground to 1200 grit SiC abrasive papers, and then polished using 3 μm, 1 μm, and 0.25 μm diamond paste, and ultrasonically cleaned in ethanol. In order to avoid crevices, the samples were masked with black wax (Apiezon Wax W)30 at least 12 h before testing and were stored in a desiccator. The black wax was dissolved in trichloroethylene to assist application.

A North American pulp and paper company supplied the white and green liquors. The WL contained sodium hydroxide (NaOH) and sodium sulfide (Na_2S) at pH > 13, the green liquor (GL) aqueous solution contained sodium carbonate (Na_2CO_3) and sodium sulfide (Na_2S) at pH >10. The

electrochemical tests were also performed in synthetic white liquor (SWL) composed of 150 g/L of NaOH and 153.8 g/L of $Na_2S.9H_2O$ (3.75 mol/L NaOH + 0.64 mol/L Na_2S)[14, 31].

All sodium components were considered based on the equivalent amount of sodium oxide (Na_2O). The definitions used were based on the Technical Association of Pulp and Paper industries (TAPPI). The effective alkali (EA) is: NaOH +1/2 Na_2S, expressed as Na_2O; the total alkali is NaOH + Na_2S + Na_2CO_3 + ½ Na_2CO_3, all expressed as Na_2O[22]. The sulphide-containing caustic solutions used were: WL consisting of 88 g/L EA as Na2O and GL consisting of 117 g/L total titratable alkali (TTA) as Na_2O. The GL and WL were originated by pulping of pine mix and hardwood mix.

A Reference 600 Gamry potentiostat was used for the electrochemical tests. The polarization curves were collected by scanning to the anodic direction at 0.167 mV/s from the corrosion potential (E_{corr}). Transpassivity was observed in all cases, and the scan was reversed when the current reached 3 mA/cm^2. All the electrochemical measurements were repeated at least three times to ensure the reproducibility.

Potentiostatic polarization was performed in GL to evaluate the efficiency of the protective layer. Three potential values were chosen for the potentiostatic tests: -500 mV_{SCE} at the first passivation (around 10^{-6} A/cm^2), -150 mV_{SCE} at the second passivation (around 10^{-5} A/cm^2), and 0 mV_{SCE} in the transpassive region.

7.3 Results and Discussion

7.3.1 Steel characterization

The microstructure of the two steels, DSS and LDSS are shown in Figure 7.2. Lighter austenite (γ) islands are embedded in the darker etched ferrite (α) matrix with no other secondary precipitates[32, 33]. The cold rolled condition of the steels showed higher yield strength, a higher tensile strength, and a lower elongation than the hot rolled condition of the steels, even though the steels were annealed at 1070 ± 25°C after rolling. Table 7.3 shows the contents of austenite and ferrite obtained using Image Pro Software.

Table 7.3: Austenite and ferrite contents obtained using Image Pro Software.

Samples	Weight percent	
	Austenite (γ)	Ferrite (Fe-α)
DSS 31803 Cold Rolled	48	52
DSS 31803 Hot Rolled	50	50
LDSS 32304 Cold Rolled	47	53
LDSS 32304 Hot Rolled	46	54

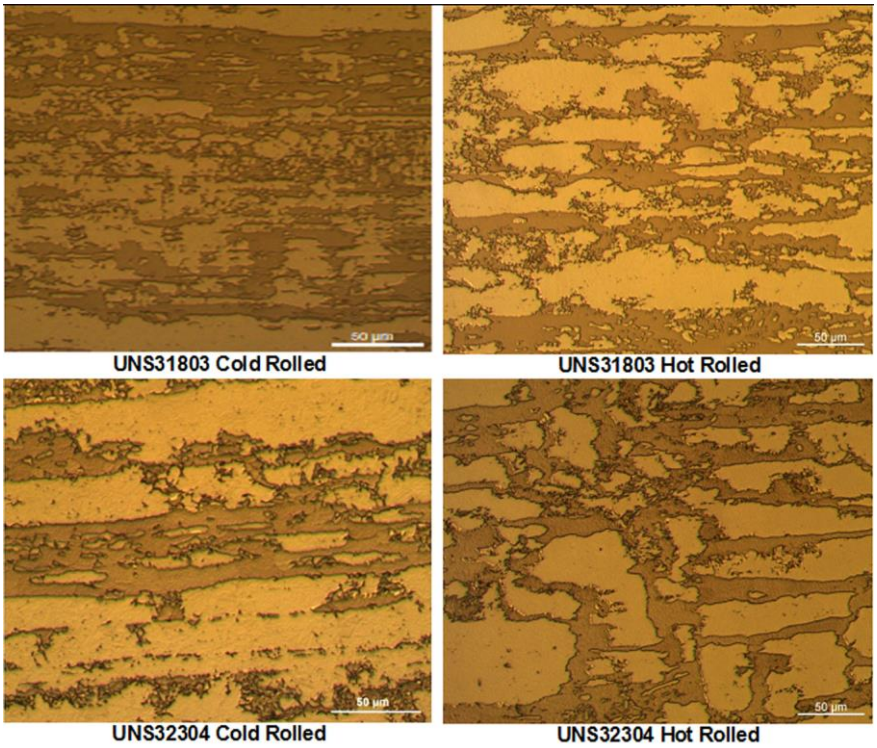

Figure 7.2: Microstructure of lean duplex and duplex stainless steels.

7.3.2 Cyclic polarization of DSS S31803 and S32304 steels in synthetic and in industrial white liquor

Studies of steel corrosion in SWL have been extensively reported in the literature12, 14, 34-35, but reports of corrosion resistance of duplex steels in industrial liquors of pulp and mill industry are not available.

The cyclic polarization curves of the S31803 duplex steel and the S32304 lean duplex steel were similar in industrial WL at room temperature as shown in Figure 7.3. Polarization curves started at open circuit potentials in the range from -500 mV_{SCE} to -300 mV_{SCE}. The current density increased slightly with potential until about –100 mV_{SCE}, was almost constant until about +100 mV_{SCE} and then increased slightly again at higher potentials. A slight but reproducible hysteresis was observed during the reverse scan for all samples. This electrochemical test was not able to distinguish differences in corrosion behavior of DSS and LDSS or any effect of the two processing conditions.

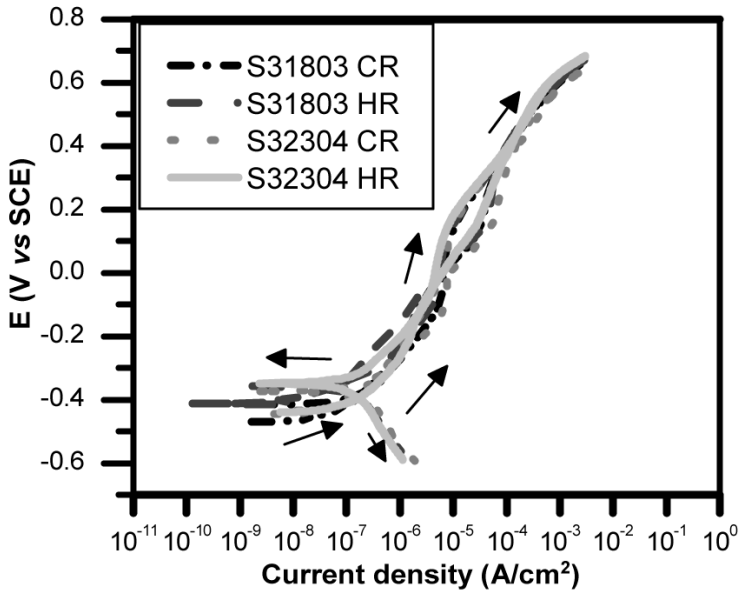

Figure 7.3: Cyclic polarization curves of S31803 and S32304 steels in industrial WL at room temperature.

Figure 7.4 shows polarization curves of S31803 steel in synthetic and industrial WL. The corrosion potential of cold rolled S31803 DSS in SWL was -1.137 ± 0.005 V_{SCE} and in the real industrial WL it was -0.459 ± 0.014 V_{SCE}. Much higher values of current density were observed in the synthetic liquor. The differences in behavior indicate that testing of steels in synthetic liquor may predict a shorter life of the material than what would be achieved in service. The industrial WL is a final product from the causticizing system and it has more chemical compounds than the synthetic solution. The WL was regenerated in the process, as the green liquor was made caustic to produce WL, which has a complex chemical composition[26]. These extra components seem to inhibit the corrosion of DSS.

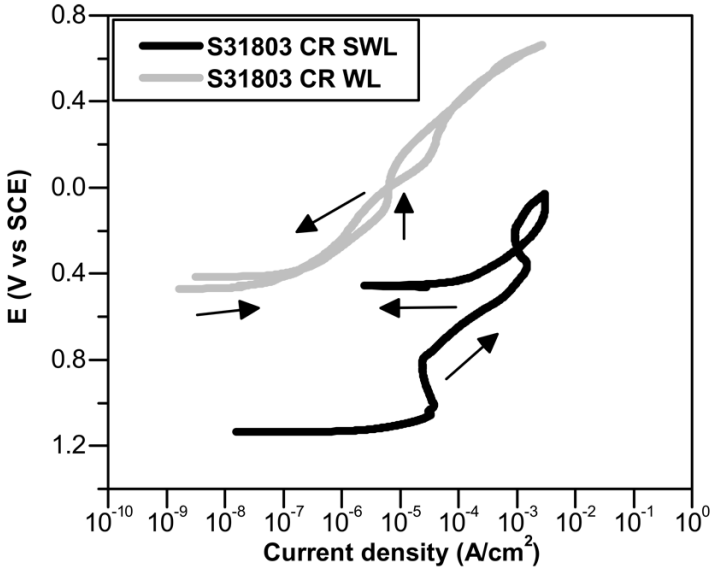

Figure 7.4: Cyclic potentiodynamic polarization curves for cold rolled S31803 steels in SWL and industrial WL at room temperature.

The S31803 DSS in SWL showed two regions of almost constant current density. In contrast, in industrial WL, only one passivation region was obtained. Bhattacharya and Singh[14] have reported a similar kind of behavior for S32205 DSS in SWL. They suggested that the current density increased in the beginning due to the dissolution of iron, and then the primary passivation was formed by the formation of nickel sulfide (Ni_2S), with Ni and Cr also contributing to the first passivation layer[14]. The current density above the primary passivation increased due to oxidation of sulfur species corresponding to the S^{2-}/SO_4^{2-} oxidation reaction, and to the dissolution of Cr in the form of CrO_4^{2-} ions. A region of constant current density of 10^{-3} A/cm^2 was observed. Finally, the current density increased due to the oxygen evolution reaction[22]. It is reasonable to assume that this explanation is also valid for the results obtained in this study.

The corrosion potential of DSS in industrial WL at 60°C was less noble than the value at room temperature (RT) as shown in Figure 7.5, which presents the cyclic potentiodynamic polarization curves of cold and hot rolled S31803 DSS at the two temperatures. The passive current density was higher at 60°C (10^{-5} A/cm^2) than at RT (10^{-6} A/cm^2), indicating a less protective passive film in sulfide-containing caustic solution at the higher temperature. At about -150 mV_{SCE} for each alloy at 60°C, the

current density increased above 10^{-5} A/cm^2. Temperature plays an important role in corrosion of duplex steels in WL and causes an increase of current densities and a decrease of open circuit potential.

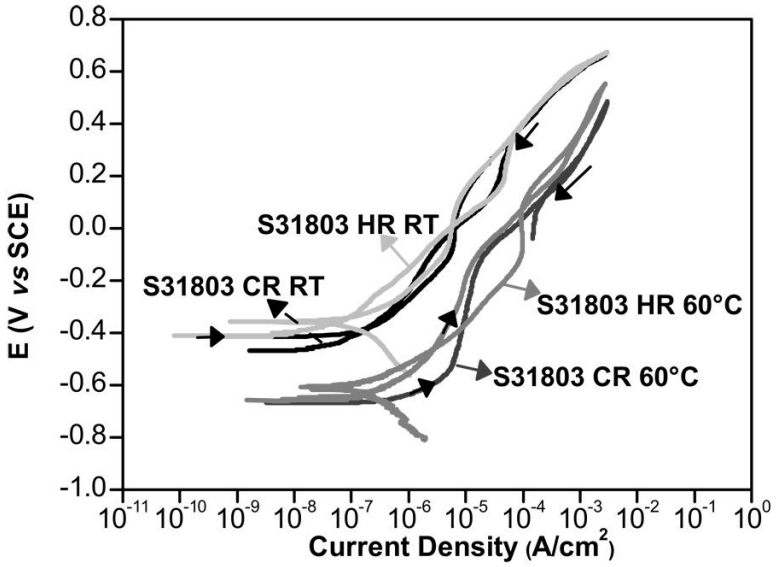

Figure 7.5: Cyclic potentiodynamic polarization curves of UNS 31803 DSS in industrial WL at room temperature and 60 ºC.

7.3.3 Cyclic polarization of S31803, S3230 DSS in green liquor

The polarization curves of the DSSs tested in GL containing sodium carbonate and sodium sulfide at pH > 10 indicate a similar behavior for the lean and duplex stainless steels as shown in Figure 7.6. Two passivation regions were identified with the first one exhibiting a range of current densities between 10^{-6} to 10^{-5} A/cm^2. The duplex and lean stainless steels showed positive hysteresis in the reverse scans indicating a possibility of localized corrosion. SEM and EDS analyses identified inclusions enriched in aluminum, magnesium, oxygen, manganese and sulfur on the surface of steels. It has been reported that MgO, Al_2O_3 and MnS inclusions on the surface of S32750 super duplex steel are the preferred sites for pit initiation[31]. In this case, pits were not observed on the surface steels but these inclusions are cathodic regions and the steel near inclusions can act as anodes, generating corrosion at inclusion/matrix interface (Figure 7.7). Figure 7.6 shows repassivation occurring at a lower

potential. Corrosion behavior of the standard duplex S31803 steel and lean duplex steel was similar in GL.

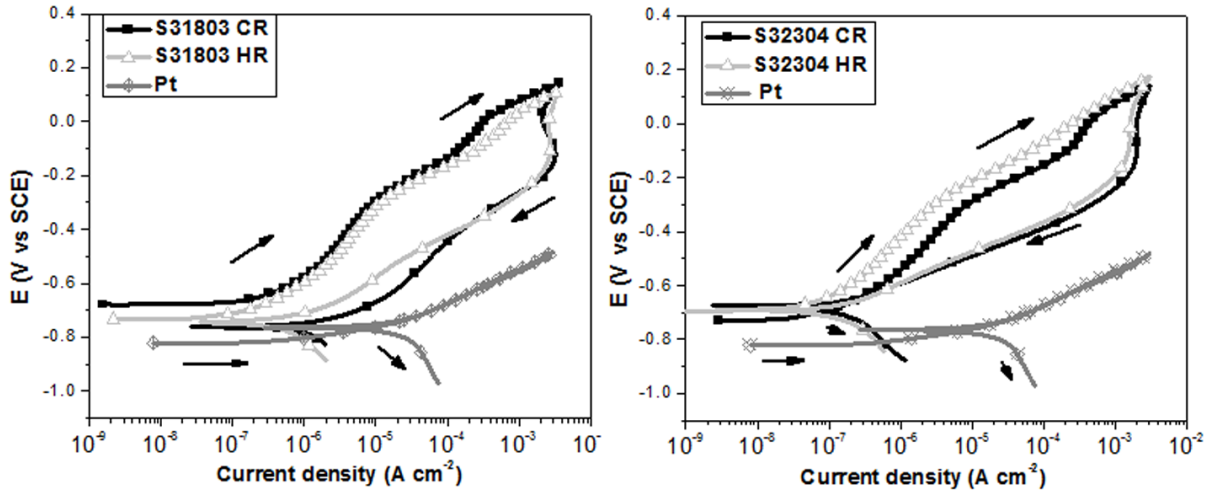

Figure 7.6: Cyclic potentiodynamic polarization curves of cold and hot rolled S31803 and S32304 steels, and Pt wire in green liquor at room temperature.

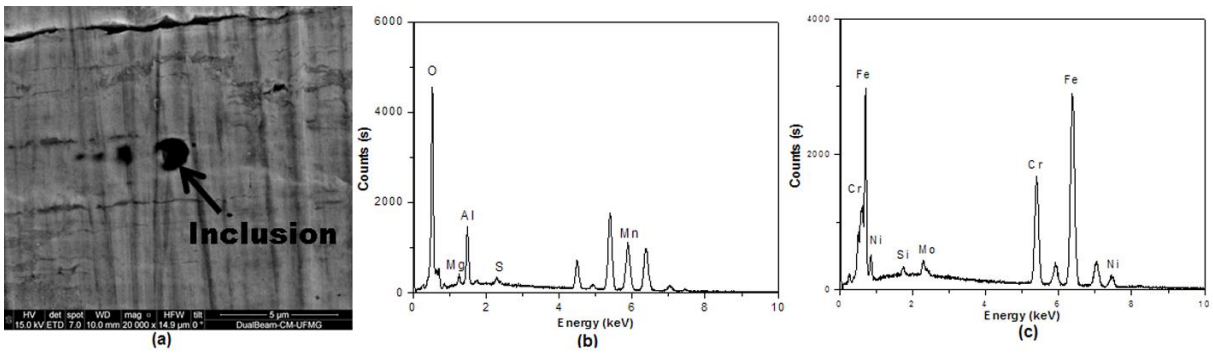

Figure 7.7: DSS surfaces after cyclic potentiodynamic polarization in GL: (a) 31803 CR, EDS analysis (b) inclusion spot, and (c) steel surface.

The behavior of platinum was compared with the DSS in these electrolytes as shown in Figure 7.5. The current densities associated with platinum are higher than the current densities exhibited by DSS, indicating that platinum surface acts as a catalyst for the redox reactions. On the other hand, the results of the DSSs were completely different from that of the platinum, and a corrosive process occurred on the surface of DSS as shown in Figure 7.5.

Potentiostatic polarization was performed to evaluate the behavior of the current density with time and thus the efficiency of the protective layer in GL. Three regions were chosen for the potentiostatic tests:

-500 mV_{SCE} at the first passivation (around 10^{-6} A/cm^2), -150 mV_{SCE} at second passivation (around 10^{-5} A/cm^2), and 0 mV_{SCE} in the transpassive region.

As is evident in Figure 7.8, the current density increased with time when the potential of 0 mV_{SCE} was applied for all steels studied, which indicates that a corrosive process occurs at a current density on the order of 10^{-3} A/cm^2.

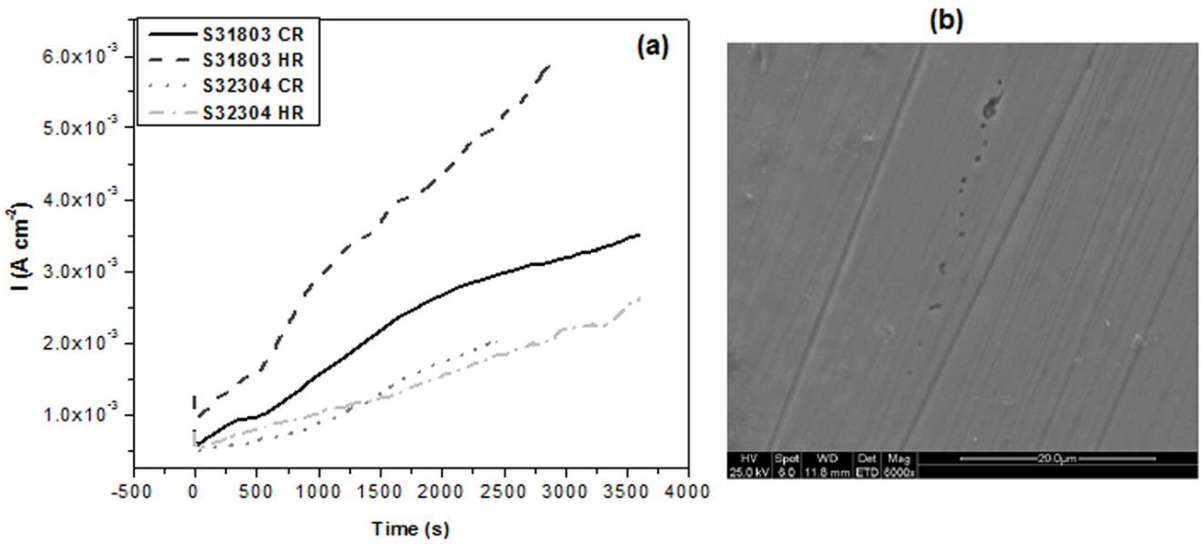

Figure 7.8: (a) Potentiostatic curves at 0 mV_{SCE} of cold and hot rolled S31803 and S32304 steels in GL at room temperature, (b) 32304 Cold Rolled surface after potentiostatic test at 0 mV_{SCE}.

The potential of -0.5 V_{SCE} was chosen to investigate the passivation region in Figure 7.6. At the applied potential of -0.5 V_{SCE}, the current density remained constant and low with time for the steels in the cold-rolled condition and showed a slight increasing trend for the steels in the hot-rolled condition as shown in Figure 7.9. The cold rolled steels showed the lowest current density in green liquor. The hot rolled S31803 steel showed the highest current density in green liquor, using the potentiostatic test. The cold and hot rolled steels were annealed at 1070°C and 1075°C, respectively. Besides the difference in mechanical properties, there is a difference in interlayer space of ferrite and austenite. In the cold rolled steel, the microstructure is finer as shown in Figure 7.10. The hot-rolled S31803 steel showed a passivation current density one order of magnitude higher (10^{-5} A/cm^2) than the current of the cold rolled S31803, and cold and hot rolled S32304 steels (10^{-6} A/cm^2). The hot-rolled S31803 steel exhibited a less protective layer than the other DSSs in GL.

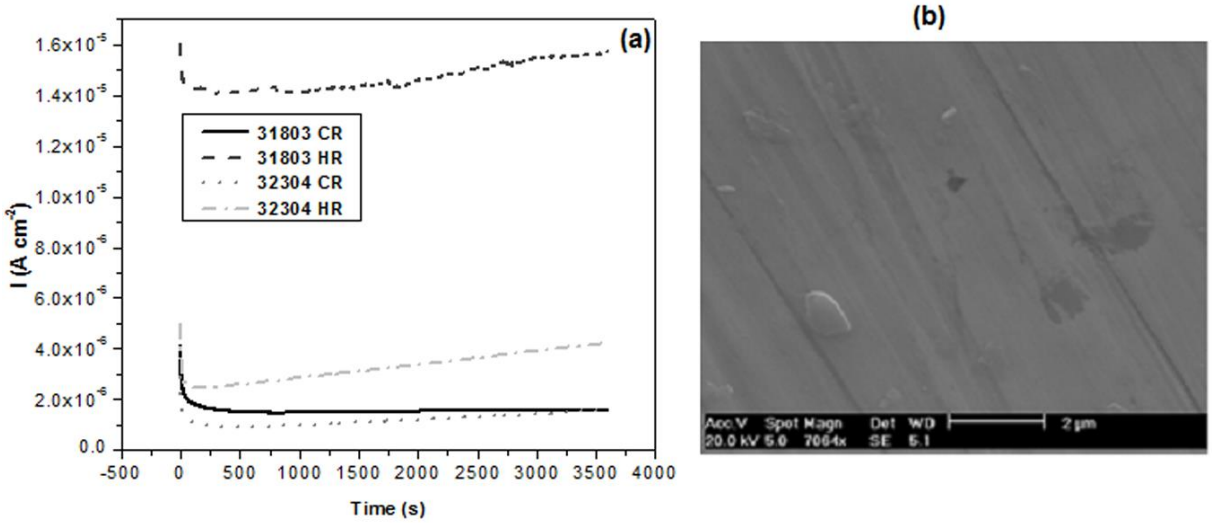

Figure 7.9: (a) Potentiostatic curves at -500 mV_{SCE} of cold and hot rolled S31803 and S32304 steels in green liquor at room temperature, (b) S31803 cold rolled surface after potentiostatic test at -500 mV_{SCE}.

In order to reveal the grain boundaries in austenite and ferrite in DSS, electrolytic etching was used with 60% HNO_3 solution at an etching potential of 2.2 V for 3 minutes. The cold rolled steels exhibited finer grains than the hot rolled steels (Figure 7.10). This finding can explain a higher tensile strength of the cold rolled steels than the hot rolled steels as shown in Table 7.2. Grain boundaries are barriers to the movement of dislocations and steels with finest grains have a higher density of grain boundaries that inhibits the dislocation movement and contributes to enhance the tensile strength of steel. The result obtained that the hot-rolled S31803 steel exhibited a less protective layer than the lower density of grain boundaries in hot rolled S31803 steel than the steel in cold rolled condition can also explain the other DSSs in GL. Finer grains contribute to improve the protective ability of the passive layer of stainless steels[36].

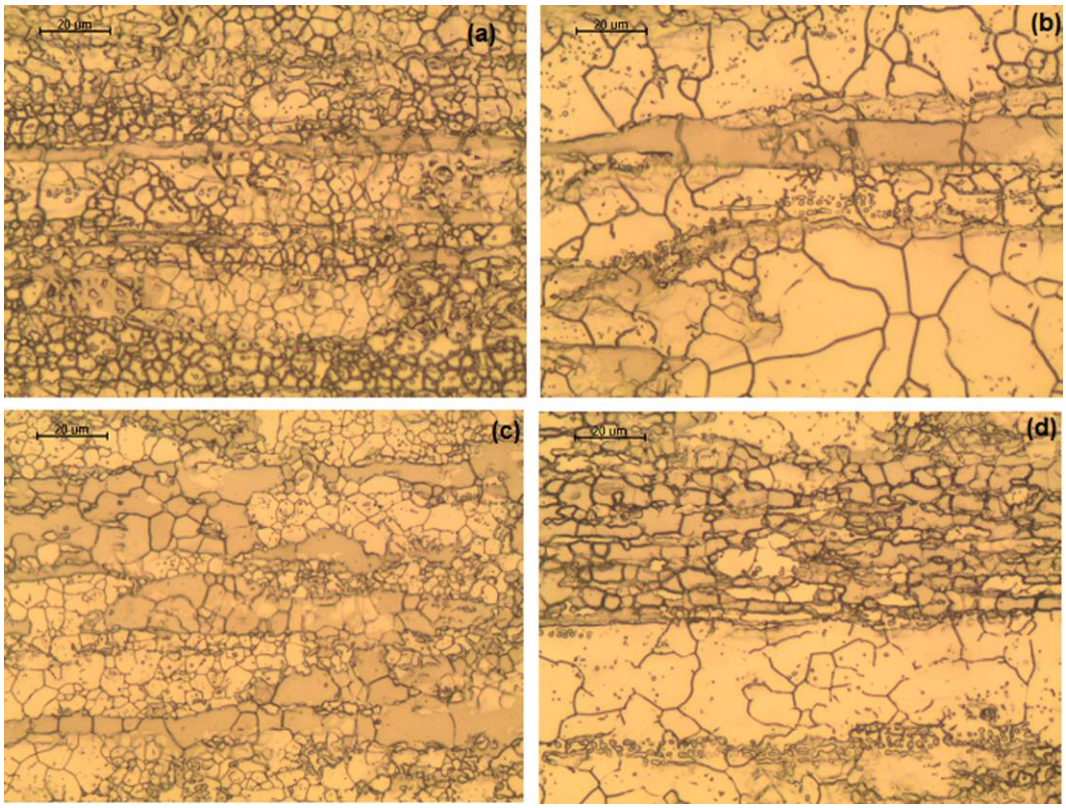

Figure 7.10: Grain boundaries of lean duplex and duplex stainless steels. (a) S31803 CR, (b) S31803 HR, (c) S32304 CR, and (d) S32304 HR.

Cyclic polarization curves (Figure 7.6) showed a possible second passivation region at current density of 10^{-4} A/cm^2. At the applied potential of -150 mV_{SCE}, the current density remained almost constant for the hot-rolled S31803 and the cold-rolled S32304 steels (Figure 7.11). The second passivation layer of hot-rolled S32304 and cold-rolled S31803 was less protective than the layer of the hot-rolled S31803 and cold rolled S32304.

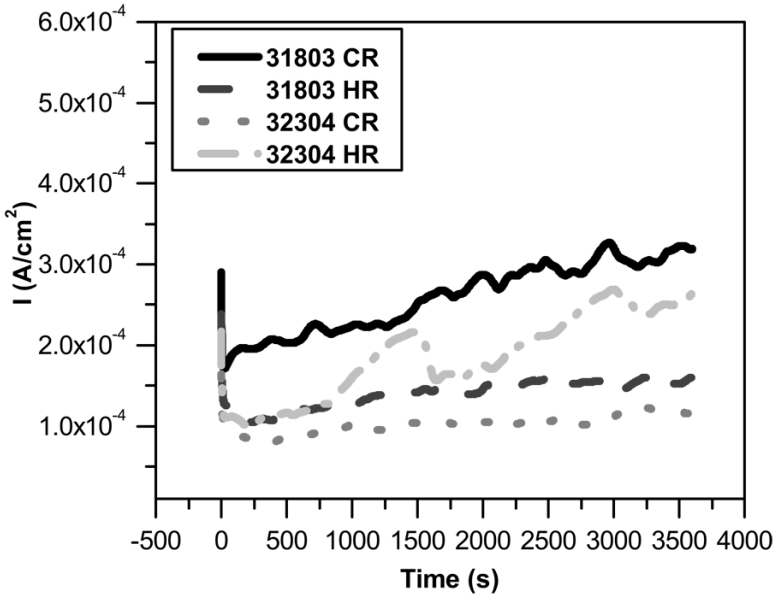

Figure 7.11: Potentiostatic curves at -150 mV_{SCE} of cold and hot rolled S31803 and S32304 steels in green liquor at room temperature.

Temperature plays an important role for steel corrosion in WL by decreasing the transpassive potential as temperature increases (Figure 7.12). The WL was the less aggressive liquor for the duplex steels, which showed the highest values of transpassive potential in this medium.

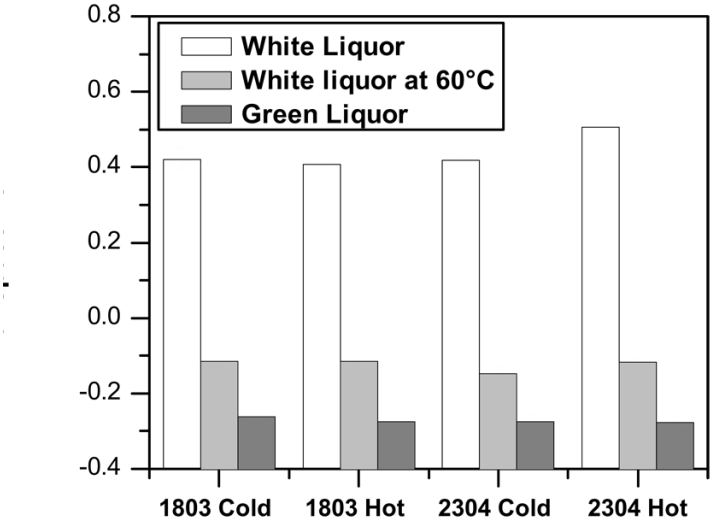

Figure 7.12: Average of the transpassive potential for all duplex stainless steels in industrial white, green liquors.

In addition, cold and hot rolled duplex and lean duplex steels in green liquor showed the lowest values of transpassive potential. Precipitation of carbonate on the steel surface in green liquor, as shown in Figure 7.13 contributed to increase of corrosion process and to decrease the transpassive potential, due to the reduction of effective anodic area.

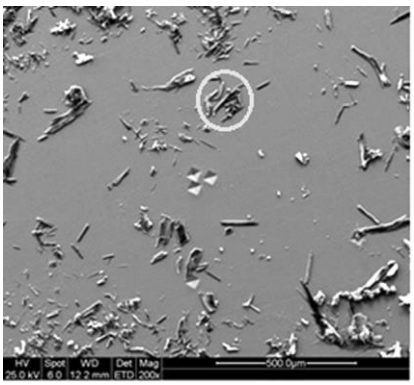

Figure 7.13: SEM micrographs after the cyclic potentiodynamic polarization showing carbonate precipitates on the hot 31803 duplex in green liquor.

Considering the passivation current density as a parameter to evaluate the corrosion behavior of steels, the GL was the most aggressive medium. It is well known that WL is more aggressive liquor due to the alkalinity. However, in this work, the carbonate precipitation plays the main role in the corrosive process, increasing corrosion, and decreasing the transpassive potential. As shown in Figure 7.14, the precipitate was not corrosion product of the steel due to the absence of Fe, Cr, and Ni in its chemical composition. Sodium, sulfur, and oxygen were found in the chemical composition of the precipitate, which is probably a carbonate or sulfide[11].

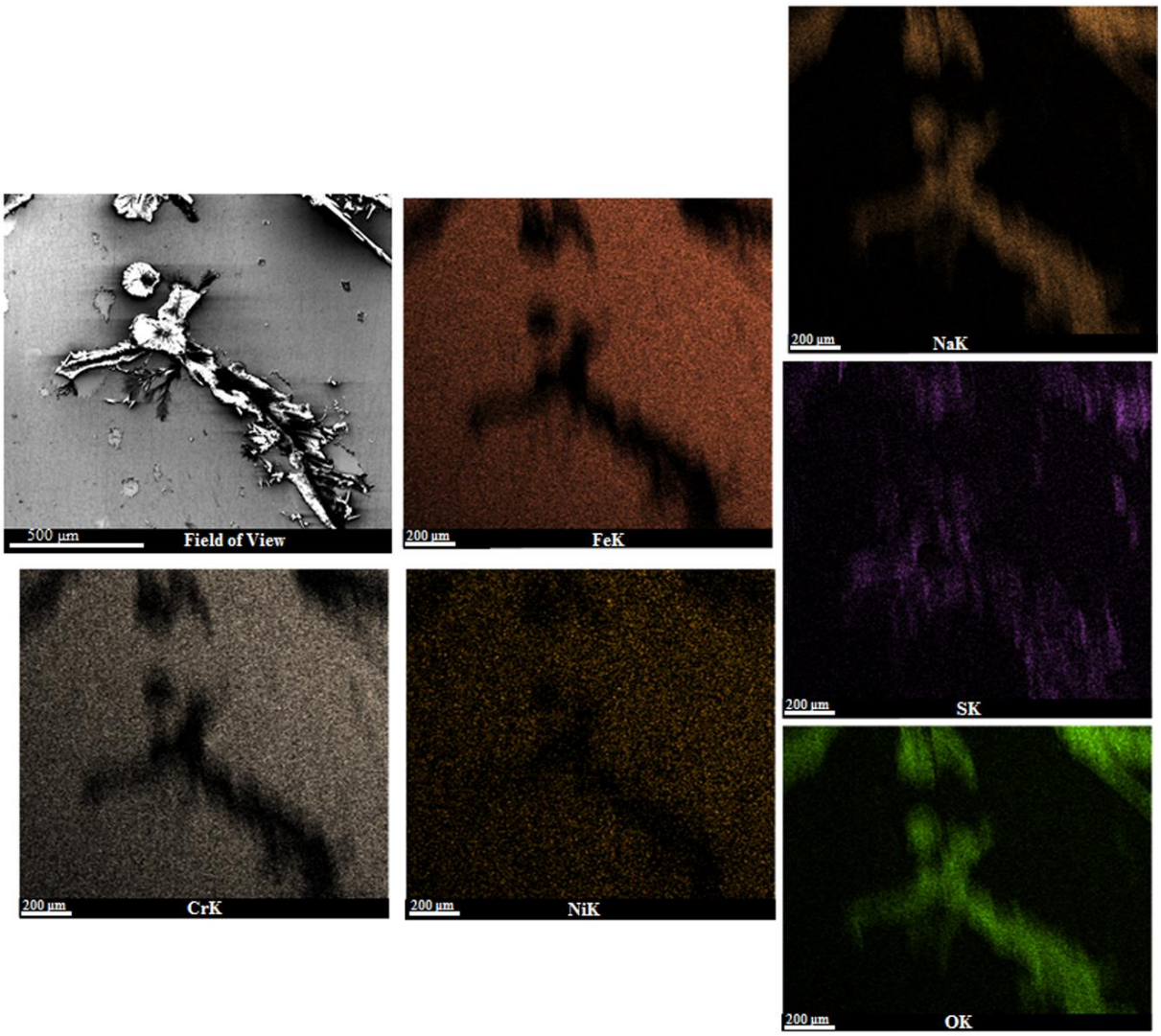

Figure 7.14: SEM micrographs after the cyclic potentiodynamic polarization showing carbonate precipitates on the hot 31803 duplex in green liquor.

7.4 Conclusions

The polarization curves of the S31803 steels in SWL were shifted to lower potentials and higher current densities in relation to the steel in industrial WL, which proved to be less aggressive to the duplex steel.

The average of transpassive potential showed that temperature plays an important role for DSS corrosion in WL decreasing the ETranspassive as temperature increases.

WL was the less aggressive liquor for the duplex steels, which showed the highest values of transpassive potential in this medium.

Cold and hot rolled duplex and lean duplex steels in green liquor showed the lowest values of transpassive potential.

Acknowledgements

The authors are grateful to the Brazilian government agencies (National Counsel of Technological and Scientific Development, Coordenação de Aperfeiçoamento de Pessoal de Nível Superior, and Fundação de Amparo à Pesquisa do Estado de Minas Gerais) for the financial support for this research.

7.5 References

1. Bajpai P. Biotechnology for Pulp and Paper Processing [Internet]. Boston, MA: Springer US; 2012.

2. Bajpai P. Chemistry and Sustainability in Pulp and Paper Industry. Patiala, India: Springer US; 2015. 1-273 p.

3. Russel EH. Near-infrared spectroscopy for on-line analysis of white and green liquors. Tappi J. 1999;82(9):101–6.

4. Hazlewood PE, Singh PM, Hsieh JS. Effect of Black Liquor Oxidation on the Stress Corrosion Cracking Susceptibility of Selected Materials. Corros Sci. 2006;62(9):765–72.

5. J. A. Kent, Handbook of Industrial Chemistry and Biotechnology, (Springer US, New York, 2012) p. 218-222.

6. Demirbas A. Pyrolysis and steam gasification processes of black liquor. Energy Convers Manag. 2002;43:877–84.

7. Wensley A. Corrosion and Cracking of Bottom Scrapers In Continuous Digesters. Natl Assoc Corros Eng. 2005;(5199).

8. Kannan, S; R.G. K. The Role of Dihydroxybenzenes And Oxygen On The Corrosion Of Steel In Black Liquor. Corros Sci. 1996;38(7):1051–69.

9. Bajpai P. Chemical Recovery in Pulp and Papermaking. Surrey, UK: Pira International Ltd; 2008. 1-166 p.

10. Kinnarinen T, Golmaei M, Jernström E, Häkkinen A. Separation, treatment and utilization of inorganic residues of chemical pulp mills. J Clean Prod. 2016;133:953–64.

11. Manskinen K, Nurmesniemi H, Pöykiö R. Total and extractable non-process elements in green liquor dregs from the chemical recovery circuit of a semi-chemical pulp mill. Chem Eng 2011;166(3):954–61.

12. H.Tuthill A. Stainless Steels and Specialty Alloys for Modern Pulp and Paper Mills. Nickel Dev Inst NiDI, Toronto, Canada, 2002;(11):1–22.

13. Cardoso M, de Oliveira ÉD, Passos ML. Chemical composition and physical properties of black liquors and their effects on liquor recovery operation in Brazilian pulp mills. Fuel [Internet]. 2009;88(4):756–63.

14. Bhattacharya A, Singh PM. Electrochemical behaviour of duplex stainless steels in caustic environment. Corros Sci. 2011;53:71–81.

15. Outokumpu. Activating Your Ideas Stainless steel for pulp & paper processes. Outokumpu. Sweden; 2008;1–15.

16. Jiang D, Ge C, Zhao X, Li J, Shi L, Xiao X. 22Cr High-Mn-N Low-Ni Economical Duplex Stainless Steels. J Iron Steel Res Int [Internet]. Central Iron and Steel Research Institute; 2012;19(2):50–56.

17. Wensley A. Pulp and Paper. Baboian R. editor. Corrosion Tests and Standards : Application and Interpretation. 2nd Edition. West Conshohocken, PA: ASM International; 2005. p. 795–811.

18. Wensley A. Corrosion Protection of Kraft Digesters. Corros 2001. (Houston, TX, NACE 2001);(1423).

19. Paoliello F, Lins VFC, Cardoso M. Influence of cooking conditions on continuous digester corrosion in a Brazilian pulp mill. Tappi J. 2011;(August):51–60.

20. Chater BJ. The pulp and paper ind turns to duplex. Stainless Steel World. 2007;7–11.

21. Munro JI. Anodic Protection of Continuous Digesters to Prevent Corrosion and Cracking. Proc TAPPI Eng Conf. 1983;13303:181–185.

22. Singh PM, Anaya A. Effect of wood species on corrosion behavior of carbon steel and stainless steels in black liquors. Corros Sci. 2007:49:497–509.

23. Wensley A. Corrosion in Alkaline Pulping Liquors. NACE. New Orleans, LA; 2004; (4248).

24. Wang, Y.; Singh P. Corrosion Behavior of Austenitic and Duplex Stainless Steels in Thiosulfate and Chloride Containing Environments. Corros Sci. 2015;71(8):1–8.

25. Bhattacharya A, Singh PM. Effect of heat treatment on corrosion and stress corrosion cracking of S32205 duplex stainless steel in caustic solution. Metall Mater Trans A Phys Metall Mater Sci. 2009;40(6):1388–1399.

26. Sharma A. In Plant Test for Corrosion Investigations in Digester of a Paper Mill. JMES. 2013;4(3):420–425.

27. Wensley, Angela; Champagne P. Effect of Sulfidity on the corrosivity of white, green, and black liquors. Corrosion 99. San Antonio, Texas; 1999 (281).

28. Aperam. Aperam,Tech. Data Sheet.2000, p. 1-4.

29. Magnabosco R. Kinetics of Sigma Phase Formation In a Duplex Stainless Steel. Mater Res. 2009;12(3):321–327.

30. Frankel GS. Pit Growth in NiFe Thin Films. J Electrochem Soc. 1992;139(8):2196–2201.

31. Feng H, Li H, Zhang S, Wang Q, Jiang Z, Li G, et al. Corrosion Behavior of Super Duplex Stainless Steel S32750 in White Liquor. Internarional J Electrochem Sci. 2015;10:4116–4128.

32. Michalska J, Sozańska M. Qualitative and quantitative analysis of σ and χ phases in 2205 duplex stainless steel. Mater Charact. 2006;56(4–5):355–362

33. Jimenez JA, Carsi M, Ruano OA. Characterization of a δ / γ duplex stainless steel. J Mater Sci. 2000;35:907–915.

34. Crowe DC. Stress Corrosion Cracking of Carbon Steel in Kraft Digester Liquors. International Conference on Corrosion in the Pulp and Paper Industry. (Helsinki, Finland, August, 1989).

35. Peterman L, Yeske RA. Thiosulfate Effects on Corrosion in Kraft White Liquor. (IPC Tech. Pap. Series, Appleton, Wisconsin, 1986).

36. Zheng ZJ, Gao Y, Gui Y, Zhu M. Corrosion behaviour of nanocrystalline 304 stainless steel prepared by equal channel angular pressing. Corros Sci. 2012;54(1):60–67.

8 CORROSION BEHAVIOR OF DUPLEX AND LEAN DUPLEX STAINLESS STEELS IN BLACK LIQUORS

Luiza Esteves [1], Vanessa F. C. Lins [1]

1 Laboratório de Corrosão e Engenharia de Superfície – UFMG, Avenida Antônio Carlos, 6627,
CEP: 13565-905, Minas Gerais, MG
e-mail: luizaeq@yahoo.com.br
e-mail: vlins@deq.ufmg.br

Abstract

Corrosion behavior of standard (UNS S31803) and lean (S32304) duplex stainless steels was studied using cyclic potentiodynamic polarization (CPP) in 15% solids weak black liquor from an American pulp and paper mill. The duplex steels were studied in cold-rolled and hot-rolled conditions. Results of electrochemical tests showed that cold rolled S32304 steel exhibited the best corrosion behavior in weak black liquor.

Keywords: Duplex stainless steels; Polarization, Alkaline corrosion; Pulp and paper industry

8.1 Introduction

Duplex stainless steel has been an important discovery in the pulp & paper industry over the past 35 years, due to its excellent corrosion resistance, high mechanical strength, and the thickness reductions. Duplex combines a low nickel content (ranging from about 1.5 to 7 wt% nickel) with a high mechanical strength, which makes it an efficient and cost alternative to the austenitic stainless steel grades [1-6].

Wensley and Champagne [6] evaluated the effect of sulfide concentration on the corrosion resistance of carbon steel specimens with different silicon contents (low-silicon A285-Grade C and medium-silicon A516-Grade 70), austenitic stainless steel (UNS S30403) and two DSS (UNS S32304 and S32205) in white, green, weak black, strong black, and flash tank liquors. Stainless steels (UNS S30403, S32304, and S32205) were all highly resistant to corrosion in all the liquors tested, regardless of sulfide content [7, 8].

Black liquor (BL) is the waste from the Kraft process and consists of residual inorganic chemicals (sodium sulfide, sulfate, sodium thiosulfate, sodium carbonate, and sodium hydroxide) after pulping process, numerous organic extractives originated from the specific wood such as organic acids and aliphatic sulfur and other constituents produced due to fragmentation reactions of lignin and its products during the pulping process [9]. The corrosion rate of the equipment in contact with BL depends on changes in pulping parameters or wood species [10, 11], for example, hardwoods result in lower corrosion rates than softwoods [12].

Cardoso *et al.* [13] reported that presence of non-processing elements (NPE) in BL (as potassium, chlorine, calcium, aluminum, silicon and iron ions) could cause incrustation on equipment walls, corroding these surfaces [13].

In this study, the corrosion behavior of DSS with two processing conditions, hot and cold rolled, in a complex solution of inorganic and organic chemicals as BL was investigated. The BL was provided by an America pulp and paper industry which is a novelty of this work as literature usually reports the corrosion behavior of DSS in synthetic liquor [10, 11, 14-15]. Nowadays, DSS and LDSS are primarily considered when selecting materials for the manufacture of digesters. To the best of our knowledge,

literature on corrosion behavior of LDSS and DSS in industrial liquors from pulp and paper industry is scarce and mechanisms involved are not fully understood. LDSS is a DSS with a lower content of molybdenum and nickel providing duplex steel with a lower cost. Nitrogen addition was used in LDSS to obtain the austenite content at a lower nickel concentration [16].

8.2 Materials And Methods

Aperam South America (Brazil) supplied the duplex stainless steels in hot rolled and cold rolled conditions and the chemical composition of steels is shown in Table 8.1. The DSS studied is the UNS S31803 with 5%wt. of nickel and 2.6%wt. of molybdenum and the LDSS is the UNS S32304 with a lower content of nickel (4%wt.) and molybdenum (0.3%wt.). The steels were examined as received: hot rolled coils, annealed at 1075 ± 25°C with 4 mm of thickness and cold rolled coils, annealed at 1070 ± 25 °C, with a thickness of 1.8 mm.

The steel sheets were cut in dimensions of 1 cm x 1 cm in the rolling direction. The samples were embedded in epoxy resin. The electrical connections necessary for the tests were made by welding a copper wire on the sample surface, which was not in contact with the electrolyte. The surface samples were wet ground consecutively to 1200 grit SiC abrasive papers and ultrasonically cleaned in ethanol. In orders to avoid crevices, the samples were masked with black wax.

A North American pulp and paper company supplied the BL. The BL consisted of residual inorganic chemicals (sodium sulfide, sulfate, sodium thiosulfate, sodium carbonate, and sodium hydroxide) and organic extractives originated from wood, and other constituents due to fragmentation reactions of lignin, at pH 13. Weak black liquor (BL) containing 15% of solids. The BL was originated by southern hardwood mix supplied by a North American company.

The metallographic analysis was performed after etching the steel samples in modified Behara reagent [80 mL distilled and deionized water, 20 mL hydrochloric acid (HCl), and 1 g of potassium metabisulfite ($K_2S_2O_5$)]; 2 g of ammonium difluoride (NH_4H HF) were added to this stock solution just before the etching [17].

Reference 600 Gamry potentiostats were used for the electrochemical tests. An electrochemical cell of three electrodes was used. The DSS and LDSS are the working electrodes; the counter electrode was

platinum and the reference electrode was saturated calomel electrode (SCE). The polarization curves were collected at a scan rate of 0.60 V/h, from the corrosion potential (Ecorr) and scanned to the anodic direction until a transpassive potential. When the current reached 3 mA/cm^2 the scan was reversed. All the electrochemical measurements were repeated at least three times to ensure the reproducibility.

Table 8.1: Chemical composition of the DSSs investigated (wt%).

Steel	Rolling	Cr	Ni	Mo	N	C	Si	Mn	S
31803	**Cold**	22.43	5.34	2.67	0.11	0.012	0.29	1.85	0.0004
31803	**Hot**	22.45	5.31	2.63	0.11	0.013	0.38	1.81	0.0005
32304	**Cold**	22.40	4.10	0.29	0.14	0.015	0.46	1.55	0.0002
32304	**Hot**	22.87	4.20	0.27	0.15	0.011	0.20	1.45	0.0004

8.3 Results

Figure 8.1 shows typical microstructures found in as-received duplex stainless (a) hot rolled UNS S31803 steel, (b) cold rolled UNS S31803 steel, (c) hot rolled UNS S32304 steel and (d) cold rolled UNS S32304 steel, respectively, containing only austenite (lighter) and ferrite phases (dark).

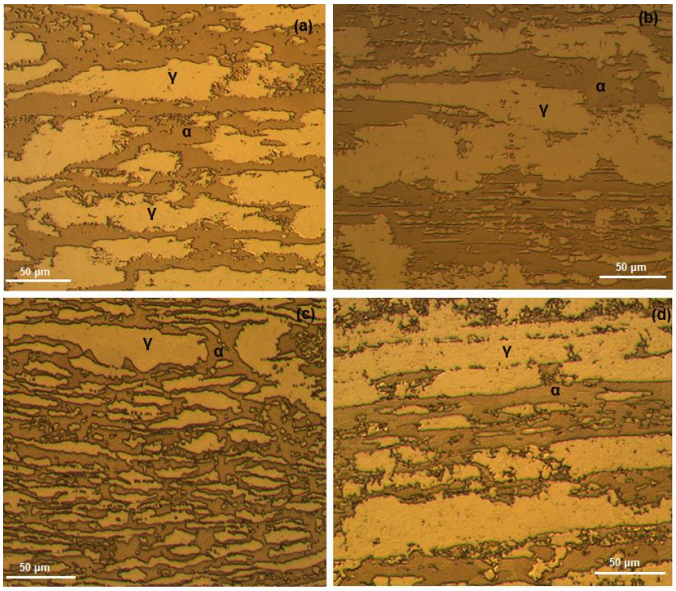

Figure 8.1: Microstructures in duplex stainless (a) hot rolled UNS S31803 steel, (b) hot rolled UNS S31803 steel, (c) hot rolled UNS S32304 steel, and (d) cold rolled UNS S32304 steel (austenite (lighter) and ferrite phases (darker)).

Corrosion resistance of duplex steels in white liquor has been widely studied; however, there is little information of steel corrosion in BL [3]. Figure 8.2 shows the polarization behavior of DSSs (S31803 cold rolled, S31803 hot rolled, S32304 cold rolled, S32304 hot rolled) in BL, pH 13, at room temperature.

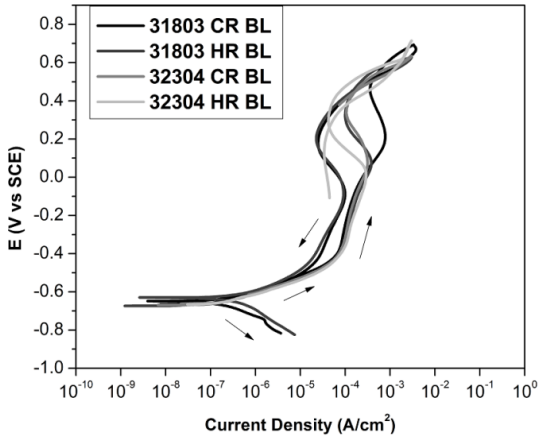

Figure 8.2: Cyclic potentiodynamic polarization curve of cold and hot rolled UNS S31803 and UNS S32304 steels in black liquor at room temperature.

Figure 8.3 shows the transpassive potential for the cold and hot rolled steels in BL provided by a pulp and paper industry.

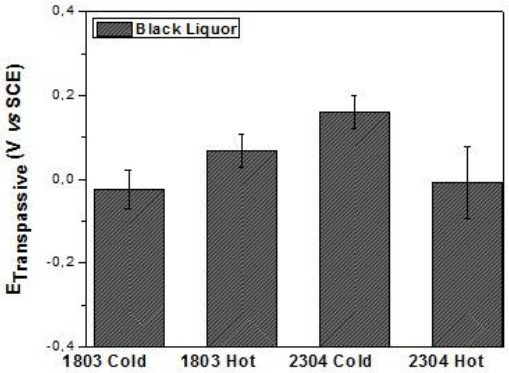

Figure 8.3: Average of the transpassive potential for all duplex stainless steels in industrial BL.

8.4 Discussions

BL is a complex solution that contains inorganic ions (Na^+, OH^-, S^{2-}, SO_4^{2-}, $S_2O_3^{2-}$, CO_3^{2-}) and organic substances originated from the decomposition of wood (lignin, catechol, cellulose) [9]. This is the source of the complexity shape of the polarization curves. It should be noted that these curves are

reproducible. A region associated with the oxidation of water with oxygen evolution, with a constant current density of 10^{-4} A/cm^2 was observed above 200 mV_{SCE}. At increasing pH, the limit potential where the water oxidation starts decreases. A negative hysteresis was observed for all curves.

Considering the passivation current density as a parameter to evaluate the corrosion behavior of steels, the BL was an aggressive medium. The duplex steels in BL showed a high passivation current density (10^{-4} A/cm^2). The characteristic passive current density values are in the range of 10^{-7}- 10^{-5} A/cm^2 [18-20]. This high passivation current density can be produced by the reduction of anode area due to precipitation of solids on the steel surface.

In BL, the cold rolled S32304 steel showed the best corrosion behavior, exhibiting the highest transpassive potential among the duplex steels studied. Besides the DSS and LDSS steels in cold rolled condition were submitted to an annealing treatment after rolling, their microstructure makes the steel surface more active than the surface of steels in hot rolled condition. A more active surface contributes to a more efficient passivation. The less noble steel (S32304) in BL electrolyte showed the highest corrosion resistance because its surface is more active and the passivation layer is more protective than the layer of DSS. This is the principle of the high protective character of a titanium oxide layer. Titanium is an active element, with a high oxidation potential, and produces a highly efficient passive layer with a great trend of repassivation [19].

8.5 Conclusions

Corrosion behavior of standard (UNS S31803) and lean (UNS S32304) duplex stainless steels was studied using cyclic potentiodynamic polarization (CPP) in 15% solids weak black liquor from an American pulp and paper mill. The duplex steels were studied in cold-rolled and hot-rolled conditions. Cold rolled S32304 steel showed the best corrosion behavior in black liquor.

2. *ACKNOWLEDGEMENTS*

The authors are grateful to the Brazilian government agencies (CNPq, CAPES, and FAPEMIG) for the financial support for this research. Thanks to Fontana Corrosion Center group.

8.6 References

[1] OUTOKUMPU, *Activating Your Ideas Stainless steel for pulp & paper processes*, Outokumpu, p. 1–15, Sweden. 2008.

[2] JIANG, D., GE, C., ZHAO, X., LI, J., SHI, L., XIAO, X., "22Cr High-Mn-N Low-Ni Economical Duplex Stainless Steels", *Journal of Iron and Steel Research, International*, v. 19, n. 2, p. 50–56, 2012.

[3] WENSLEY, A., "Pulp and Paper", In: SCULLY, Robert Baboian; Sheldon W. Dean Jr; Harvey P. Hack; Edward L. Hibner; John R. (Org.), *Corrosion Tests and Standards: Application and Interpretation*, 2nd Edition. West Conshohocken, PA: ASM International, 2005, p. 795-811.

[4] BENDALL, K. C., "Duplex stainless steel in the pulp and paper industry", Anti-Corrosion Methods and Materials, v. 44, n. 3, p. 170–174, 1997.

[5] AGUIAR, I.V., ESCOBAR, D.P., SANTOS, D.B., MODENESI, P.J., "Microstructure characterization of a duplex stainless steel weld by electron backscattering diffraction and orientation imaging microscopy techniques", Revista Materia, v. 20, n. 1, p. 212–226, 2015.

[6] VILLALOBOS, D.; ALBITER, A.; MALDONADO, C., "Microstructural changes in SAF 2507 superduplex stainless steel produced by thermal cycle", Revista Materia, v. 14, n. 3, p. 1061–1069, 2009.

[7] WENSLEY, A.; CHAMPAGNE, P., "Effect of Sulfidity on the corrosivity of white, green, and black liquors", In: *Corrosion 99*, n. 281, p. 1–5, San Antônio, Texas, April, 1999.

[8] WENSLEY, A., "Corrosion in Alkaline Pulping Liquors", In: NACE, New Orleans, LA, p. 1–13, 2004.

[9] FREDERICK, W.J., Chapter 3 “Black Liquor Properties” In: *Kraft Recovery Boilers*, Adams, T. N. (Eds). TAPPI Press, p.61, Atlanta, 1987.

[10] SINGH, P. M.; ANAYA, A., "Effect of wood species on corrosion behavior of carbon steel and stainless steels in black liquors", Corrosion Science, v. 49, p. 497–509, 2007.

[11] ANAYA, A.; SINGH, P., "Effect of Wood Species on Corrosivity of Black Liquors", In: *Corrosion 2001*, n. 885, p. 1–16, Houston, Texas, 2001.

[12] BAUER, A. D.; LUNDBERG, M., "Choosing materials to solve corrosion problems in the pulp and paper industry", Anti-Corrosion Methods and Materials, v. 44, n. 3, p. 161–169, 1997.

[13] CARDOSO M., OLIVEIRA E. D.; PASSOS, M.L., "Chemical process simulation for minimizing energy consumption in pulp mills", Applied Energy, v. 86, n. 1, p. 45–51, 2009.

[14] HAZLEWOOD, P. E.; SINGH, P. M., HSIEH, J. S., "Linking Extractives to Black Liquor Corrosivity", In: Corrosion Nace, San Diego, California: 06245, v. 61, p. 1–10, 2006.

[15] KANNAN, S., Kelly, R.G., "The Role Of Dihydroxybenzenes And Oxygen On The Corrosion Of Steel In Black Liquor", Corrosion Science, v. 38, n. 7, p. 1051–1069, 1996.

[16] SICUPIRA, D. C., FRANKEL, G.S., DE F. C. LINS, V., “Pitting corrosion of welds in UNS S32304 lean duplex stainless steel". Materials and Corrosion, v. 67, p. 440-448, 2016.

[17] MAGNABOSCO, R., "Kinetics of Sigma Phase Formation In a Duplex Stainless Steel", Materials Research, v. 12, n. 3, p. 321–327, 2009.

[18] MCCAFFERTY, E., *Introduction to Corrosion Science*, Alexandria, VA: Springer-Verlag New York, 2010.

[19] KIM, H. S.; KIM, W. J., Annealing effects on the corrosion resistance of ultrafine-grained pure titanium, Corrosion Scienc**e**, v. 89, n. C, p. 331–337, 2014.

[20] DENG, B., JIANG, J., GONG, J., ZHONG, C., GAO, J., LI, J., "Critical pitting and repassivation temperatures for duplex stainless steel in chloride solutions", Electrochimica Acta, v. 53, p. 5220–5225, 2008.

9 HIGH-TEMPERATURE AND HIGH-PRESSURE CORROSION BEHAVIOR OF DUPLEX STAINLESS STEEL IN WHITE LIQUOR FROM BRAZILIAN PAPER AND PULP MILL

Luiza Esteves*, G. S. Frankel, W. R. C. Campos, M. M. A. M. Schvartzman Vanessa F.C. Lins

LuizaEsteves

Federal University of Minas Gerais, Department of Chemical Engineering, Antônio Carlos Avenue 6627, Brazil, Zip Code 13565-905 Phone Number +553134091737

Wagner reis da Costa Campos
Comissão Nacional de Energia Nuclear, Centro de Desenvolvimento da Tecnologia Nuclear, Antônio Carlos Avenue 6627, Brazil, Zip Code 31270-901

Mônica Maria Abreu Mendonça Schvartzman
Comissão Nacional de Energia Nuclear, Centro de Desenvolvimento da Tecnologia Nuclear, Antônio Carlos Avenue 6627, Brazil, Zip Code 31270-901

Gerald S. Frankel
Fontana Corrosion Center, Department of Materials Science and Engineering, The Ohio State University, Columbus, OH 43210, USA

Vanessa Freitas Cunha Lins
Federal University of Minas Gerais, Department of Chemical Engineering, Antônio Carlos Avenue 6627, Brazil, Zip Code 13565-905 Phone Number +553134091775

luizaeq@yahoo.com.br

Abstract

Specimens of duplex stainless steel (DSS) were exposed at high temperature (200 ºC) in industrial white liquor from a Brazilian kraft mill using an autoclave to simulate the same conditions of a digester processing. Tafel extrapolation method and weight loss were used to evaluate corrosion behavior of duplex steel in white liquor. The corrosion rates of DSSs increase as the temperature increases. Moreover, selective dissolution of the ferrite phase occurred.

Keywords: Duplex stainless steels; Polarization, Alkaline corrosion; Pulp and paper industry

9.1 Introduction

Duplex stainless steel (DSS) has been an important discovery in the pulp & paper industry over the past 35 years, due to its excellent corrosion resistance, and high mechanical strength that allows thickness reductions. Duplex combines a low nickel content (ranging from about 1.5 to 7wt% nickel) with a high mechanical strength, which makes it an efficient and cost alternative to the austenitic stainless steel grades [1-4].

DSS have a dual phase microstructure with equal amounts of austenite and ferrite [5, 6]. Laboratory autoclaves are used to investigate the effect of organic species on steel corrosion in digester liquors [7-15].

The effect of high (40%) sulfidity and low (30%) sulfidity on the steel corrosion was studied in white (98°C), green (96°C), weak black (92°C), strong black (102°C), and flash tank liquors (170°C) using carbon steel specimens with different silicon contents (low-silicon A285-Grade C and medium-silicon A516-Grade 70), austenitic stainless steel (UNS S30403) and two DSS (UNS S32304 and S31803) [9]. The corrosion tests were carried out in stainless steels autoclaves and a reference electrode of pure molybdenum (Mo) was used due to compatibility with sulfides in these liquors. Stainless steels (UNS S30403, S32304, and S31803) were all highly resistant to corrosion in all the liquors tested, regardless of sulfidity [9, 10]. Another study evaluated the electrochemical behavior of carbon steel at 150°C in alkaline sulfide solutions using an autoclave; counter electrode was a graphite rod and an external silver/silver sulfide as a reference electrode was used, they developed potential-pH (E-pH) diagrams indicating thermodynamically stable compounds at given potentials and pH that were used to interpret the observed corrosion behavior. The polarization behavior indicated increased anodic currents resulted from sulfide interfering with passivation. Dissolution, which increased in the presence of sulfide, was associated with formation of iron sulfides, producing a less protective film composed of iron oxides and iron sulfides. Thus, higher corrosion rates and difficulty to generate the passive layer on the surface of the steel in liquor with higher sulfide concentration occur [16].

In the pulp and paper mill industry, corrosion in digesters is a relevant problem due to the presence of sulfate, sulfide, and chloride in liquors. Sharma *et al*., (2013) developed a study in-plant of six months

duration of a bottom part of a batch digester, made of mild steel of 85 m^3 in volume. The wood chips are filled in the digester and cooking liquor is then charged keeping liquor to the wood ratio as 1:2.8. The volume of cooking liquor inside the digester was kept between 37 and 42 m^3. The cooking liquor consists of mainly sodium hydroxide (NaOH) (92 gpl as NaOH) and sodium sulfide (Na_2S) (22.4 gpl as NaOH) having pH ~13.2. Maximum temperature attained during the pulping process is 168ºC and it operates at a pressure of 6.2 $kgf.cm^{-2}$. The materials studied in-plant test are mild steel, austenitic (stainless steel) SS 304L and SS 316L, DSS32205 and lean duplex stainless steel (LDSS). The results showed that mild steel (MS) experienced the highest corrosion rate while DSS showed the lowest corrosion rate. The bottom part of the digester can be constructed of DSS without severe risk of corrosion [17].

The current manuscript aims at evaluating the corrosion behavior of duplex steels in industrial white liquor. The study was developed by using an autoclave for electrochemical measurements and weight loss comparing the standard DSS (UNS 31803) and lean duplex (LDSS) (UNS 32304) in industrial white liquor (WL) provided by a Brazilian paper and pulp mill.

9.2 Materials and Methods

The UNS S31803 and UNS S32304 duplex steels had the chemical composition given in Table 9.1 and were received as a 3.85 mm thickness sheet, annealed at 1075 ± 25°C. The length described was maintained parallel to the rolling direction.

Table 9.1: Chemical composition of the investigated DSS (wt. (%)).

Steel	Cr	Ni	Mo	Mn	Si	N	C	Fe
S31803	22.45	5.31	2.63	1.81	0.38	0.11	0.013	Balance
S32304	22.87	4.20	0.27	1.45	0.20	0.15	0.011	Balance

9.2.1 Steel characterization

Metallographic samples were prepared with conventional polishing and electrolytic etching in 10% acid oxalic solution at 1.5 V for 30 s. Austenite and ferrite volume fractions were estimated by using the

Image pro software. The microstructure analyses were carried out using an optical light microscope (LOM, LeitzMetalloplan).

9.2.1 Electrolyte

Tests performed in industrial white liquor (WL) provided by Cenibra - Belo Oriente, MG – Brazil (the liquor was shipped in full container and stored cold to minimize decomposition or oxidation). According to Brazilian standards WL: TTA (total titratable alkali): 140 ± 10 $g.L^{-1}$ (as NaOH), EA (effective alkali): 110 ± 10 $g.L^{-1}$ (as NaOH), sulfidity: 25 ± 2%, causticizing efficiency: 82 ± 2%, total suspended solids <100 $mg.L^{-1}$, and pH > 12.

9.2.2 Electrochemical tests

An Autolab PGSTAT 100 potentiostat was used for the electrochemical tests at room temperature (RT). The polarization curves were collected by scanning to the anodic direction at 0.167 mV/s from the corrosion potential (E_{corr}). Transpassivity was observed in all cases, and the scan was reversed when the current reached 5 mA/cm^2.

In order to simulate the cooking process inside the digester an autoclave made of a 316 L stainless steel (1 L) was used at 200ºC and at 18 bars (1.8 Mpa). Precautions were taken to avoid any contact between the test samples and the autoclave to eliminate any galvanic effect. The samples were placed on a polytetrafluoroethylene (PTFE) plate [18] to isolate from the autoclave. Samples for the Tafel extrapolation tests had a dimension of 10 mm in length and 10 mm in width. The samples were ground with SiC up to 1200 grit, cleaned with acetone, and the surface was measured. Tafel tests were carried out using the DSS as a working electrode, a platinum foil as a counter electrode and a yttrium-stabilized zirconia (YSZ) electrode filled with a mixture of Ni/NiO powder as the reference electrode (YSZ(Ni/NiO) (Figure 9.1). A conversion factor of -1.32 V for the temperature and pH conditions of the test was used to convert the measured values to saturated calomel electrode (V_{SCE}) according to the Boch's work [19-22]. The scan rate was 0.167 $mV.s^{-1}$. Open circuit potential (OCP) data were collected for 15 min; this time was optimized after a study of OCP for 24 h. All electrochemical measurements were repeated at least three times to ensure the reproducibility.

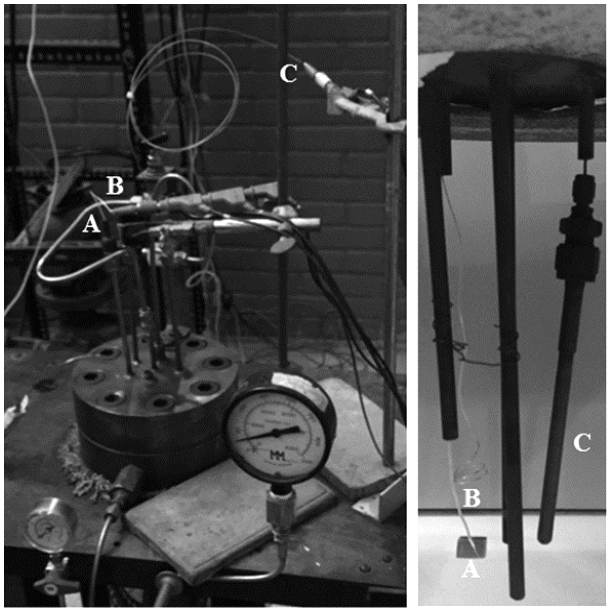

Figure 9.1: (a) Electrodes in an autoclave and (b) details of electrochemical measurements, A: work electrode, B: platinum counter electrode, C: YSZ(Ni/NiO) as reference electrode.

9.2.3 Weight loss

The corrosion rate was measured by using the weight loss method. Samples for the corrosion rate tests had a dimension of 15 mm in length and 10 mm in width. The samples were scraped with SiC paper up to 2000 grit. Then, the samples were cleaned, degreased, dried and weighed using an analytical balance and their area was measured before mounting. Precautions were taken to avoid any contact between the test samples (Teflon rods) and the autoclave (PTFE jacket) to avoid any galvanic effects. Autoclave with a volume of 0.3 L type was constructed using type 316 L stainless steel. Up to 3 samples were tested simultaneously (Figure 9.2). They were immersed in the autoclave at 170 ± 5ºC for 15 days. There was no agitation. After the experiment, the samples were rinsed with distilled water and acetone, dried, and then corrosion products on the metal surface were removed using Clarke's solution. The final weight of each sample was measured and was used to calculate the rate of general corrosion for each sample. It was confirmed that Clarke's solution (a combination of hydrochloric acid and inhibitors) [23] neither attacked the base DSS metal during the cleaning time nor affected the final weight measurements [18]. A Jeol JXA-840 microscope was used. EDS analyses were made using a Jeol JXA-8900 RL WD/ED combined with a microanalyser.

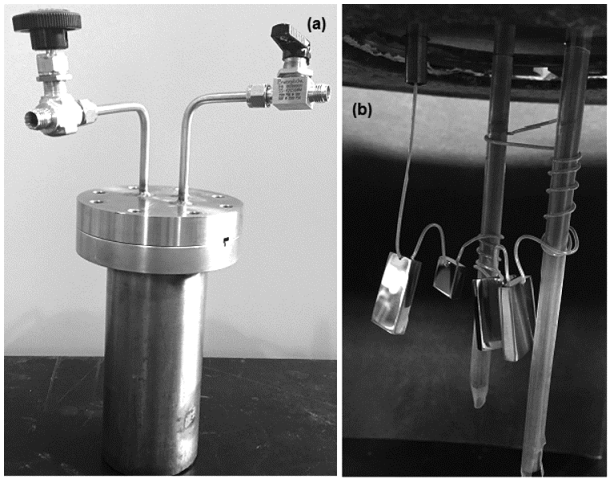

Figure 9.2: (a) Autoclave set up, and (b) Electrodes disposition in autoclave used to evaluate weight loss.

9.3 Results and Discussion

9.3.1 Steel characterization

Figure 9.3 shows the microstructure of the DSS as received. Lighter austenite (γ) islands are embedded in the darker etched ferrite (α) matrix with no other secondary precipitates [24]. The Image pro software was used to determine the contents of austenite and ferrite in DSS as received. The hot rolled S31803 contained 50% of austenite and 50% of ferrite and the hot rolled S32304 had 46% of austenite and 54% of ferrite [25].

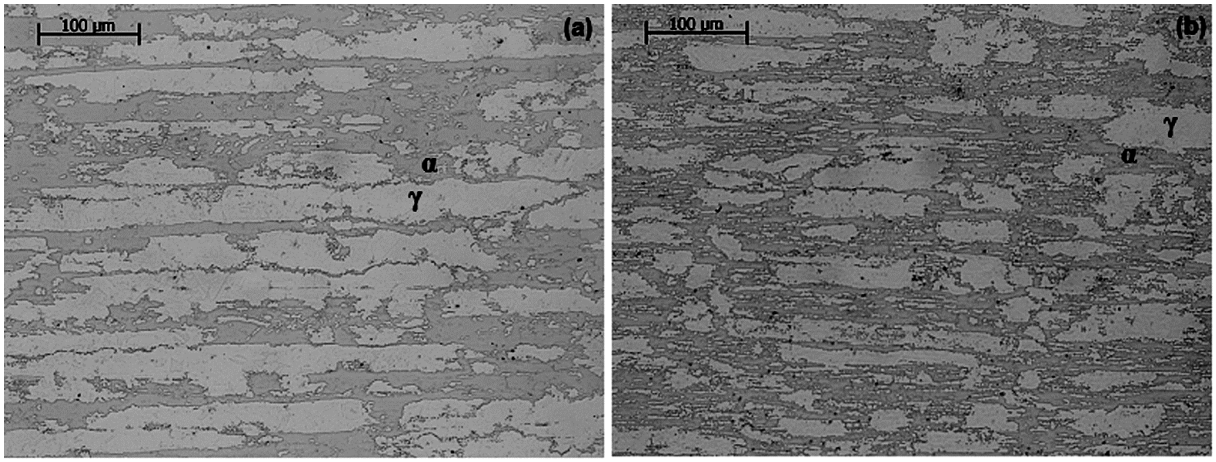

Figure 9.3: Typical microstructures found in the studied: a) hot rolled UNS S31803 DSS and b) UNS 32304, showing ferrite (darker) and austenite (lighter).

Figure 9.4 and Table 9.2 show the microstructure and microanalysis of austenite and ferrite phases in hot rolled DSS S32304 as received. The chemical composition of austenite and ferrite phases was different due to different contents of Cr, Ni, and Mo. The microstructure depends on the chemical composition of the alloy and the heat treatment conditions [26]. The ferrite stabilizers are chromium, silicon, molybdenum, titanium and niobium and the austenite stabilizers are nickel, carbon, copper, nitrogen, manganese [27].

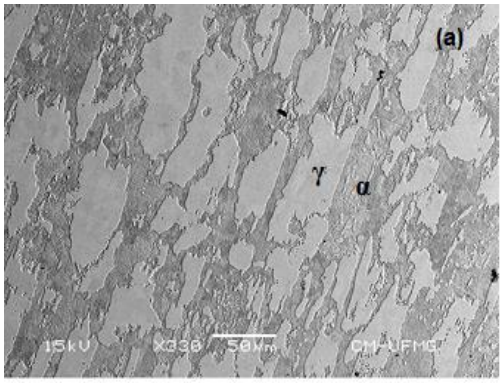

Figure 9.4: Typical microstructure of the hot rolled UNS S32304 DSS studied as received, showing ferrite (dark phase) and austenite (light gray phase). Etching: Behara Modified used to EDS analysis.

Table 9.2: Chemical composition of austenite and ferrite in DSS using EDS analysis.

		Content of Chemical Elements (wt%)				
Material	**Phase**	**Cr**	**Ni**	**Mo**	**Mn**	**Fe**
S32304	Austenite	20.62	4.90	0.09	0.90	71.38
	Ferrite	24.17	2.99	0.19	0.71	69.87
S31803	Austenite	20.22	6.43	1.59	1.48	67.72
	Ferrite	23.71	3.83	2.76	1.21	66.15

9.3.2 Electrochemical tests at room temperature (RT)

Cyclic potentiodynamic polarization (CPP) shows positive hysteresis (Figure 9.5), but pits were not obseved using an optical microscope (OM) analysis after linear polarization. However, as shown in Figure 9.6, a corrosion attack at interfaces between ferrite and austenite was found. The phases were also revealed after the linear polarization. Pits were not observed on the steel surfaces, in contrast,

the phase boundaries were attacked in both DSSs. Hence, the curves for DSSs showed a wide passivation region (around -800 mV_{SCE} to 0 mV_{SCE}) at room temperature in contrast what occurred in high temperature. In conclusion, temperature plays an important role in attaining protective layers on DSSs. An aggressive condition of high temperature and pressure inhibits the formation of a protective layer on DSS surfaces as in the other severe conditions such as very low pH.

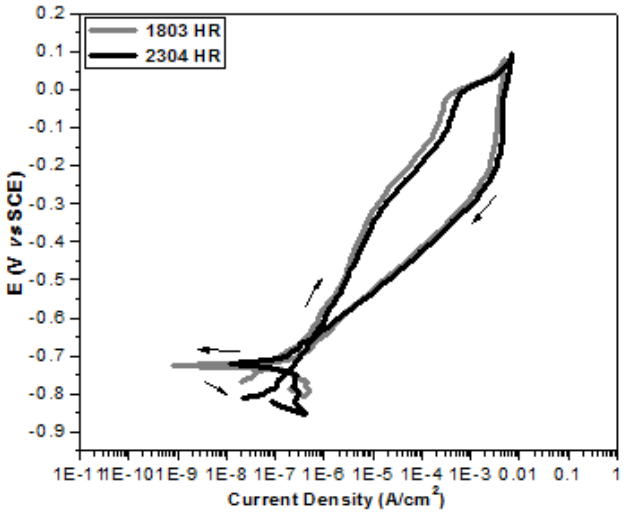

Figure 9.5: Cyclic polarization curves of S31803 and S32304 in industrial white liquor at 200 ºC.

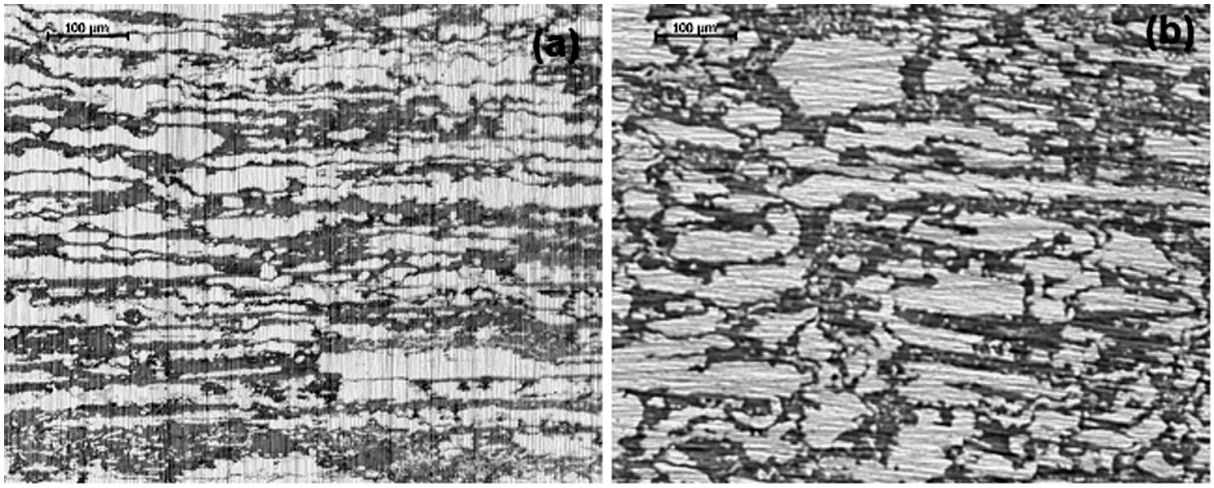

Figure 9.6: Optical microscope (OM) after linear polarization: (a) S31803 and (b) S32304.

9.3.3 Tafel tests of DSS S31803 and S32304 in industrial white liquor at 200ºC

Figure 9.7 and 9.8 showed stabilized Open Circuit Potential (OCP). DSS 31803 had the noblest corrosion potential which could be associated with the higher content of Cr and Ni, which might have contributed to the corrosion resistance of the steel. In prior study is related that Mo can be detrimental to the corrosion resistance of the steel at high temperatures [14]. The stabilization time of OCP was studied in advanced for 24 h and the optimized time of 15 minutes was determined.

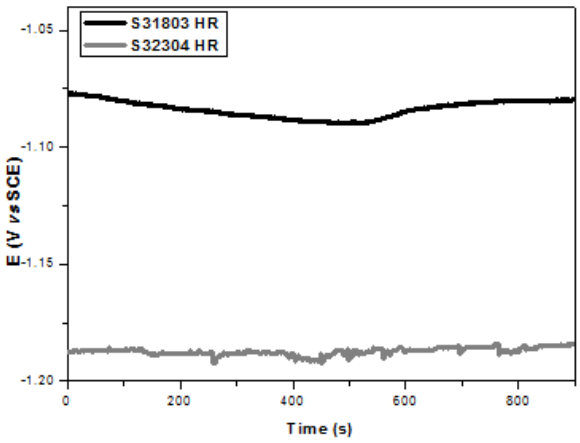

Figure 9.7: Comparing OCP stabilized of S31803 and S32304 in industrial white liquor at 200 ºC.

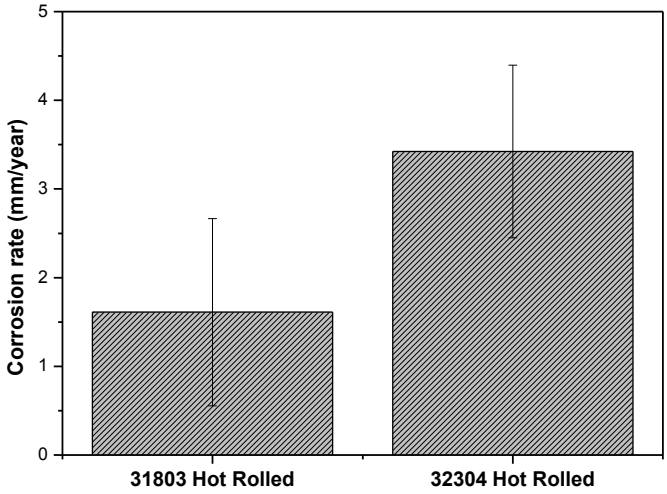

Figure 9.8: Comparing corrosion rate of S31803 and S32304 in industrial white liquor at 200 ºC.

Figure 9.9 shows the results of Tafel extrapolation of DSS in industrial WL at 200ºC. The increase of temperature and pressure in this caustic-sulfide medium may affect passive film formation. The current density increased quickly and did not show any passive region. For this reason, Tafel extrapolation method was used to evaluate the corrosion rate. On the other hand, a generalized corrosion did not occur as previously expected, and ferrite and austenite phases did not corrode uniformly. In DSSs, Cr, Mo, Ni and N are not uniformly distributed between ferrite and austenite phases and this heterogeneity may lead to galvanic interactions, which result in a difference in corrosion behavior between these phases [28]. And also, more corrosion products were visualized on the surface of austenite phase (Figure 9.8a), which indicated that ferrite corroded preferentially. Selective dissolution was already reported in literature [29-32]. This selective attack was more evident for the DSS S31803 than the DSS S32304 (Figure 9.10). EDS (Figure 9.11) showed corrosion products concentrated in the austenite phase, due to the formation of a film containing elements from electrolyte, such as Na, S, O, and a higher content of Ni, an austenite stabilizer. Moreover, the steel showed a higher content of Cr (ferrite former) in the local without corrosion products. The metal ions generated on the ferrite surface probably had higher diffusion rates than the anions formed on the austenite region and the corrosion products were found on the cathode area (austenite). The corrosion rate can be calculated using Tafel analysis for general corrosion and using immersion tests to determine the corrosion rate for the DSS at high temperature.

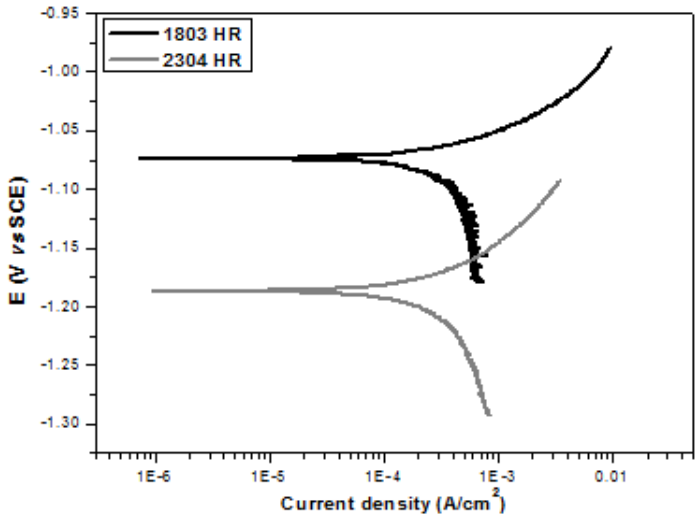

Figure 9.9: Tafel plots: S31803 and S32304 in industrial white liquor at 200ºC.

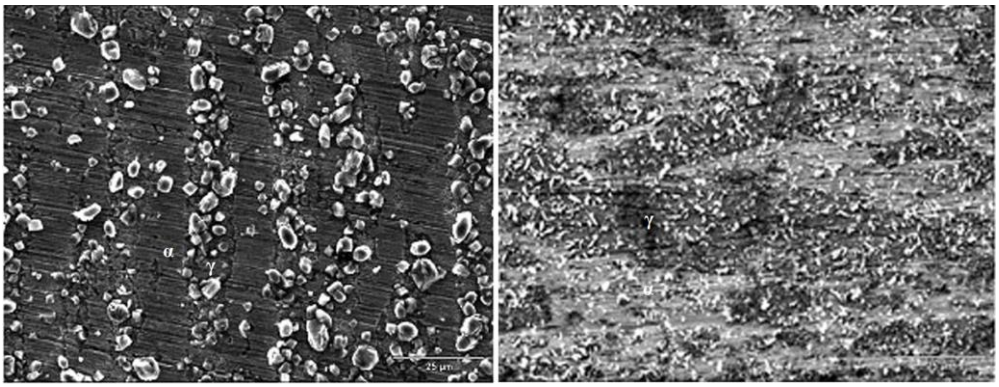

Figure 9.10: SEM micrographs of (a) S31803 and (b) S32304 after Tafel extrapolation method in industrial white liquor at 200ºC.

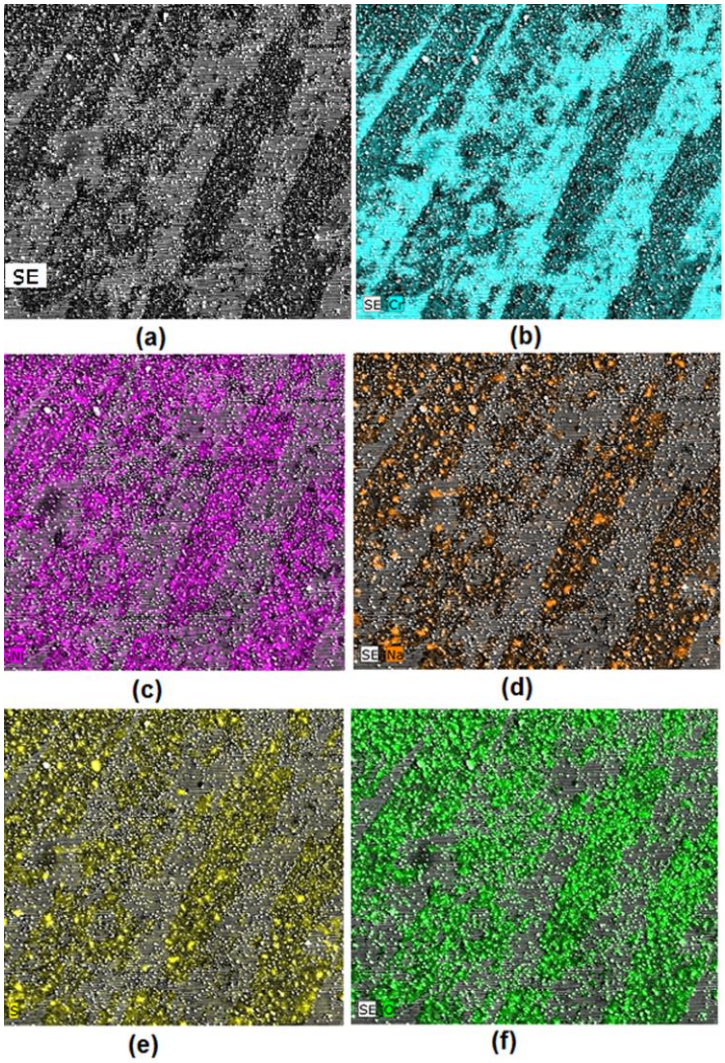

Figure 9.11: Mapping data obtained by EDS: (a) field of view in S31803, distribution maps of (b) Cr, (c) Ni, (d) Na, (e) S, and (f) O, after Tafel extrapolation in industrial white liquor at 200°C.

9.3.4 Weight loss

The corrosion rate was determined using immersion tests for 15 days at 170°C. The operation temperature of a digester in paper and pulp mill is 170°C, and this temperature was used to simulate industrial conditions. For the electrochemical tests, a higher temperature was used (200°C) due to the characteristic of the reference electrode. Table 9.3 shows the corrosion rate obtained using weight loss for three samples of DSSs.

Table 9.3: The weight loss measurements test results.

Corrosion rate (mm/year)		
S31803	Sample 1	0.04
	Sample 2	0.11
	Sample 3	0.07
S32304	Sample 1	0.14
	Sample 2	0.07
	Sample 3	0.08

The average of corrosion rate for S31803 was 0.07 ± 0.04 mm.year^{-1} and for S32304 was 0.09 ± 0.04 mm.year^{-1}. As has been noted in Table 9.3, the heterogeneity of the DSSs probably affected the corrosion behavior by using the weight loss method for 15 days. Assuming that the immersion test could reproduce a similar process of the digester, this analysis is more reliable than the Tafel extrapolation. The DSS S31803 and DSS 32304 had very low corrosion rates [33] in industrial white liquor as already reported by Wensley (2004) for 2205 duplex stainless steel [10, 14].

The average corrosion rate obtained by using the immersion tests for S31803 was 1.61 ± 1.06 mm.year^{-1} and by using Tafel analysis was 3.42 ± 0.97 mm.year^{-1}. It is important to be aware that immersion tests were carried out at 170 ± 5ºC and Tafel plots were performed at 200°C, the temperature played an importante role in the corrosion process, and the weight loss method is more similar to the service conditions than the Tafel extrapolation, an accelerating corrosion test. These could explain the differences observed between the results of immersion tests and Tafel extrapolation. Hence, the selective attack identified after Tafel measurements suggests that corrosion rate can not

be calculated by Tafel extrapolation, it is known that this tecnique should be applied for uniform corrosion. For this reason, immersion tests may be better tool to evaluate the corrosion rate for DSS in sulfide-containing caustic enviroment.

9.4 Conclusions

The S31803 steel showed a selective corrosion attack on the ferrite regions after Tafel analysis at 200ºC and high pressure. Corrosion product was identified mainly on the austenite islands. The S31803 and S32304 did not show a passivation region in industrial white liquor at 200°C and high pressure.

The corrosion rate of S31803 steel after immersion for 15 days in industrial white liquor was lower than the corrosion rate of S32304 steel.

Acknowledgements

The authors are grateful to the Brazilian government agencies (CNPQ, CAPES and FAPEMIG) for the financial support for this research and Centro de Desenvolvimento da Tecnologia Nuclear – CDTN for the technical support. They also thank Antônio Edicleto Gomes Soares for his help during the performance of electrochemical tests at high temperature.

9.5 References

[1]Outokumpu; Activating Your Ideas: Stainless steel for pulp & paper processes, Outokumpu, Finland **2008**.

[2] D. Jiang, C. Ge, X. Zhao, J. Li, L. Shi, X. Xiao, J. Iron Steel Res. **2012**, Int. 19, 50.

[3] A. Wensley, Pulp and Paper, in: Corros. Tests Stand. Appl. Interpret., ASM International, West Conshohocken, PA **2005**.

[4] K. C. Bendall, Anti-Corrosion Methods Mater. **1997**, 44, 170.

[5] G. Krauss, Steel Processing, Structure, and Performance, ASM International, Ohio **2005**.

[6] P. Marcus, F. Mansfeld, F. Marcus, Philippe Mansfeld, Analytical Methods In Corrosion Science and Engineering, Taylor & Francis Group, Boca Raton, Florida **2006**.

[7] Anaya, A.; Singh, presented at Corrosion 2001, Houston, Texas, 11-16 March **2001**, pp. 1-16.

[8] A. Wensley, presented at Eng. Conf. in TAPPI Proceedings, Chicago, IL, 16-19 September, **1996**, pp.1-8.

[9] A. Wensley, P. Champagne, presented at Corrosion 99, San Antonio, Texas, 25-30 April, **1999**, pp. 1-5.

[10] A. Wensley, presented at Corrosion 2004, New Orleans, Louisiana, 28 March-1 April, **2004**, pp.1-16.

[11] A. Wensley, Corrosion 2006, San Diego, California, 12-16 March, **2006**, pp.1-19.

[12] P. E. Hazlewood, PhD. Thesis, Georgia Institute of Technology, USA, **2006**.

[13] J. Alfonsson, E.; Olsson, presented at Corrosion 99, San Antonio, Texas, 25-30 April, **1999**, pp. 1-7.

[14] A. Bhattacharya, P.M. Singh, Corros. Sci. **2011**, 53, 71.

[15] D. C. Crowe, D. Tromans, Corrosion,**1988**, 44,142.

[16] D.C. Crowe, D. Tromans, Corrosion, **1986**, 42, 409.

[17] A. Sharma, JMES. **2013**, 4, 420.

[18] A. Bhattacharya, P.M. Singh, Corrosion, **2008**, 64, 532.

[19] R-W. Bosch, Z. Kerner, G. Nagy, D. Féron, M. Navas, W. F. Bogaerts, D. Kárnik, T. Dorsch, R. Kilian, M. Ulberg, A. Molander, K. Mäkelä, T. Saario, presented at Proc. 11th Int. Conf. Env. Deg. of Mater. in Nuclear Power Syst., Stevenson, WA, August, **2003**.

[20] R-W, Bosch; D. Féron; J.-P; Celis; Electrochemistry in light water reactors: Reference Electrodes, measurement, corrosion and tribocorrosion issues. Woodhead Publishing Limited (England) and CRC Press LLC (Washington, DC). Published by European Fed. of Corr. Pub. Nº49 **2007**.

[21] L. I. L. Lima, M.M.A.M. Schvartzman, C.A. Figueiredo, A.Q. Bracarense, Corrosion. **2011**, 67, 085004-1.

[22] C. De Araújo Figueiredo, R.W. Bosch, M. Vankeerberghen, Electrochim. Acta. **2011**, 56, 7871.

[23] S. A. Wade, presented at Corros. Prev., Adelaide, South Australia, 15-18 November, **2015**, pp. 1-9.

[24] J. Michalska, M. Sozańska, Mater. Charact. **2006**, 56, 355.

[25] L. Esteves, V.F.C. Lins, A.K.N. Viana, P.R.P. Paiva, , Materials Research. **2016**.

[26] A. Itman, F.; R. V. Silva, W. S. Cardoso, L. C. Casteletti. Materials Research. **2014**, 17, 801.

[27] A. E. Yonekubo, MSc Thesis, Universidade Estadual De Ponta Grossa, Brazil, **2010**.

[28] M. Femenia, J. Pan, C. Leygraf, J. Electrochem. Soc. **2004**, 151, B581.

[29] I. H. Lo, Y. Fu, C. J. Lin, W. T. Tsai, Corros. Sci. **2005**, 48, 696.

[30] M. Femenia, J. Pan, C. Leygraf, P. Luukkonen, Corros. Sci. **2001**, 43, 1939.

[31] F. Zanotto, V. Grassi, A. Balbo, C. Monticelli, F. Zucchi, Corros. Sci. **2014**, 80, 205.

[32] M. Femenia, J. Pan, C. Leygraf, J. Electrochem. Soc. **2002**, 149, B187.

[33] E. Mattsson, Basic electrochemical concepts, 2nd Edition, The Chameleon Press Ltd, London, 2001.

10 MICROELECTROCHEMICAL TESTING: MICROCELL TECHNIQUE

The microcell technique could be applied to study the influence of the corrosion resistance of the single-phase austenite and ferrite of duplex stainless steels (DSS) on the entire metal (Marcus, 2006).

Microelectrochemical techniques using microcapillaries as microcells are powerfull methods to study local processes on metal surfaces (Suter, 1997). The cell setup for the microelectrochemical investigations is shown in Figure 10.1 and consists of three electrodes (counter, reference and working). The microcapillary replaces the objective in the microscope and is filled with the electrolyte/solution studied (Suter, 1998). Suter and Böhni, (2001), have described capillary preparation.

The microcell consists of a pulled microcapillary filled with solution. The tip diameter of the capillary can be varied from about 1 to 1000 µm depending on the experimental requirements (Marcus, 2006; Suter, 2001; Birbilis, 2005).

Suter (2001) evaluated the localized corrosion processes of stainless steel 304 in 1 M NaCl. The setup for microelectrochemical investigations is shown in Figure 10.1. Different modifications of the microcells allow evaluating additional parameters during a corrosion experiment or to perform corrosion measurements under different conditions such as pH measurements, measurement with temperature control, with mechanical stress, with friction, and with flow. Local potentiodynamic polarization curves were measured at random sites on a low sulfur 304 plate (0.003%S) in 1 M NaCl. The diameter used of the microcapillaries varied from 1 to 1000 µm. Usual large-area measurements show a pitting potential of about 300 mV (SCE) and measurements performed with 1000 µm microcapillaries showed similar pitting potentials and measurements with a lower area, 50 µm in diameter, leads to an increase of the pitting potential to about 1200 mV (SCE). These microelectrochemical experiments revealed that the pitting potential is an area-dependent value. The study showed that the presence of MnS inclusions is of primary importance for pit initiation, whereas the size and geometry, as well as the amount of chlorides and the temperature, are critical for the transition from metastable to stable pit growth (Suter, 2001).

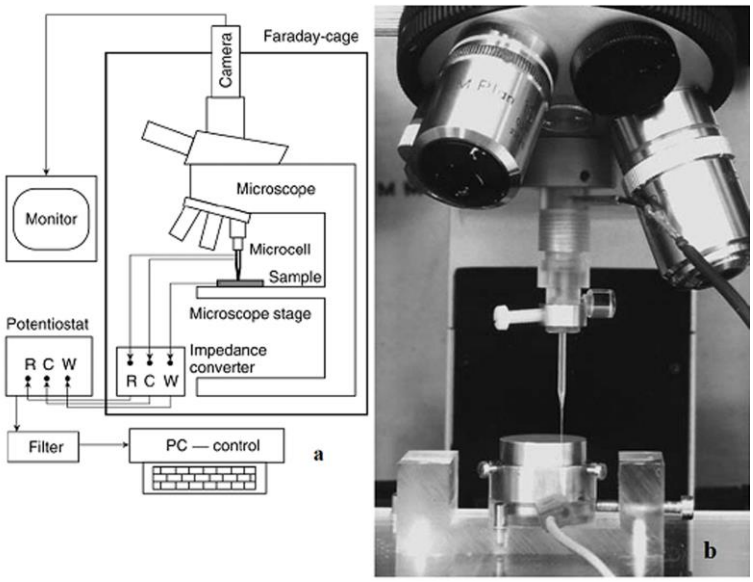

Figure 10.1: Setup for microelectrochemical investigations. A glass microcapillary is used as an electrochemical cell; (a) schematic drawing of microcell technique; (b) picture of the assembled microcell. Source: Bohni, 1995; Suter, 1988; Suter, 2001.

The range of current for microelectrochemical polarization measurements is pA (10^{-12}) and fA (10^{-15}) due to small area, this way is necessary good shielding (Faraday cage), high-resolution potentiostat (Perren *et al.*, 2001; Suter and Bohni, 2001, Lohrengel, 2001; Lohrengel *et al.*, 2004).

Microelectrochemical techniques allow performing local electrochemical investigations of single areas of special interest (Pereda *et al.,* 2011). The electrochemical microcell technique has been used to measure the behavior of a microstructurally complex material on a phase-by-phase basis for the evaluation of the electrochemical behavior that showed good correspondence between electrochemical reaction rate maps for different environmental conditions and observations of localized corrosion of 7075 samples after free corrosion exposures (Buchheit, 2010).

Corrosion resistance of super DSS in chloride ion containing environments using microcell was studied with potentiodynamic polarization measurements in the area around 10 μm, which was possible to evaluate the behavior of each single phase (ferrite and austenite) in hydrochloric acid. The results showed a good relation between the pitting resistance equivalent number (PREN) of the each phase and the corrosion behavior was measured (Perren *et al.,* 2001).

10.1 Experimental procedure

The Microelectrochemical set up used in these experiments is shown in Figure 10.2. The microcell is formed of a microcapillary, which was fixed an objective and filled with the appropriate electrolyte. The tip was sealed with a layer of silicon rubber between the front end of the microelectrode and working electrode to avoid leaking of the electrolyte (Sánchez *et. al.*, 2012).

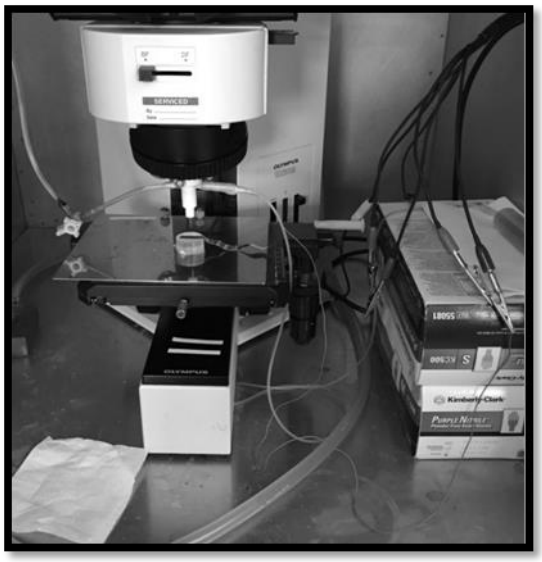

Figure 10.2: Set up for the microcell to measure the diameter of the capillary.

Capillary preparation starts with small glass tubes with a length of some centimeters and a diameter of around 1mm. Then they are heated in the middle and pulled in the special set- ups using a laboratory capillary puller (World Precision Instruments) to create a capillary with a fine tip as shown in Figure 10.3. The tip was subsequently ground using 1200 grit to guarantee flatness tip (Lohrengel *et al.*, 2006). A silicone seal was applied to the front end of the capillary in order to avoid any solution leakage and to allow an interference contact with the working electrode (Birbilis *et al.*, 2005; Lohrengel *et al.*, 2006).The solution in the capillary was refreshed before each measurement.

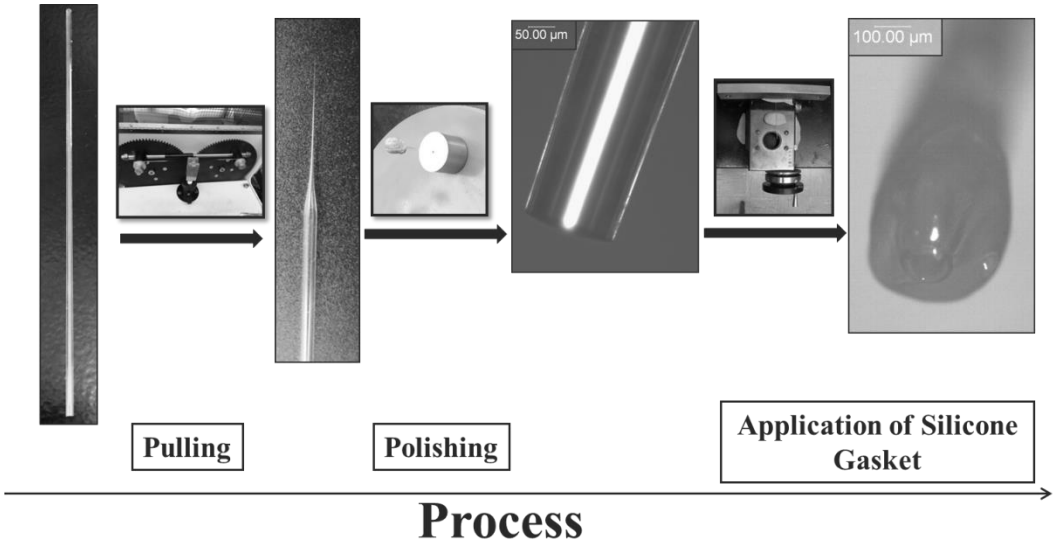

Figure 10.3: Manufacturing the capillaries.

The difficult to apply the rubber increases when the area the tip reduces. Nevertheless, the current is smaller.

10.1.1 Cyclic Anodic Potentiodynamic Polarization

Tests were performed three times to ensure the reproducibility. The polarization curves were collected at a scan rate of 1 mV/s (Perren *et al*., 2001; Birbilis, 2008, Buchheit, 2010; Cavanaugh *et al,*, 2007; Li, 2015) using a GAMRY reference 600 potentiostat in a standard three-electrode set up. Saturated calomel electrode (SCE) as reference electrode, platinum wire as counter electrode, and the working electrode, which had the area controlled by tip size as shown in Figure 10.4. Scans were begun bellow the corrosion potential (E_{corr}), were stabilized for a period of 2 minutes and the anodic polarization measurements were initiated from -0.01 V *vs.* OCP until a breakdown potential. When the current had reached 5 mA/cm^2 the scan was reversed until the hysteresis loop is close or until the $E_{corr.}$ Tests were performed at the Ohio State University (OSU) in the United States.

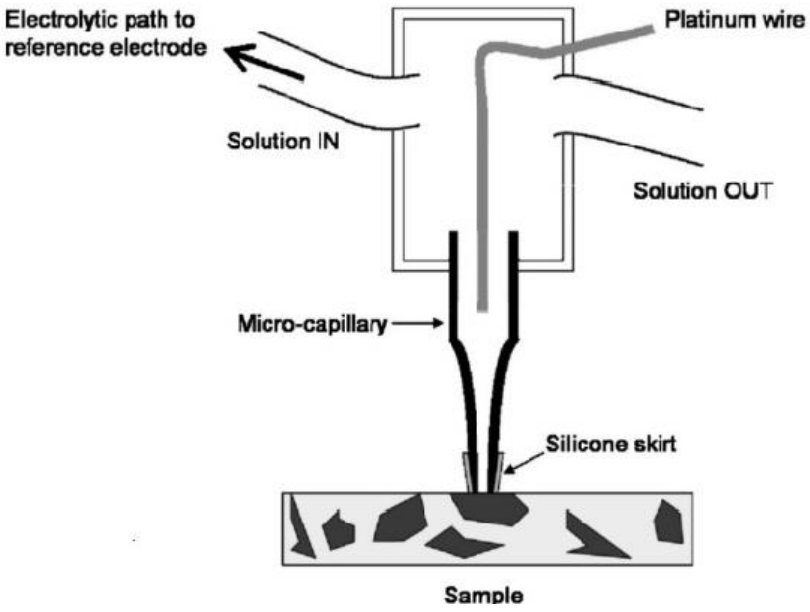

Figure 10.4: Schematic representation of microcell test. Adapted: Birbillis, 2005.

10.2 Results and Discussion

The white liquor was selected as an electrolyte for the microelectrochemical analysis due to the highest aggressiveness reported from pulp and paper mill and due to this medium does not contain solids, which can obstruct capillary. Figure 10.5(a) shows the cyclic potentiodynamic polarization curves of hot rolled DSS 32205 in white liquor at room temperature. In these measurements the area of the tip was 3.5 x 10^{-5} cm^2, the scan rate was 1 mV/s to avoid cell leakage, and also to avoid corrosion products block the capillary mouth during cyclic polarization (Andreatta *et al.*, 2003, Birbilis *et al.*, 2005), and it was reached a 5 mA/cm^2 before the reverse scan. Figure 10.5 (b) shows the corroding area. The behavior of microelectrochemical measurements was similar to macroelectrochemical.

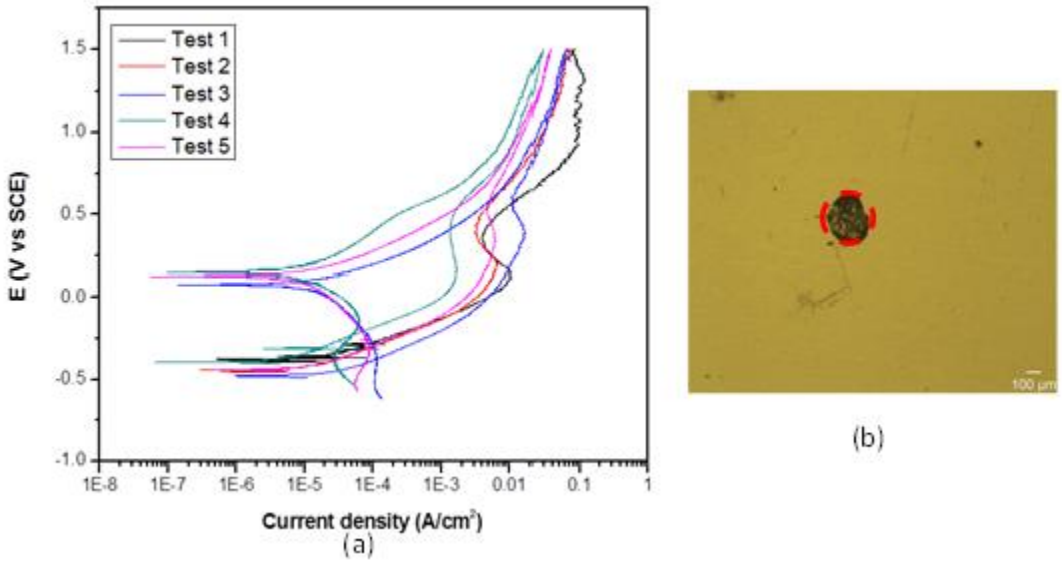

Figure 10.5: (a) Microelectrochemical cyclic potentiodynamic polarization curves in white liquor of hot rolled DSS S31803, (b) measurement area.

Figure 10.6 (a) illustrated the corroding area which the sample was prepared by polishing until 0.25 µm to permit evaluate which phase the area of the tip is taking on the measurement. Without etching was possible to distinguish the phase austenite and ferrite. Figure 10.6 (b) shows that the brighter phases are austenite with diameter around 20 µm, for this reason, the tip must be reduced to reach only one phase in each measurement.

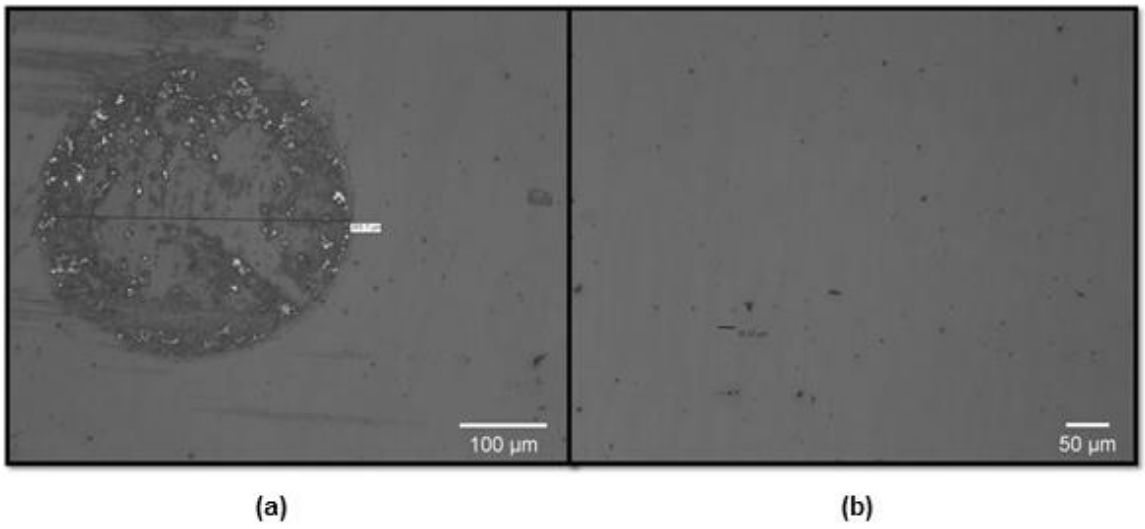

Figure 10.6: (a) Corroding area after cyclic potentiodynamic polarization test in white liquor at room temperature, (b) austenite size (around 20 µm).

First, is necessary to find a way to reduce the area of the tip to allow the measurement of each phase in DSS. For this improve the skill to seal a small area of the tip and figure out how to work white liquor which has high viscosity and some particles precipitating inside of the microcell due to the high concentration of salt in the composition of the electrolyte.

10.3 Conclusion

- Reduce the area of tip to allow the measurement of each phase in duplex stainless steel;
- Improve the skill to seal a small area of tip;
- Figure out how to work white liquor, which has high viscosity and some particles precipitating inside of the microcell due to the high concentration of salt in the composition of the electrolyte.

10.4 References

ANDREATTA, F.; Lohrengel, M.; Terryn, H.; Wit, J. H. W , **Electrochemical characterisation of aluminigum AA7075-T6 and solution heat treated AA7075 using a micro-capillary cell,** Electrochimica Acta, vol. 48, no. 20-22, p. 3239–3247, 2003.

BIRBILIS, N.; BUCHHEIT, R. G., Electrochemical Characteristics of Intermetallic Phases in Aluminum Alloys, **Journal of The Electrochemical Society**, v. 152, n. 4, p. B140, 2005.

BIRBILIS, N.; PADGETT, B. N.; BUCHHEIT, R. G., Limitations in microelectrochemical capillary cell testing and transformation of electrochemical transients for acquisition of microcell impedance data, **Electrochimica Acta**, v. 50, n. 16–17, p. 3536–3544, 2005.

BIRBILIS, N.; BUCHHEIT, R. G., Investigation and Discussion of Characteristics for Intermetallic Phases Common to Aluminum Alloys as a Function of Solution pH, **Journal of The Electrochemical Society**, v. 155, n. 3, p. C117, 2008.

BÖHNI, H.; SUTER, T.; SHREYER, A.; **Micro and nanotechniques to study localized corrosion.** Electrochimica Acta.v.40, p.1361-1368 (1995).

BUCHHEIT, R.G.; BIRBILIS, N., Electrochemical microscopy: An approach for understanding localized corrosion in microstructurally complex metallic alloys, **Electrochimica Acta**, v. 55, n. 27, p. 7853–7859, 2010.

CAVANAUGH, M. K. *et al*, Investigating localized corrosion susceptibility arising from Sc containing intermetallic Al3Sc in high strength Al-alloys, **Scripta Materialia**, v. 56, n. 11, p. 995–998, 2007.

LI, J.; HURLEY, B.; BUCHHEIT, R., Inhibition Performance Study of Vanadate on AA2024-T3 at High Temperature by SEM, FIB, Raman and XPS, **Journal of the Electrochemical Society**, v. 162, n. 6, p. C219–C227, 2015.

LOHRENGEL, M. M.; MOEHRING, a.; PILASKI, M., Capillary-based droplet cells: Limits and new aspects, **Electrochimica Acta**, v. 47, n. 1, p. 137–141, 2001.

LOHRENGEL, M. M., Electrochemical capillary cells, **Corrosion Engineering, Science and Technology**, v. 39, n. 1, p. 53–58, 2004.

LOHRENGEL, M. M.; Heiroth, S.; Kluger, K.; Pilaski, M.; Walther, B.**, Microimpedance - Localized material analysis**, Electrochimica Acta, v. 51, n. 8-9, p. 1431–1436 (2006).

MARCUS, PHILIPPE MANSFELD, Florian, **Analytical Methods in Corrosion Science and Engineering**, Boca Raton: Taylor &Francis Group, 2006.

PEREDA, M. D.; GERVASI, C. A.; LLORENTES, C. L.; BILMES, P.D.; **Microelectrochemical corrosion study of super martensitic welds in chloride-containing media**. Corrosion Science. v. 53, p. 3934-3941 (2011).

PERREN, R.; Suter, T.A.; Uggowitzer, P. J.; Weber, L.; Magdowski, R.; Bohni, H.; Speidel, M. O.; **Corrosion resistance of super duplex stainless steels in chloride ion containing environments: Investigations by means of a new microelectrochemical method. II. Influence of precipitates**, Corrosion Science, v. 43, n. 4, p. 727–745, 2001.

SÁNCHEZ, M. *et al*, Assessment of the electrochemical microcell geometry by local electrochemical impedance spectroscopy of copper corrosion, **Electrochimica Acta**, v. 62, p. 276–281, 2012.

SUTER, T.; BÖHNI, H., **A new microelectrochemical method to study pit initiation on stainless steels, Electrochimica Acta**, v. 42, n. 70, p. 3275–3280 (1997).

SUTER, T.; BÖHNI, H.; **Microelectrodes for studies of localized corrosion processes.**ElectrochimicaActa. (43) P. 2843-2849 (1998).

SUTER, T.; BÖHNI, H.; **Microelectrodes for corrosion studies in microsystems.** ELECTROCHIMICA ACTA. (47) P. 191-199 (2001).

11 FUTURE WORKS

- Increase the period of immersion test to formed the corrosion products and using X-ray photoelectron spectroscopy (XPS) and DRX to study the chemical composition and oxides morphology;
- Characterize the samples using Mott-Schottky technique after the potentiostat test to increase the layer of the corrosion product.